CFD ANALYSIS OF ELECTRONICS CHIP COOLING

A THESIS SUBMITTED IN PARTIAL FULFILMENT
OF THE REQUIREMENTS FOR THE DEGREE OF

Master of Technology

in

Mechanical Engineering

By

SAROJ KUMAR PATRA

Department of Mechanical Engineering

National Institute of Technology

Rourkela

2007

CFD ANALYSIS OF ELECTRONICS CHIP COOLING

A THESIS SUBMITTED IN PARTIAL FULFILMENT
OF THE REQUIREMENTS FOR THE DEGREE OF

Master of Technology

in

Mechanical Engineering

By

SAROJ KUMAR PATRA

Under the Guidance of

Prof. ASHOK KUMAR SATAPATHY

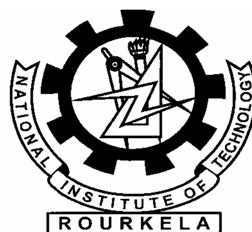

Department of Mechanical Engineering

National Institute of Technology

Rourkela

2007

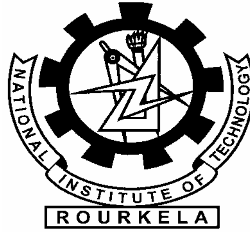

National Institute of Technology
Rourkela

CERTIFICATE

This is to certify that thesis entitled, "**CFD ANALYSIS OF ELECTRONICS CHIP COOLING**" submitted by Mr. SAROJ KUMAR PATRA in partial fulfillment of the requirements for the award of Master of Technology Degree in Mechanical Engineering with specialization in "Thermal Engineering" at National Institute of Technology, Rourkela (Deemed University) is an authentic work carried out by him under my supervision and guidance.

To the best of my knowledge, the matter embodied in this thesis has not been submitted to any other university/ institute for award of any Degree or Diploma.

Prof. Ashok Kumar Satapathy
Date:
Dept. of Mechanical Engineering
National Institute of Technology

ACKNOWLEDGEMENT

It is with a feeling of great pleasure that I would like to express my most sincere heartfelt gratitude to **Prof. Ashok Kumar Satapathy**, **Asst. Professor, Dept. of Mechanical Engineering, NIT, Rourkela** for suggesting the topic for my thesis report and for his ready and able guidance through out the course of my preparing the report. I am greatly indebted to him for his constructive suggestions and criticism from time to time during the course of progress of my work.

I express my sincere thanks to **Prof. R.K.Sahoo of the Department of Mechanical Engineering, NIT, Rourkela** for providing me the necessary facilities in the department.

I am also thankful to all the staff members and all the M.Tech 2nd year students of the department of Mechanical Engineering and to all my well wishers for their inspiration and help.

Date :

Saroj Kumar Patra

Roll No.:- 20503028

National Institute of Technology

Rourkela-769008, Orissa, India.

Abstract

Since the development of the first electronic digital computers in the 1940s, the effective removal of heat has played a key role in ensuring the reliable operation of successive generations of computers. As day by day the size of the electronic instruments decreases drastically and simultaneously the number of functions per chip increases hugely. So it's a great challenge to packaging engineers to remove the heat generated by the chip efficiently. Many researches are going on in this direction for the past few decades. In the last decade or so CFD simulations have become more and more widely used in studies of electronic cooling. Validation of these simulations has been considered to be very important.

In this study we are analyzing the cooling effects of the chip by modeling the geometry numerically. We have considered a single chip module. The modeling is carried out by solving the governing equations for a flow through a channel via obstruction. The case we have considered is transient laminar flow. The method we have used here to discretize the governing equations, namely the continuity equation, the momentum equation and the energy equation is Finite Difference Method (FDM). To solve the problem the algorithm we have used is Marker and Cell (MAC) method, and to discretize the convective term we have used the weighted second upwind and space centered difference. The diffusive terms are discretized by central difference scheme. The entire algorithm was written in FORTRAN-90.

The geometry and the boundary conditions we have considered is for general applicability, that's why we have non-dimensionalized the variables. In the discretization we have considered equal increment in both x-direction and y-direction. We have considered the domain 198 nodes in x-direction and 32 in y-direction. The case we are considering is constant temperature conditions. The temperature of the wall and that of the chip were considered to be unity and that of the inlet velocity temperature is considered to be zero. So the entire temperature range falls in between zero and one. The obstruction size we have considered are 3x3, 7x7, 11x11, and 15x 15, that means the blockage ratio nearly varies from 0.1 to 0.5. All the above cases are considered by varying the Reynolds number as 300, 600, 900, and 1200 that means all are in the laminar zone.

After conducting the simulations we found the results, and by using different software packages like Surfer-32, Origin 6.1, and Grapher 1.09, we have plotted different contours of pressure and temperature, velocity profiles and variation of Nusselt number. Finally the outputs or graph and contours are analyzed for the process. In appendix-A, we have presented the output of FLUENT, which is simulated with same boundary conditions. So the results can be compared with it.

Table of Contents

Certificate i
Acknowledgement ii
Abstract iii
Table of Contents v
List of Figures viii
Nomenclature xi
1. Introduction 1
1.1 General 2
1.2 History of Chip Cooling 2
1.3 Major Concern Areas 6
1.3.1 Traditional Thermal Design Requirements 6
1.3.2 New Thermal Design Requirements 7
1.4 Current Methods Used in Industry 7
1.4.1 Module Level Cooling 7
1.4.1.1 Internal Module Cooling 7
1.4.1.2 External Module Cooling 8
1.4.1.3 Immersion Cooling 8
1.4.2 System Level Cooling 9
1.4.2.1 Air Cooling 9
1.4.2.2 Hybrid Air-Water Cooling 10
1.4.2.3 Liquid-Cooling Systems 11
1.4.2.4 Refrigeration Cooled Systems 12
1.4.3 Data Center Thermal Management 12
1.5 Objective of the Work 14
1.6 Organization of the Thesis 14
2. Literature Review 15
2.1 Introduction 16

2.2 Analytical Solutions 18
2.3 Numerical Solutions 20
2.4 Experimental Investigations. 27
2.5 Closure 32
3. Mathematical Formulation 33
3.1 Introduction 34
3.2 Governing Equations 34
3.2.1 Expanded Form of Navier-Stokes Equation. 34
3.2.2 Non-Dimensionalization 35
3.3 Staggered Grid 36
3.4 Solution of the Navier-Stokes Equation 36
3.4.1 Introduction to the Marker and Cell (MAC) Method 36
3.4.2 Outline of Procedure. 37
3.4.3 The Algorithm of MAC Method. 38
3.4.4 MAC Formulation. 40
3.4.5 Pressure-Velocity Correction. 44
3.4.5.1 The Philosophy of Pressure Correction Method. 44
3.4.5.2 Pressure-Velocity Correction Procedure by MAC method. 45
3.4.6 Boundary Conditions 48
3.4.7 Numerical Stability Considerations 51
3.5 Solution of the Energy Equation 52
3.5.1 Solution Procedure. 53
3.6 Computational Domain and Boundary Conditions 55
3.6.1 Computational Domain 55
3.6.2 Boundary Conditions 57
3.7 Closure. 58
4. Results and Discussions 59
4.1 Introduction 60
4.2 Pressure Contours 60

4.3 Temperature Contours 66
4.4 Velocity Profiles 71
4.5 Nusselt Number 76
4.6 Closure 79

5. Conclusions and Suggestions for Further Work 80

5.1 Conclusion 81
5.2 Suggestions for further work 82

Appendices 83

Appendix-A: Results of FLUENT 83
Appendix-B: Programme for chip cooling 90

Bibliography 110

List of Figures

Figure Number	Title of the Figure	Page number
Fig. 1.1	Increase in circuit complexity	4
Fig. 1.2	The Chronological Evolution of chip level Heat Flux.	4
Fig. 1.3	The Chronological Evolution of Module level Heat Flux in Mainframe Computers.	5
Fig 1.4	Major Causes of Electronics Failure	5
Fig. 1.5	Cross Section of a Typical Module Denoting Internal Cooling Region and External Cooling Region	8
Fig 1.6	Heat load per product Footprint	13
Fig. 3.1	Discretization of a Three-Dimensional Domain	43
Fig. 3.2	Boundary Conditions and Imaginary Boundary Cells	50
Fig. 3.3	Discretization of the Domain	57
Fig. 3.4	Boundary Conditions and Fictitious Boundary Cells	58
Fig. 3.5	Geometry of the Computational Domain Showing B, H	59
Fig. 4.1	Pressure Contours for an obstruction size of 3x3 for various Reynolds No.s (a) Re = 300 (b) Re = 600 (c) Re = 900 (d) Re = 1200.	62
Fig. 4.2	Pressure Contours for an obstruction size of 7x7 for various Reynolds No.s (a) Re = 300 (b) Re = 600 (c) Re = 900 (d) Re = 1200.	63
Fig. 4.3	Pressure Contours for an obstruction size of 11x 11 for various Reynolds No.s (a) Re = 300 (b) Re = 600 (c) Re = 900 (d) Re = 1200.	64
Fig. 4.4	Pressure Contours for an obstruction size of 15x15 for various Reynolds No.s (a) Re = 300 (b) Re = 600 (c) Re = 900 (d) Re = 1200.	65
Fig. 4.5	Temperature Contours for an obstruction size of 3x3 for various Reynolds no.s (a) Re = 300 (b) Re = 600 (c) Re = 900 (d) Re = 1200.	68
Fig. 4.6	Temperature Contours for an obstruction size of 7x7 for various Reynolds no.s (a) Re = 300 (b) Re = 600 (c) Re = 900 (d) Re = 1200.	69
Fig. 4.7	Temperature Contours for an obstruction size of 11x11 for various Reynolds no.s (a) Re = 300 (b) Re = 600 (c) Re = 900 (d) Re = 1200.	70

Fig. 4.8 Temperature Contours for an obstruction size of 15x15 for various Reynolds no.s (a) Re = 300 (b) Re = 600 (c) Re = 900 (d) Re = 1200. 71

Fig. 4.9 Velocity Profile for an obstruction size of 3x3 for various Reynolds Numbers (a) Re = 300 (b) Re = 600 (c) Re = 900 (d) Re = 1200. 73

Fig. 4.10 Velocity Profile for an obstruction size of 7x7 for various Reynolds Numbers (a) Re = 300 (b) Re = 600 (c) Re = 900 (d) Re = 1200. 74

Fig. 4.11 Velocity Profile for an obstruction size of 11x11 for various Reynolds Numbers (a) Re = 300 (b) Re = 600 (c) Re = 900 (d) Re = 1200. 75

Fig. 4.12 Velocity Profile for an obstruction size of 15x15 for various Reynolds Numbers (a) Re = 300 (b) Re = 600 (c) Re = 900 (d) Re = 1200. 76

Fig. 4.13 Variation of Nusselt Number along the Axial Direction for an Obstruction Size of 3x3, at Different Reynolds Number 78

Fig. 4.14 Variation of Nusselt Number along the Axial Direction for an Obstruction Size of 7x7, at Different Reynolds Number 78

Fig. 4.15 Variation of Nusselt Number along the Axial Direction for an Obstruction Size of 11x11, at Different Reynolds Number 79

Fig. 4.16 Variation of Nusselt Number along the Axial Direction for an Obstruction Size of 15x15, at Different Reynolds Number 79

Fig.A.1 Pressure Contours for an Obstruction Size of 3x3 at Various Reynolds No. (a) 300, (b) 600, (c) 900, (d) 1200 84

Fig.A.2 Temperature Contours for an Obstruction Size of 3x3 at Various Reynolds No. (a) 300, (b) 600, (c) 900, (d) 1200 84

Fig.A.3 Velocity Profile for an Obstruction Size of 3x3 at Various Reynolds Number (a) 300, (b) 600, (c) 900, (d) 1200 85

Fig.A.4 Pressure Contours for an Obstruction Size of 7x7 at Various Reynolds No. (a) 300, (b) 600, (c) 900, (d) 1200 85

Fig.A.5 Temperature Contours for an Obstruction Size of 7x7 at Various Reynolds No. (a) 300, (b) 600, (c) 900, (d) 1200 86

Fig.A.6 Velocity Profiles for an Obstruction Size of 7x7 at Various Reynolds No. (a) 300, (b) 600, (c) 900, (d) 1200 86

Fig.A.7 Pressure Contours for an Obstruction size of 11x11 at Various Reynolds Number (a) 300, (b) 600, (c) 900, (d) 1200 87

Fig.A.8 Temperature Contours for an Obstruction Size of 11x11 at various Reynolds Number (a) 300, (b) 600, (c) 900, (d) 1200 87

Fig.A.9 Velocity Profiles for an Obstruction Size of 11x11, for Various Reynolds No. (a) 300, (b) 600, (c) 900, (d) 1200 88

Fig.A.10 Pressure Contours for an Obstruction of 15x15, for Various Reynolds Number (a) 300, (b) 600, (c) 900, (d) 1200 88

Fig.A.11 Temperature Contours for an Obstruction Size of 15x15 at various Reynolds Number (a) 300, (b) 600, (c) 900, (d) 1200 89

Fig.A.12 Velocity Profiles for an Obstruction Size of 15x15, for Various Reynolds Number (a) 300, (b) 600, (c) 900, (d) 1200 89

Nomenclature

English Figures

C_p	Specific heat at constant pressure
Ec	Eckert number
i	Node value along X-direction.
ia	Initial node value of the obstruction along X-direction
ib	Final node value of the obstruction along X-direction
iim	Imaginary node value along X-direction.
Ire	Real node value along X-direction.
J	Node value along Y-direction
ja	Initial node value of the obstruction along Y-direction
jb	Final node value of the obstruction along Y-direction
jim	Imaginary node value along Y-direction.
jm	Horizontal mid plane
jre	Real node value along Y-direction.
k	Node value along Z-direction
kim	Imaginary node value along Z-direction.
kre	Real node value along Z-direction
n	Unit normal vector
Nu	Nusselt number.
p	Non-dimensional form of Pressure
$P^n_{i,j,k}$	Pressure at the centre of the cell (*i, j, k*) at nth time level
Pe	Peclet number
Re	Reynolds number
t	Non dimensional form of time‘t*’.

t^*	Time
T	Temperature of air.
T_∞	Free stream temperature of air at inlet
T_w	Temperature of wall and chip.
u	Nondimensionalized form of velocity
u^*	X-component of velocity
U_∞	Free stream velocity at inlet.
v	Y-component of velocity
w	Z-component of velocity

Greek Symbols

α	Upwind factor.
δx	Small increment along the x-direction of the discretized domain.
δy	Small increment along the y-direction of the discretized domain.
δz	Small increment along the z-direction of the discretized domain.
δt	Small increment of time.
ρ	Density of air.
μ	Coefficient of viscosity
Φ	Nondimensional form of Φ^*
Φ^*	Viscous dissipation.
θ	Nondimensional form of temperature, T.
ω_0	Over relaxation factor.

Subscripts

av	Average.

(i, j, k)	Nodal location of a cell.
w	Wall condition.
θ	Condition at free stream.

Superscripts

n	Represents the nth time level.
$*$	Represents the non-dimensionalization.

Operators

$\mid \; \mid$	Modulus.
∇	Gradient operator

Abbreviations

CFL	Courant-Friedrichs-Lewy
CONVT	Convective
MAC	Marker and Cell
DPDX	Differentiation of P with respect to X.
SDISCU	Spatial discretization of the convective and diffusive terms

Chapter-1

Introduction

- **General**
- **History of Chip Cooling**
- **Major Concern Areas**
- **Current Methods Used in Industry**
- **Objective of the Work**
- **Closure**

INTRODUCTION

1.1 General

Electronics devices and equipment now permeate virtually every aspect of our daily life. Among the most ubiquitous of these is the electronic computer varying in size from the hand held personal digital assistant to large scale mainframes or servers. In many instances a computer is embedded within some other devices controlling its function and is not even recognizable as such. For example in automobiles, space crafts, missiles, satellite etc. The applications of computers vary from games for entertainment to highly complex systems supporting vital heath, economic, scientific, mobile phones, and defense activities. The dimensions of the instruments also decreasing day by day but simultaneously the number of functions increases as a result the functions per unit volume are increasing hugely, this is most visible in portable electronic component, such as laptops, cell phones, digital cameras and other items around us, where an increasing number of functional components are squeezed into an ever shrinking system box. Compact packaging is also in progress in desktops and in server computers, driven by the needs to reduce the box dimensions and cut wiring distances between electronic devices. In a growing number of applications computer failure results in a major disruption of vital services and can even have life-threatening consequences. As a result, efforts to improve the reliability of electronic computers or electronics chips are as important as efforts to improve their speed and storage capacity.

1.2 History of Chip Cooling

Since the development of the first electronic digital computers in the 1940s, the effective removal of heat has played a key role in ensuring the reliable operation of successive generations of computers. The Electrical Numerical Integrator and Computer (ENIAC), dedicated in 1946, has been described as a ‘‘30 ton, boxcar-sized machine requiring an array of industrial cooling fans to remove the 140 KW dissipated from its 18,000 vacuum tubes’’. As with ENIAC, all early computers up to 1957 used vacuum-tube electronics and were cooled with forced air. The

invention of the transistor by Bardeen, Brattain, and Shockley at Bell Laboratories in 1947 foreshadowed the development of generations of computers yet to come. As a replacement for vacuum tubes, the miniature transistor generated less heat, was much more reliable, and promised lower production costs. For a while it was thought that the use of transistors would greatly reduce if not totally eliminate cooling concerns. This thought was short-lived as packaging engineers worked to improve computer speed and storage capacity by packaging more and more transistors on printed circuit boards, and then on ceramic substrates.

The trend toward higher packaging densities dramatically gained momentum with the invention of the integrated circuit by Kilby at Texas Instruments and Noyce at Fairchild Semiconductor in 1959. During the 1960s small scale and then medium scale integration (SSI) and (MSI) led from one device per chip to hundreds of devices per chip. The trend continued through the 1970s with the development of large scale integration (LSI) technologies offering hundreds to thousands of devices per chip, and then through the 1980s with the development of very large scale integration (VLSI) technologies offering thousands to tens of thousands of devices per chip [see Fig.1.1]. This trend continued with the introduction of the microprocessor. It continues to this day with INTEL and others projecting that a microprocessor chip with a billion or more transistors will be a reality before 2010.

In many instances the trend toward higher circuit density has been accompanied by increased power dissipation per circuit to provide reductions in circuit delay (i.e., increased speed). The need to further increase packaging density and reduce signal delay between communicating circuits led to the development of multi chip modules beginning in the late 1970s and is continuing to this day. Fig.1.2 and Fig.1.3 represents the chip heat flux and module heat flux. As can be seen the chip heat flux increases at a cumulative growth rate (CGR) of 7 % per year, and heat flux associated with bipolar circuit technologies steadily increased from the very beginning and really took off in the 1980s. There was a brief respite with the transition to CMOS circuit technologies in the 1990s; but the demand for increased packaging density and performance reasserted itself and heat flux is again increasing at a challenging rate.

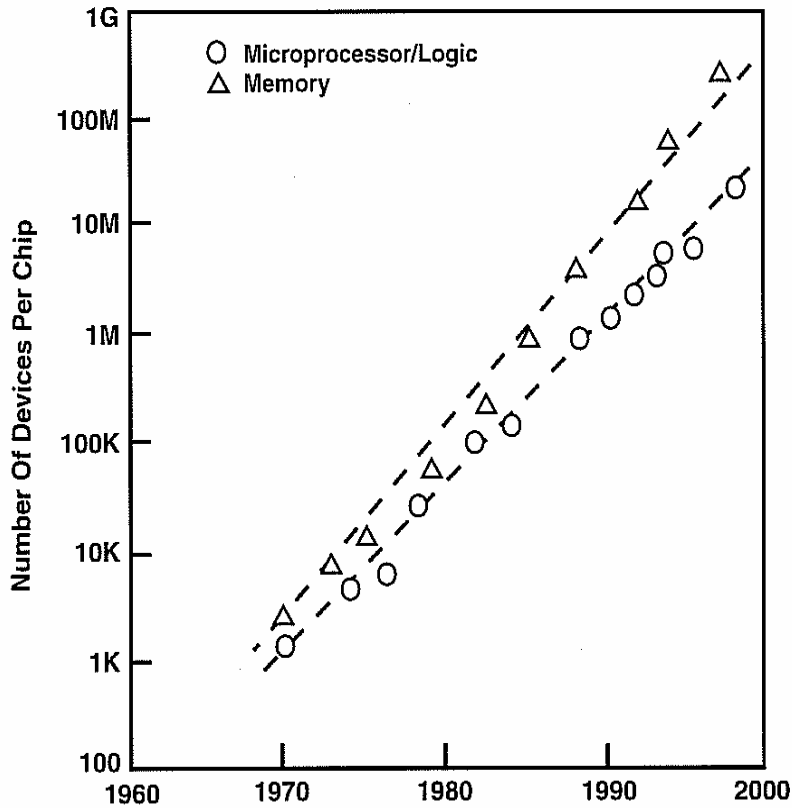

[Fig.1.1] Increase in circuit complexity

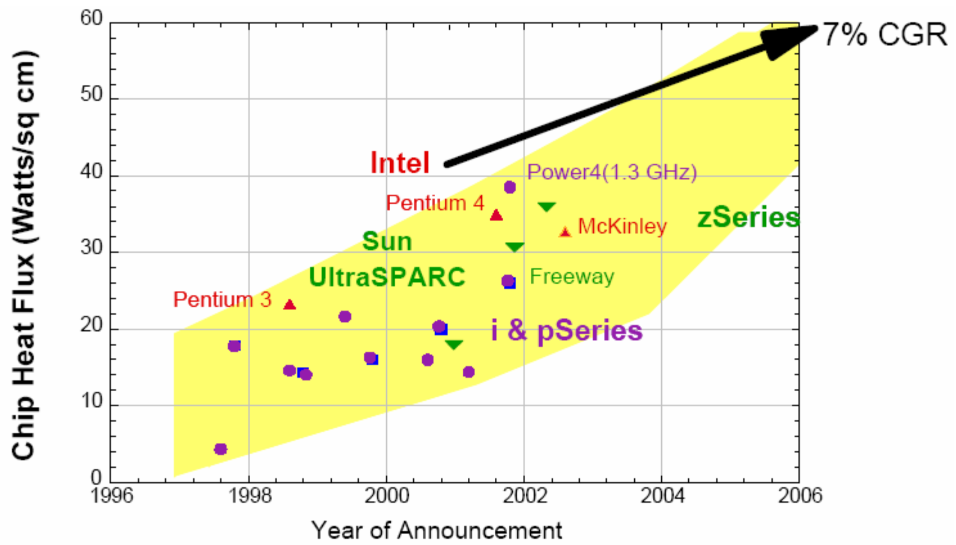

[Fig.1.2] The Chronological Evolution of chip level Heat Flux.

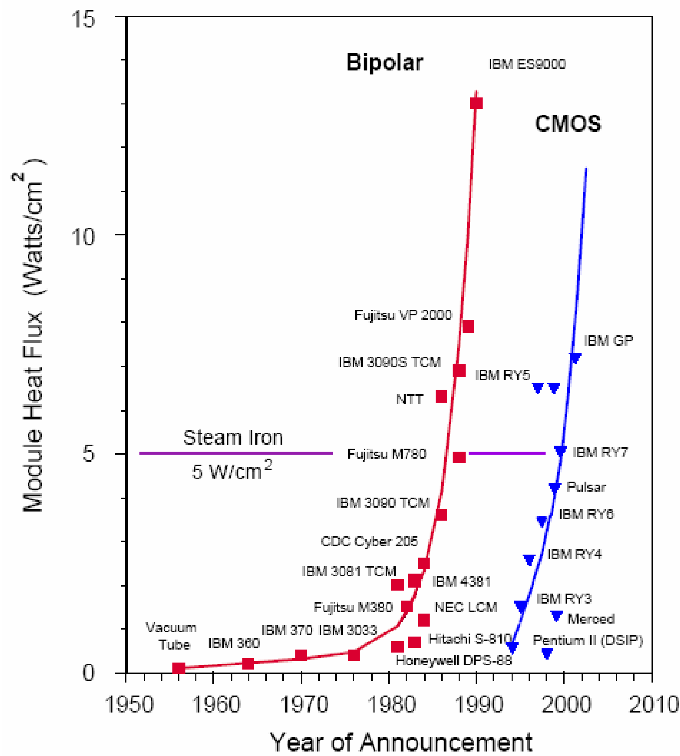

[Fig.1.3] The Chronological Evolution of Module level Heat Flux in Mainframe Computers.

It has been found that for every 2° C temperature rise, the reliability of a silicon chip will be decreased by about 10 %. The major cause of a electronic chip failure is due to temperature rise (55%) as against other factors which accounts 20 % vibration, 19 % humidity and 6 % dust [Fig.1.4]. So it's a great challenge for the packaging engineers to remove the heat from the electronics chips very effectively.

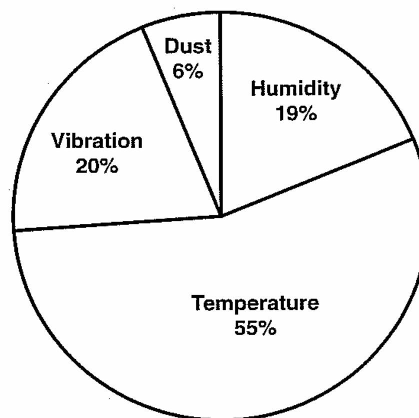

[Fig.1.4] Major Causes of Electronics Failure

1.3 Major Concern Areas

Throughout the past 50 years, cooling and thermal management have played a key role in accommodating increases in power while maintaining component temperatures at satisfactory levels to satisfy performance and reliability objectives. Thermal management will play a pivotal role in the coming decade for all types of electronics products. Increased heat fluxes at all levels of packaging from chip to system to facility pose a major cooling challenge. To meet the challenge, significant cooling technology enhancements will be needed in each of the following areas.

- Thermal interfaces
- Heat spreading
- Air cooling
- Indirect and direct water cooling
- Immersion cooling
- Refrigeration cooling
- Thermoelectric cooling
- Data center cooling

So the thermal design requirements to meet the growing demands are as follows, it is here grouped as traditional thermal design requirements and new thermal design requirements.

1.3.1 Traditional Thermal Design Requirements

- Design for Performance
- Design for Reliability
- Design for Serviceability
- Design for Extensibility
- Design for minimal Cost
- Design on minimal Impact on User
-

1.3.2 New Thermal Design Requirements

- Design for improved coolability at the package level via optimized internal thermal conduction paths.
- Design for direct air cooling at the product level via enhanced convection process over the packages.
- Design for special cooling needs at the module level via spot cooling devices attached to the packages.
- Design for low temperature applications- Sub ambient to cryogenic.
- Design for low cost via computer aided thermal engineering (CATE) and improved manufacturability.

1.4 Current Methods Used in Industry

Here are the various types of methods used in electronics (Computer) industry to cool Modules, Systems, and Data centers

1.4.1 Module Level Cooling

Processor module cooling is typically characterized in two ways: cooling internal and external to the module package and applies to both single and multi chip modules. Fig. 1.5 illustrates the distinction between the two cooling regimes in the context of a single-chip module.

1.4.1.1 Internal Module Cooling

The primary mode of heat transfer internal to the module is by conduction. The internal thermal resistance is therefore dictated by the module's physical construction and material properties. The objective is to effectively transfer the heat from the electronics circuits to an outer surface of the module where the heat will be removed by external means which will be discussed in the following section.

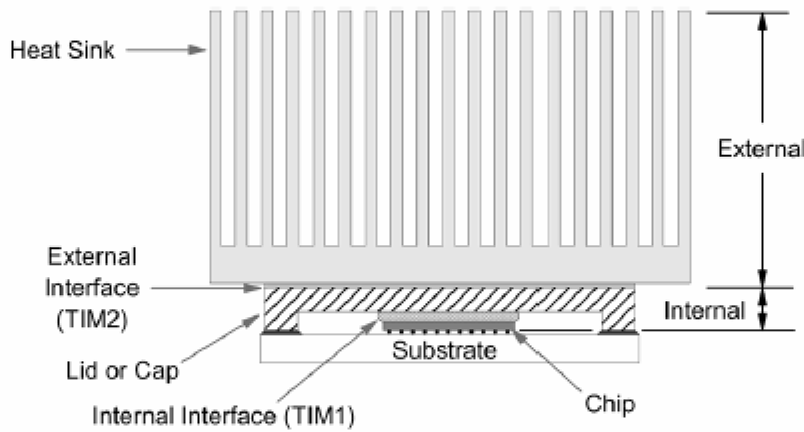

Fig.1.5 Cross Section of a Typical Module Denoting Internal Cooling Region and External Cooling Region

1.4.1.2 External Module Cooling

Cooling external to the module serves as the primary means to effectively transfer the heat generated within the module to the system environment. This is accomplished primarily by attaching a heat sink to the module. Traditionally, and preferably, the system environment of choice has been air because of its ease of implementation, low cost, and transparency to the end user or customer. This section, therefore, will focus on air-cooled heat sinks. Liquid-cooled heat sinks typically referred to as cold plates will also be discussed.

1.4.1.3 Immersion Cooling

Immersion cooling has been of interest as a possible method to cool high heat flux components for many years. Unlike the water-cooled cold plate approaches which utilize physical walls to separate the coolant from the chips, immersion cooling brings the coolant in direct physical contact with the chips. As a result, most of the contributors to internal thermal resistance are eliminated, except for the thermal conduction resistance from the device junctions to the surface of the chip in contact with the liquid. Direct liquid immersion cooling offers a high heat transfer coefficient which reduces the temperature rise of the heated chip surface above the liquid coolant temperature. The magnitude of the heat transfer coefficient depends upon the thermo-physical

properties of the coolant and the mode of convective heat transfer employed. The modes of heat transfer associated with liquid immersion cooling are generally classified as natural convection, forced convection, and boiling. Forced convection includes liquid jet impingement in the single phase regime and boiling (including pool boiling, flow boiling, and spray cooling) in the two-phase regime.

1.4.2 System-Level Cooling

Cooling systems for computers may be categorized as air-cooled, hybrid-cooled, liquid-cooled, or refrigeration- cooled. An air-cooled system is one in which air, usually in the forced convection mode, is used to directly cool and carry heat away from arrays of electronic modules and packages. In some systems air-cooling alone may not be adequate due to heating of the cooling air as it passes through the machine. In such cases a hybrid-cooling design may be employed, with air used to cool the electronic packages and water-cooled heat exchangers used to cool the air. For even higher power packages it may be necessary to employ indirect liquid cooling. This is usually done utilizing water-cooled cold plates on which heat dissipating components are mounted, or which may be mounted to modules containing integrated circuit chips. Ultimately, direct liquid immersion cooling may be employed to accommodate high heat fluxes and a high system heat load.

1.4.2.1 Air Cooling

Although liquid forced convection and boiling offer the highest heat transfer rates, air cooling has been and continues to be the most widely used technique for heat rejection. The principal advantages of cooling with air are its ready availability and ease of application. Prior to 1964, all computers were cooled solely by forced air. Air moving devices took in room air and provided a serial flow of air over columns of boards carrying printed circuit cards with single chip modules. In many cases air moving devices at either the bottom or top of a column of boards provided sufficient cooling air flow. A push–pull airflow arrangement with air moving devices at both the bottom and top of the column of boards was used for those cases requiring higher pressure drop capability.

Forced air-cooled systems may be further subdivided into serial and parallel flow systems. In a serial flow system the same air stream passes over successive rows of modules or boards, so that each row is cooled by air that has been preheated by the previous row. Depending on the power dissipated and the air flow rate, serial air flow can result in a substantial air temperature rise across the machine. The rise in cooling air temperature is directly reflected in increased circuit operating temperatures. This effect may be reduced by increasing the air flow rate. Of course to do this requires larger blowers to provide the higher flow rate and overcome the increase in air flow pressure drop. Parallel air flow systems have been used to reduce the temperature rise in the cooling air. In systems of this type, the printed circuit boards or modules are all supplied air in parallel. Since each board or module is delivered its own fresh supply of cooling air, systems of this type typically require a higher total volumetric flow rate of air.

1.4.2.2 Hybrid Air–Water Cooling

An air-to-liquid hybrid cooling system offers a method to manage cooling air temperature in a system without resorting to a parallel configuration and higher air flow rates. In a system of this type, a water-cooled heat exchanger is placed in the heated air stream to extract heat and reduce the air temperature. The cooling system incorporated an air-to-water finned tube heat exchanger between each successive row of circuit boards. The modules on the boards were still cooled by forced convection with air, however; the heated air exiting a board passed through an air-to-water heat exchanger before passing over the next board. Approximately 50% of the heat transferred to air in the board columns was transferred to the cooling water. Ultimately air-to-liquid hybrid cooling offers the potential for a sealed, recirculating, and closed-cycle air-cooling system with total heat rejection of the heat load absorbed by the air to chilled water. Sealing the system offers additional advantages. It allows the use of more powerful blowers to deliver higher air flow rates with little or no impact on acoustics. In addition, the potential for electromagnetic emissions from air inlet/outlet openings in the computer frame is eliminated. Another variant of the hybrid cooling system is the liquid-to-air cooling system. In this system liquid is circulated in a sealed loop through a cold plate attached to an electronic module dissipating heat. The heat is then transported via the liquid stream to an air-cooled heat exchanger where it is rejected to ambient air. This scheme provides the performance advantages of indirect liquid cooling at the module level while retaining the advantages of air cooling at the

system or box level. Most recently, a liquid-to-air cooling system is being used to cool the two processor modules in the Apple Power Mac G5 personal computer shipped earlier this year.

1.4.2.3 Liquid-Cooling Systems

Either the air-to-water heat exchangers in a hybrid air–water-cooled system or the water-cooled cold plates in a conduction-cooled system rely upon a controlled source of water in terms of pressure, flow rate, temperature, and chemistry. In order to insure the physical integrity, performance, and long-term reliability of the cooling system, customer water is usually not run directly through the water-carrying components in electronic frames. This is because of the great variability that can exist in the quality of water available at computer installations throughout the world. Instead a pumping and heat exchange unit, sometimes called a coolant distribution unit (CDU) is used to control and distribute system cooling water to computer electronics frames. The primary closed loop (i.e., system) is used to circulate cooling water to and from the electronics frames. The system heat load is transferred to the secondary loop (i.e., customer water) via a water-to-water heat exchanger in the CDU. Within an electronics frame a combination of parallel-series flow networks is used to distribute water flow to individual cold plates and heat exchangers. Water flow in the primary loop is provided at a fixed flow rate by a single operating pump, with a stand-by pump to provide uninterrupted operation if the operating pump fails. The temperature of the water in the primary loop is controlled by using a mixing valve to regulate the fraction of the flow allowed to pass through the water-to-water heat exchanger and forcing the remainder to bypass the heat exchanger. A CDU is also required for direct immersion cooling systems. In addition, because of the relatively high vapor pressure of the coolants suitable for direct immersion applications (e.g., fluorocarbons), the cooling system must be both "vapor-tight" and "liquid-tight" to ensure against any loss of the relatively expensive coolant.

1.4.2.4 Refrigeration Cooled Systems

The potential for enhancement of computer performance by operating at lower temperatures was recognized as long ago as the late 1960s and mid-1970s. Some of the earliest studies focused on Josephson devices operating at liquid helium temperatures (4K). The focus then shifted to CMOS devices operating near liquid nitrogen temperatures (77 K). A number of researchers have identified the electrical advantages of operating electronics all the way down to liquid nitrogen temperatures (77 K). In summary, the advantages are:

- Increased average carrier drift velocities (even at high fields);
- Steeper sub-threshold slope, plus reduced sub-threshold currents (channel leakages) which provide higher noise margins;
- Higher transconductance;
- Well-defined threshold voltage behavior;
- No degradation of geometry effects;
- Enhanced electrical line conductivity;
- Allowable current density limits increase dramatically (i.e., electro migration concerns diminish).

1.4.3 Data Center Thermal Management

Due to technology compaction, the information technology (IT) industry has seen a large decrease in the floor space required to achieve a constant quantity of computing and storage capability. However, the energy efficiency of the equipment has not dropped at the same rate. This has resulted in a significant increase in power density and heat dissipation within the footprint of computer and telecommunications hardware. The heat dissipated in these systems is exhausted to the room and the room has to be maintained at acceptable temperatures for reliable

operation of the equipment. Cooling computer and telecommunications equipment rooms is becoming a major challenge. The increasing heat load of datacom equipment has been documented by a thermal management consortium of 17 companies and published in collaboration with the Uptime Institute as shown in Fig. 28.

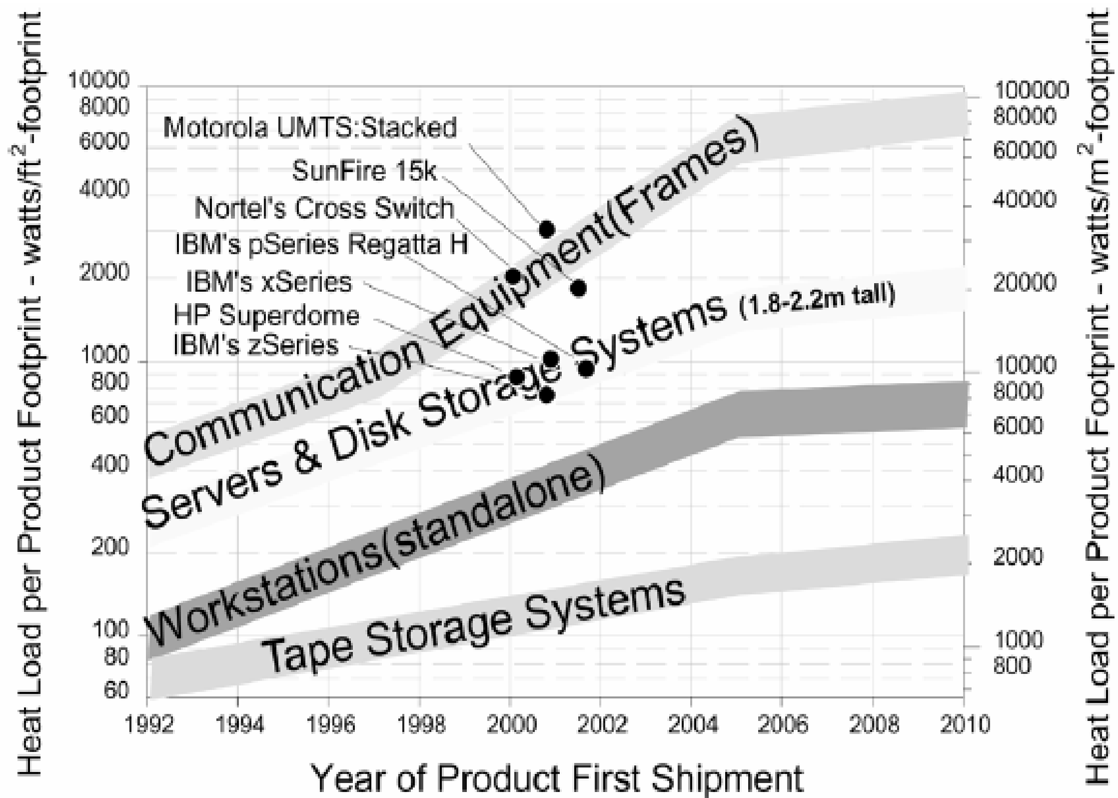

[Fig. 1.6] Heat load per product Footprint

Also shown in this figure are measured heat fluxes (based on product footprint) of some recent product announcements. The most recent shows a rack dissipating 28500 W resulting in a heat flux based on the footprint of the rack of 20900 W/m. With these heat loads the focus for customers of such equipment is in providing adequate air flow at a temperature that meets the manufacturer’s requirements.

1.5 Objective of the Work

In the analysis of electronics chip cooling. We are analyzing the flow through a square obstruction with given boundary conditions. By the process we are solving the Continuity equation and Momentum equation and Energy equation by Marker and Cell algorithm. The method is finite difference method. Here our aim is to predict the pressure distribution, temperature distribution, velocity distribution contours and Nusselt number variation with respect to different Reynolds number and different body sizes; consequently what are the effects on the cooling process. We have considered only the transient steady state condition.

1.6 Organization of the Thesis

This thesis has been organized in total five chapters. Chapter 1-2 is for foundation of the subject; chapter-3 is for mathematical formulation, while chapter-4 is for results and discussions and at last chapter-5 is for conclusion and scope for future work.

Chapter-1 contains the introduction to the subject of different types of chip cooling process at the chip level, module level and data center level. Wide varieties of methods that are used in industry are discussed here.

Chapter-2 contains literature survey, which presents a verity of research results done regarding chip cooling. This chapter is classified as numerical analysis, analytical results and experimental investigation.

Chapter-3, in this chapter mathematical formulation of the problem has been discussed. Complete Marker and cell method is discussed to discretize the governing equations. And finally the computational domain and the boundary conditions are discussed here.

Chapter-4, here the result outputs are discussed. Different contours and velocity profiles are presented in this chapter.

Chapter-5 contains the final conclusion and the scope of future work

Reader can also get the benefit of Appendices. Appendix-A shows the results of FLUENT output with the same geometry and boundary conditions that we have considered. Appendix-B consists of the code that has been developed during the process for the calculations of different parameters.

Chapter-2

Literature Review

- **Introduction**
- **Analytical Solutions**
- **Numerical Solutions**
- **Experimental Investigation**
- **Closure**

LITERATURE RIVIEW

2.1 Introduction

Components packed in a tight space constitute geometrically complex heat flow paths that pose enormous difficulty to the attempt to perform thermal analysis. In the industry today, Computational Fluid Dynamics (CFD) codes are widely used as a tool of thermal analysis. CFD solutions of high spatial and temporal resolutions can be obtained on a desktop computer or even a laptop. However, CFD-based thermal analysis is not necessarily easy to perform where the object of analysis is geometrically complex. Before embarking on CFD analysis the analyst has to devise a model, omitting some geometric features of structures and approximating complex configurations by simpler ones. This first phase of analysis is an art that often determines the accuracy of the end result no matter how rigorously the subsequent CFD analysis is performed. Although CFD code vendors are providing the tools for the user to set up pre-CFD models and generate meshes, the modeling still remains in the realm of art, increasingly difficult art with the growth of geometric complexity in the system box. Even after some simplifications, the model tends to be complex, reflecting the situation in the actual equipment. The CFD simulation on such a model involves a large number of meshes and, thus, requires a powerful computer and long computing time. Also, the analyst often has to iteratively search for a better mesh system to improve the confidence in the simulation result, and such a search is time consuming where heat transfer paths are complex. So, with the progress of compact packaging, the time and the computational resource required for CFD-based thermal analysis are increasing. On the other hand, the market force demands shorter design time to accelerate product development. It is now an industry-wide concern how to raise the productivity of thermal analysis. The cycle of product development must become ever-increasingly shorter. To meet such stringent demands, highly efficient tools are required for the design and manufacturing. To this end, a host of techniques. Design tools and software have been developed and are now indispensable tools for

meeting the marketplace demands. These also need to be continuously improved and upgraded which leads to computers of today breeding computers and other electronic devices of the next generation. It is perhaps fair to say that, the development and application of software tools in the electrical aspects of packaging has been more advanced than those dealing with cooling problems. Those programs to deal with cooling problems made relatively recent arrivals in the industry design room. With the advent of Computational Fluid Dynamics (CFD) in the recent years, flow and heat transfer computations have become quite readily possible. In particular, with the recent introduction of high power workstations and personal computers the cost of such computations has been drastically reduced and as a result many CFD codes have come into the market. More recently, such computations have become very popular in the application area of cooling of electronic components. In fact, this popularity has led to several purposes developed CFD codes coming into the market which are specifically tailored for use by heat transfer engineers in the electronic industry.

The relatively recent adoption of CFD simulation studies in electronic cooling applications has prompted some interest in validation of these codes for these types of problems. In general, validation and benchmarking of CFD codes has been an on-going research area attracting a lot of attention from both users and code developers

Many research papers were published about forced air cooling of electronics chips, some of the results will be discussed in this chapter. The literature reviewed in this chapter can be broadly classified under three categories. The first part of the survey deals with the analytical solutions for forced air convection type chip cooling, as described in Chapter 2.2. The second part of the survey deals with numerical solutions for forced convection air cooling and flow via an obstruction. The various numerical techniques used for this purpose are described, in Chapter 2.3. The third part of the survey deals with experimental investigations in various geometries or positions of chips, which is presented in Chapter 2.4.

2.2 Analytical Solutions

Culham, J. R. , Yovanovich, M. M. , Lemczyk T. F., [1],[2000], Presented an analytical approach for characterizing electronic packages, based on the steady-state solution of the Laplace equation for general rectangular geometries, where boundary conditions are uniformly specified over specific regions of the package.. The basis of the solution is a general three dimensional Fourier series solution which satisfies the conduction equation within each layer of the package. The application of boundary conditions at the fluid-solid, package board and layer-layer interfaces provides a means for obtaining a unique analytical solution for complex IC packages. They compared the values with published experimental data for both a plastic quad flat package and a multichip module to demonstrate that an analytical approach can offer an accurate and efficient solution procedure for the thermal characterization of electronic packages.

Davies, Mark R. D., Cole, Reena., Lohan, John., [2],[2000] Presented the method to correct the thermal resistance of electronics components is to adjust the junction-to-ambient thermal resistance to account for operational conditions. For forced convection applications, they proposed two factors; the first accounts for any upstream aerodynamic disturbance and the second addresses purely thermal interaction. Thus if an upstream powered component interacts with a downstream component, the two factors are combined. They found that both factors may be quantified in terms of readily measured temperatures and then used as coefficients to adjust the standard thermal resistance data for operational conditions. They applied this approach to a symmetrical array of board mounted 160-lead devices and the data shows how the factors vary with component position, non-dimensional power distribution and Reynolds number. Based on data they proposed a new method of generating operational component thermal resistances.

Chen , Han-Ting ., Horng, Jenn-Tsong ., Chen, Po-Li ., Hung, Ying-Huei.,(2004)[3], Developed an effective method for predicting and optimizing the thermal performance of heat sinks with Parallel-Plain Fin under a given design constraint of pressure drop. They developed the thermal and hydrodynamic performance analyzers for PPF heat sinks. A screening experimental design

using the Taguchi method has been performed to determine key factors that are critical to the design and screen out unimportant design factors; and a Response Surface Methodology is then applied to establish analytical models for the thermal resistance and pressure drop in terms of the key design factors with a CCD experimental design. By employing the Sequential Quadratic Programming technique, a series of constrained optimal designs can be efficiently performed. After comparing between these predicted optimal designs and those evaluated by the theoretical calculations the agreement they got was satisfactory.

Pucha, Raghuram V., Tunga,James, Krishna.,[(2004)[4], presented a field-use induced damage mapping methodology that can take into consideration the field-use thermal environment profile to develop accelerated thermal cycling guidelines for packages intended to be used in military avionics thermal environment. They considered the board-level assembly process mechanics and critical geometric features with appropriate material models while developing the methodology. The models they developed are validated against in-house and published accelerated thermal cycling experimental data. The developed mapping methodology was employed to design alternate accelerated thermal cycles by matching the creep and plastic strain contributions to total inelastic strain accumulation in solder under military field-use and accelerated thermal cycling environments, while reducing the time for accelerated thermal cycling and qualification.

Zhao, C.Y. , Lu, T.J.,(2002) [5] Presented an analytical and numerical study on the heat transfer characteristics of forced convection across a micro channel heat sink. Two analytical approaches are used by them: the porous medium model and the fin approach. In the porous medium approach, the modified Darcy equation for the fluid and the two-equation model for heat transfer between the solid and fluid phases are employed. Firstly, the effects of channel aspect ratio (as) and effective thermal conductivity ratio on the overall Nusselt number of the heat sink are studied in detail. The predictions from the two approaches both show that the overall Nusselt number (Nu) increases as α_s increased and decreases with increasing k.. The effect of porosity (e) on the thermal performance of the micro channel was also examined by them. They found

that, whereas the porous medium model predicts the existence of an optimal porosity for the micro channel heat sink, the fin approach predicts that the heat transfer capability of the heat sink increases monotonically with the porosity. They also studied the effect of turbulent heat transfer within the micro channel, and they found that turbulent heat transfer results in a decreased optimal porosity in comparison with that for the laminar flow. They proposed a new concept of micro channel cooling in combination with micro heat pipes, and the enhancement in heat transfer due to the heat pipes is estimated. Finally, they conducted two-dimensional numerical calculations for both constant heat flux and constant wall temperature conditions to check the accuracy of analytical solutions and to examine the effect of different boundary conditions on the overall heat transfer.

2.3 Numerical Solution

Mukhopadhyay, A., Biswas, G., Sundararajan, T., (1992) [6], investigated numerically the structure of confined wakes behind a square cylinder in a channel of the unsteady Navier-Stokes equations. Vortex shedding behind the cylinder induces periodicity in the flow field. They simulated the details of the phenomenon through numerical flow visualization. The unsteady periodic wake can be characterized by the Strouhal number, which varies with the Reynolds number and the blockage ratio of the channel. The periodicity of the flow is, however, damped in the downstream region of a long duct. This damping may be attributed to the influence of side walls on the flow structure.

Lee, Tien-Yu Tom., Chambers, Ben., and Mahalingam, Mali.,(1995) [7] assessed the Application of a computational fluids dynamics (CFD) tool to the thermal modeling of free convection cooled handheld/portable products and component level products. The results of two case studies were reviewed by them. The first case focuses on a sealed, system level enclosure typical of portable consumer products; while the second case looks at a component level analysis of a sealed multichip module (MCM) package possessing an internal cavity. Temperatures predicted by the simulations are compared to available experimental data as a means of assessing

the software's (FLOTHERM) ability to adequately solve the coupled fluid dynamics heat transfer problem. All simulation results were within 10 % of experimental results for these two cases, indicating that the software is readily capable of providing good thermal performance predictions.

Hung, T. C., Wangi S. K., & Peter F.(1997) [8], performed numerical simulations to investigate convective-conductive heat transfer due to a laminar boundary layer flow of air over a two dimensional array of rectangular chip blocks which represent the finite heat sources. A time-accurate numerical scheme algorithm, PISO (pressure-implicit with splitting of operators), has been used to simulate the conjugate heat transfer between the fluid and solid phases.. The results of the simulations show that the existence of the array of blocks results in stagnant flow regions between blocks in which heat convected to the ambient flow field is limited. It was found that heat transfer can be enhanced passively, especially in the areas between blocks, by opening the chip board between blocks. The enhancement of heat transfer thus occurring is presumably due to a pseudo-suction force which induces a vertical flow between blocks. The enhancement of heat transfer for the chips on-board is reflected by a global increase of the Nusselt number on the chip blocks, especially on the west sides of the chips located further downstream of the flow direction. Further investigation shows that the chip-to-chip temperature variations diminish if the openings located upstream of the front end block and downstream of the rear end block are sealed. The optimal cooling configuration for the array of chip blocks can be utilized by the electronics industry.

Masud, Nakayama, and Wan (1998) [9] tried to validate the CFD package FLUENT with the experimental data obtained by then earlier. Here they have taken a heated chip with temperature 353 K and the air inlet velocity at temperature 293 K. The inlet velocities were varied from 1 m/s to 7 m/s. Various turbulence models have been tested, and the effect of the channel inlet flow on the heat transfer rate has been determined by considering both a uniform and fully-developed condition. The substrate adiabatic heat transfer rate has been determined by considering both uniform and fully-developed condition. The substrate adiabatic heat transfer coefficient is also

numerically determined. The results indicate that the flow in the vicinity of the module is three dimensional, and exhibits flow separation and vortex formation, hence leading to a complex distribution of the local heat transfer coefficient on the substrate. In general the flow structure was in good agreement with the experiments. The predicted turbulence intensity did not agree well with the measurements. The turbulence treatment near the wall is very important and wall functions are not suitable.

Egan, Eric., Amon, Cristina. H., (2000) [10], in order to understand the thermal phenomena of embedded electronics design and to explore the thermal design space, analyzed the finite element numerical simulations, physical experimentation, and analytical models. Numerical models ascertain the effect of heat spreaders and polymer composite substrates on the thermal performance, while physical experimentation of an embedded electronic artifact ensures the accuracy of the numerical simulations and the practicality of the thermal design. Analytical models using thermal resistance networks predict the heat flow paths within the embedded electronic artifact as well as the role of conductive fillers used in polymer composites. The results show that the exposed surface area of the heat spreader and the conductivity of the substrate are the most important parameters affecting the thermal performance of the embedded electronic artifact.

Gauch, Paul., and Xu, Weiran.,(2000) [11], Presented an method for modeling phase change using the conventional material properties' and a transient analysis for system level thermal models'. This' provides a reliable thermal analysis using an existing Computational Fluid Dynamics (CFD) tool. They considered a case study in which a system level CFD model of an electronic enclosure is' modeled without PCM and with PCM retro-fitted in three configurations. The proposed method greatly simplifies the analysis without compromising the thermal integrity of the model and solutions can be obtained quickly.

Chang, J. Y. , Yu, C. W., Webb, R. L.,(2001)[12], Conducted CFD analysis of a 30-W socketed CPU of a desktop computer with minimum air flow rate and minimum heat sink size. They

achieved this using only the fan in the power supply for all air movement in the chassis. A duct was employed to direct the air flow over the CPU and then to the inlet air vents of the power supply. They allowed the use of this duct more than 10°C reduction of the CPU case temperature, relative to an unducted design. The CFD analysis results were confirmed by experiment, and the predicted CPU case temperatures agreed within 62.9°C of the experimental values for the ducted cases. Here they have described the methodology of CFD analysis for the heat sink/duct design, and described experimental procedures to validate the predictions.

Rodgers, Peter J., Eveloy, Valerie C., Davies, Mark R. D.,(2003) [13], Assessed the numerical predictive accuracy for component-printed circuit board (PCB) heat transfer in forced convection using a widely used computational fluid dynamics (CFD) software, as component junction temperature prediction accuracy for the populated board case is typically within 65°C or 610%, which would not be sufficient for temperature predictions to be used as boundary conditions for subsequent reliability and electrical performance analyses. Neither the laminar nor turbulent flow model resolves the complete flow field, suggesting the need for a turbulence model capable of modeling transition. They show that the full complexity of component thermal interaction is not to be fully captured.

Leon1, Octavio., Mey, Gilbert De., Jan Vierendeels, Erik Dick.,(2003)[14], compared, the performance of an array of staggered and non-staggered cooling fins is looking not only into the traditional objective of maximum heat transfer flux, but also to obtain it with the minimum flow resistance. They studied three different models to obtain the ratio between the heat removed and the energy spent for the coolant flow going through the cooling fins. The study is done numerically using the computational fluid dynamic software FLUENT. The results show the advantages of the staggered model compared to the standard model since for a given incoming velocity, the use of a staggered heat sink always leads to a maximization of the heat transfer flux. The significant positive difference in the thermal performance of the staggered model permits the reduction of the incoming velocity with the consequent reduction in the pressure drop, and power consumption.

Kitamura, Yoji., Ishizuka, Masaru., (2004) [15] emphasized on heat transfer by natural convection. They observed that one of the methods of promoting the capacity of natural air cooling is to incline the electronics casing, thereby, induce draft air by what is called the chimney effect. However, the effect of inclination on thermal behavior and cooling capacity has not yet been fully understood due to the involvement of many parameters in driving the draft air. They presented the results of experimental and numerical studies on the effect of casing inclination on the temperature rise across the casing. They implemented the numerical simulation to find out the thermal behavior inside a thin electronic casing. The simulation results are in good agreement with the experiment data. They obtained a thermal design guide regarding how the cooling effect is improved by increasing the inclination angle.

Nakayama, Matsuki, Hacho, and Yajima, (2004) [16] conducted CFD simulations on a set of hardware models to gain insight into the effects of component placement on the junction temperature. They introduced two algorithms before and after CFD simulations. They found that the CFD code allows one to find detailed temperature and air-flow distributions inside the system box of electronic equipment. A substantial part of the knowledge produced by CFD simulations is unobtainable by experimental measurements, and detailed three-dimensional pictures of the temperature field on the computer display or in print are reassuring to the packaging designer. As a tool to navigate through various design options, the CFD code is inefficient. The method was applied to the thermal analysis of a simplified hardware model (benchmark model) having a simulated package (Heater), a printed cardboard (PCB), dummy blocks, and three small fans in a flat system box. From singular value decomposition of a starter placement pattern of the components the geometric parameters and their levels were defined. Then, eight patterns of components placement were created in correspondence with the two-level factorial table of the Taguchi method. CFD simulations were performed on these patterns, and the thermal resistance solutions were subjected to a test to measure contributions from the geometric parameters. An important identified parameter includes the location of the Heater/PCB assembly, in agreement with physical interpretations. This technique will help to deal with more geometrically complex systems of actual electronic equipment.

Bhopte, Siddharth.,. Alshuqairi, Musa S., Agonafer, Dereje., Ahmed, Gamal., Refai., (2004) [17], Investigated numerically the effect of an impinging mixed convection air jet on the heat transfer rate of a parallel flat plate heat sink. A three dimensional numerical model was developed by them to evaluate the effects of the nozzle diameter d, nozzle-to-target vertical placement H/d, Rayleigh number, and the jet Reynolds number on the heat transfer rates from a discrete heat source. They performed the simulations for a Prandtl number of 0.7 and for Reynolds numbers ranging from 100 to 5000. The governing equations were solved in the dimensionless form using a commercial finite volume package. They have obtained the average Nusselt numbers, at H/d 53 and two jet diameters, for the bare heat source, for the heat source with a base heat sink, and for the heat source with the finned heat sink. The heat transfer rates from the bare heat source surface have been compared with the ones obtained with the heat sink in order to determine the overall performance of the heat sink in an impingement configuration.

Jin , L.F. , Tou , K.W. , Tso , C.P.,(2004)[18], studied a two-dimensional unsteady numerical on an air-filled enclosure rotated about its horizontal axis with an array of three rows of heat sources on one of the walls, revealing three physically realizable phenomena, namely, uniperiodic oscillation, multi-periodic oscillation and chaotic oscillation. They studied the evolutionary process of flow field and natural convection characteristics from stationary to rotating situation are studied. The results they found that in an imbalance between clockwise and counter-clockwise circulations, increases heat transfer in the worst scenario, reduces the oscillation of Nusselt number, and improves or reduces mean performance in each cycle. The optimal distribution of heaters in rotating fluid is close to the results in the stationary situation if they have same dominated circulation direction.

Roy, A., Bandyopadhyay, G. (2004) [19], conducted a similar type investigation by developing a fully explicit two-dimensional incompressible laminar Navier-Stokes solver in primitive variable formulation using a Cartesian staggered grid. The governing flow equations have been solved on the physical plane using a finite volume discretisation scheme. They discretized the convective terms of the solver using the weighted second upwind SOLA scheme. The pressure is solved by

using the SOLA pressure correction algorithm. The diffusive terms of the momentum equations are discretised by using central differencing scheme. In their investigation, flow past a square cylinder placed inside a channel with two different blockage ratios, namely, 0.125 and 0.250 have been computed at four different Reynolds numbers, namely, 150, 300, 750 and 1500. The average drag coefficient increases with an increase in blockage ratio for a given Reynolds number. The vortex shedding frequency also increases with increase in blockage ratio. Recirculation zones are formed on the channel wall surfaces for Reynolds numbers 750 and 1500, respectively. Recirculating zones on the walls are affected by the vortex shedding process. Their structure and location get modified from time to time. Streamlines, vorticity contours and pressure contours are provided to analyze the important characteristics of the flow field. The results compare well with those available from literature.

Srikanth, J., and.Tulapurkara, E.G., Biswas. G.,(2005)[20], Investigated the complex flow past a delta winglet-pair placed in a rectangular channel and studied numerically using the Large eddy Simulation (LES) approach. They used the Reynolds number based on the channel height and inlet velocity 10000, and a grid of 165*45*95. The code was based on Marker and Cell algorithm with third order upwind scheme for the convective term. They compared the computed results with experimental data at Reynolds number of 134000. Computation show that the longitudinal velocities generated by the winglet–pair disrupt the growth of boundary layer and would serve ultimately to bring about enhancement of heat transfer between the fluid and neighboring surface.

Dhiman, A.K., , Chhabra, R.P., Eswaran, V.,(2005)[21], Investigated the flow and heat transfer characteristics of an isolated square cylinder in crossflow placed symmetrically in a planar slit for a range of conditions. They obtained the heat transfer correlations in the steady flow regime for the constant temperature and constant heat flux boundary conditions on the solid square cylinder in crossflow. In addition, variation of the local Nusselt number on each face of the obstacle and representative isotherm plots are presented to elucidate the role of Prandtl number and blockage ratio on drag coefficient and heat transfer.

Kumara, K. S., Tulapurkaraa, E.G., Biswasb, G., Gowdac, B.H.L., (2005)[22] investigated the complex unsteady flow through and around a channel in the presence of an obstruction at the entry is studied by solving directly the unsteady Navier–Stokes equations. They considered the Reynolds number of 4000, as experimental results are available for comparison. The computed results are in close agreement with experiments. The computations help with better understanding of the phenomenon of reverse flow and fluid pumping.

Cheng.Y.P, Lee.T.S & Low.H.T, (2006) [23], numerically investigated the fluid flow and heat transfer characteristics of mixed convection in three-dimensional rectangular channel with four heat sources. The SIMPLEC algorithm was applied to deal with the coupling between pressure and velocity, and new high-order stability guaranteed second-order difference (SGSD) scheme was adopted to discretize the convection term. They studied the influence of four parameters: Richardson number, heat source distribution, channel height and inclination angle. They analyzed the numerical results from the viewpoint of the field synergy principle, which says that the enhanced convective heat transfer is related not only to the velocity field and temperature field, but also to the synergy between them. They found that the effects of the four parameters on the thermal performance can all be explained with the field synergy principle. To obtain better electronic cooling, the synergy between the velocity and temperature gradient should be increased when other conditions are unchanged.

2.4 Experimental Investigation

In the latter part of the 1980s, ETA Systems Inc. developed a commercial supercomputer system using CMOS logic chips operating in liquid nitrogen [24]. The processor modules were immersed in a pool of liquid nitrogen maintained in a vacuum-jacketed cryostat vessel within the CPU cabinet. Processor circuits were maintained below 90 K. At this temperature, circuit speed was reported to be almost double that obtained at above ambient temperatures. Heat transfer experiments were conducted to validate peak nucleate boiling heat flux limits of approximately 12 W/cm. A closed-loop Stirling refrigeration system (cryogenerator) was developed to recondense the gaseous nitrogen produced by the boiling process. In 1991, IBM initiated an effort to demonstrate the feasibility of packaging and cooling a CMOS processor in a form

suitable for product use [25]. In 1999, Fujitsu released its Global Server GS8900 that utilized a refrigeration unit to chill a secondary coolant and then supply the coolant to liquid-cooled Central Processor Unit (CPU) MCMs [26]

DeVoe, Jason., Ortega, Alfonso., (2000) [27] performed a systematic study of the influence of board conduction on the predictive accuracy of Compact Thermal Models of BGA and CPGA package styles. Various resistance network topologies were assessed by them for each package style. They created the detailed (FE) isotropic board models with conductivities spanning three orders of magnitude to test the influence of board conductivity on CTM accuracy. They compared the results to equivalent fully-detailed (FE) package models on detailed board models. The predictive capability of the optimized topologies was strongly correlated to the existence of strong local temperature gradients in the board, whenever the sensitivity to board heat conduction was high. When the board is poorly conducting (k=l W/m-K), board heat conduction is too low to matter. When the board is highly conducting (k= lOO W/m-K), the high conductivity smoothes out local board temperature gradients, and the CTMs are accurate even though the board heat flow path is dominant. In general, they found that optimized network topologies that included shunt resistances to predict the junction temperature to within 5% to 8% over a wide range of board conductivities, while star-shaped networks were generally only accurate to 10-15 %.

Wong, Henry., Peck, Robert E., (2001)[28], evaluated experimentally The effect of altitude on electronic cooling . As material properties of air vary as a function of altitude due to changes in atmospheric pressure and temperature. These changes have a negative impact on the heat transfer effectiveness and result in higher component temperature when compared to sea level conditions. They carried out the experiments in a hypobaric chamber using electronic printed circuit boards populated with heated rectangular blocks placed in a small wind tunnel. The altitude was varied between 0 and 5000 m above sea level and the air speed is varied between 1 and 5 m/s. The results show the local adiabatic heat transfer coefficient and thermal wake function diminish with altitude. This information is useful for design and analysis of electronic equipment for operation

over a range of altitudes and air speeds typically encountered in forced air convection cooling applications.

Haider, S. I.,. Joshi, Yogendra, K ., Nakayama, Wataru.,(2002) [29], studied a model for the two-phase flow and heat transfer in the closed loop, two-phase thermosyphon (CLTPT) involving co-current natural circulation. The focus was on CLTPTs for electronics cooling that exhibit complex two-phase flow patterns due to the closed loop geometry and small tube size. They used homogeneous two-phase flow model to evaluate the friction pressure drop of the two-phase flow imposed by the available gravitational head through the loop. They used the boiling characteristics of the enhanced structure to predict the chip temperature. The comparison with experimental data for dielectric working fluid PF-5060 and was in general agreement with the observed trends.

Lorenzini, Giulio., Biserni, Cesare.,(2003)[30] Investigated by experimental means a possible use of the Vapotron Effect for the cooling of electronic devices. The problem deals with a particular kind of sub cooled boiling which is able to enhance heat exchange between a non isothermal finned surface, simulating the packaging of an electronic component, and a refrigerant fluid (water in the case here presented) flowing on it. The experimental tests have shown the existence of a relation that couples temperature trend of water in the cavities between the fins and cycle of events characterizing the phenomenon. These results will be helpful to apply in the future to the study of more dynamic phenomena.

Yoo, Seong-Yeon., Park, Jong-Hark., Chung, Min-Ho., (2003) [31] Investigated how the flow via an obstruction in forced convection influence the local heat transfer from electronic modules. They have conducted experiments on a three-dimensional array of hexahedral elements as well as on a two-dimensional array of rectangular elements. Naphthalene sublimation technique was employed to measure three-dimensional local mass transfer, and the mass transfer data are converted to their counterparts of the heat transfer process using the analogy equation between heat and mass transfer. Module location and stream wise module spacing were varied, and the

effect of vortex generators on heat transfer enhancement was also examined. The results show dramatic change of local heat transfer coefficients on each surface of the module, and three-dimensional modules have a little higher heat transfer value than two-dimensional modules because of bypass flow. Longitudinal vortices formed by vortex generator enhance the mixing of fluids and thereby heat transfer, and the rectangular wing type vortex generator is found to be more effective than the delta wing type vortex generator.

Grimes, Ronan., Davies, Mark.(2004) [32], measured the surface temperature and air velocity for the case of a printed circuit board with heated metal elements in a fan induced flow. They measured the surface temperature using infra red thermography, while air flow measurements were performed using Particle Image Velocimetry (PIV). They found that, the flow was parallel and uniform. There were symmetrical temperature gradients across the board that was readily explained in terms of board conduction and boundary layer growth. In the second part of the paper, deals with the board mounted in the fan exit flow. The flow here is unsteady and swirling, giving rise to significantly higher Nusselt numbers over the whole of the board. The implications for increased system reliability, due to both the measured low component temperatures and the lower operational temperature of the fan are significant.

Gima, Satoru., Nagata, Takashi., Zhang, Xing., and Fujii, Motoo., (2005) [33], Carried out experiments on an indirect cooling method of high-power CPU of notebook computers using a closed-loop two-phase thermosyphon with Fluorinert (FC-72) as the working fluid. The experimental setup consists of an evaporator with an electric heater, a condenser, and flexible tube connecting them. The heater and condenser act as a high-power CPU and a cooling plate located behind the display of a notebook computer, respectively. The evaporator and the condenser have the outer dimensions of 50 mm × 50 mm × 20 mm and 150 mm × 200 mm × 20 mm, respectively. They examined four possible boiling surfaces of an evaporator, i.e., a smooth surface (Type A), rough one, ones with smooth plate fins and rough plate fins (Type D). The results show that type D evaporator shows the highest performance, i.e., it reduces the temperature at the evaporator/heater interface by about 18% in comparison with that of the

smooth surface evaporator (Type A). Type D evaporator keeps the temperature difference between the evaporator/heater interface and the ambient to be around 55 K at the highest heat input Q = 30 W. They examined experimentally the effects of the heat input Q, the volumetric amount of Fluorinert liquid F in the thermosyphon, and the evaporator type on the heat transfer characteristics of the cooling system.

Simionescu, F., Meir, A. J., and Harris, D. K., (2006) [34], studied a heat source (electronic chip) placed on the top surface of a flat thermal spreader which is cooled by convection on the opposite surface. They found an optimal convection heat transfer coefficient yielding maximal heat removal from the chip an optimal control technique. They control the solution of the heat equation with the convective boundary condition, taking the heat transfer coefficient as the control. They used a conjugate gradient method to solve the optimal control problem. The results show that the temperature distributions corresponding to the controlled solution are lower and display a flatter profile than those corresponding to the uncontrolled solution.

Rhee, Jinny., Moffat, Robert J.,(2006)[35] Estimated experimentally the continuous, one-dimensional kernel function in a rectangular duct subject to forced convection with air using liquid crystal thermography techniques. They manipulated the Analytical relationships between the kernel function for internal flow and the temperature distribution resulting from a known heat flux distribution to accomplish this objective. They proposed a model for the kernel function in the hydrodynamic entry region of the rectangular duct, and used in its experimental determination. The kernel functions obtained by the work were shown to be capable of predicting the highly non uniform surface temperature rise above the inlet temperature resulting from an arbitrary heat flux distribution to within the experimental uncertainty. This is better than the prediction obtained using the analytically derived kernel function for turbulent flow between parallel plates, and the prediction obtained using the conventional heat transfer coefficient for constant heat flux boundary conditions. The latter prediction fails to capture both the quantitative and qualitative nature of the problem. The results of their work are relevant to applications

involving the thermal management of non uniform temperature surfaces subject to internal convection with air, such as board level electronics cooling.

Tae Ho Ji a, Seo Young Kim b, and Jae Min Hyuna, (2006)[36], Performed experiments to investigate heat dissipation from a heated square cylinder in a channel by oscillating flow. During the experiments, the input power and oscillating amplitude (A) were fixed. The effects of the Reynolds number based on the mean flow velocity and the oscillating frequency on the heat transfer enhancement are examined. They determined the time averaged Nusselt number and the Strouhal number for each oscillating condition. The measured Strouhal numbers according to the Reynolds number are compared with the previous results and good agreement is found. The occurrence of the "lock-on" phenomenon is demonstrated for a square cylinder. When the pulsating frequency is in the lock-on regime, the heat transfer from a square cylinder is dramatically enhanced. They found that the heat transfer enhancement is pronounced as the Reynolds number increases.

2.5 Closure

Many research papers were published regarding electronics chip cooling. Some of them investigated analytically, some are numerically and rest experimentally predicted. Mostly analytical solutions are newly developed techniques which needs validations. Numerical solutions are, solving the governing equations by different techniques, or using the commercially available codes. But validating the codes is also an ongoing process, which is still going on. And finally the experimental investigation results are practically needed results. So the experimental results are also required to validate the CFD codes and analytical results. In this study we will solve the governing equations by MAC method and analyze the results obtained.

Chapter-3

Mathematical Formulation

- **Introduction**
- **Governing Equations**
- **Staggered Grid**
- **Solution of the Navier-Stokes Equation**
- **Solution of the Energy Equation**
- **Computational Domain and Boundary Conditions**
- **Closure**

MATHEMATICAL FORMULATION

3.1 Introduction

In this chapter the governing equations are solved by Marker and Cell method. Here no assumption is made about the relative magnitude of the velocity components; consequently the full Navier-Stokes equations are solved. The method is based on the finite difference discretizations and on the solution of a Poisson equation to determine the pressure distribution. These methods use primitive variables *u, v, w* and *p* as function of *x, y, z, t* and Reynolds number Re.

In the primitive variable approach, it is implicitly assumed that the x- component momentum equation determines the x-component velocity, and so on, while the mass balance equation solves for pressure. The fact that pressure does not appear in the mass balance equation at all is solved by the algorithm, which is presented here. Attention is also given to the nonlinearity of the of the Navier-Stokes equations. After solving it finally energy equation is solved and the algorithms are written to solve the governing equations. At the end of this chapter my computational geometry is presented with single obstruction, which varies in dimension.

3.2 Governing Equations

For flow of the fluid the governing equations are the Continuity equation and the Momentum (Navier-Stoke) equation. The Navier- Stokes Equations in original form is as follows

3.2.1 Expanded forms of Navier-stokes Equation

Let (X, Y, Z) be the orthogonal components of the body force field in the Cartesian coordinate system; then

$$\text{x:} \quad \rho\left(\frac{\partial u^*}{\partial t^*}+\frac{\partial\left(u^{*2}\right)}{\partial x^*}+\frac{\partial\left(u^* v^*\right)}{\partial y^*}+\frac{\partial\left(u^* w^*\right)}{\partial z^*}\right)=\mathrm{X}-\frac{\partial p^*}{\partial x^*}+\mu\left[\frac{\partial^2 u^*}{\partial x^{*2}}+\frac{\partial^2 u^*}{\partial y^{*2}}+\frac{\partial^2 u^*}{\partial z^{*2}}\right]$$

$$\text{y:} \quad \rho\left(\frac{\partial v^*}{\partial t^*}+\frac{\partial\left(u^* v^*\right)}{\partial x^*}+\frac{\partial\left(v^{*2}\right)}{\partial y^*}+\frac{\partial\left(u^* w^*\right)}{\partial z^*}\right)=\mathrm{Y}-\frac{\partial p^*}{\partial y^*}+\mu\left[\frac{\partial^2 v^*}{\partial x^{*2}}+\frac{\partial^2 v^*}{\partial y^{*2}}+\frac{\partial^2 v^*}{\partial z^{*2}}\right]$$

$$\text{z:} \quad \rho\left(\frac{\partial w^*}{\partial t^*}+\frac{\partial\left(u^* w^*\right)}{\partial x^*}+\frac{\partial\left(v^* w^*\right)}{\partial y^*}+\frac{\partial\left(w^{*2}\right)}{\partial z^*}\right)=Z-\frac{\partial p^*}{\partial z^*}+\mu\left[\frac{\partial^2 w^*}{\partial x^{*2}}+\frac{\partial^2 w^*}{\partial y^{*2}}+\frac{\partial^2 w^*}{\partial z^{*2}}\right]$$

(3.1)

3.2.2 Non-Dimensionalization

In order to obtain a solution for the general applicability, the governing equations are non-dimensionalized with following variables

$$u=\frac{u^*}{U_\infty}, \quad v=\frac{v^*}{U_\infty}, \quad w=\frac{w^*}{U_\infty}, \quad p=\frac{p^*}{\rho U_\infty^2} \quad t=\frac{t^*}{L/U_\infty}$$

$$x=\frac{x^*}{L}, \quad y=\frac{y^*}{L}, \quad z=\frac{z^*}{L}, \quad \text{and} \quad \theta=\frac{T-T_\infty}{T_w-T_\infty} \quad \text{(for Energy equation)} \quad (3.2)$$

In Cartesian coordinates, the governing equations for unsteady incompressible three-dimensional laminar viscous flow, neglecting body forces are as follows

$$\frac{\partial u}{\partial x}+\frac{\partial v}{\partial y}+\frac{\partial w}{\partial z}=0 \quad (3.3)$$

$$\frac{\partial u}{\partial t}+\frac{\partial (u^2)}{\partial x}+\frac{\partial (uv)}{\partial y}+\frac{\partial (uw)}{\partial z}=-\frac{\partial p}{\partial x}+\frac{1}{\mathrm{Re}}\left[\frac{\partial^2 u}{\partial x^2}+\frac{\partial^2 u}{\partial y^2}+\frac{\partial^2 u}{\partial z^2}\right] \quad (3.4)$$

$$\frac{\partial v}{\partial t}+\frac{\partial (uv)}{\partial x}+\frac{\partial (v^2)}{\partial y}+\frac{\partial (vw)}{\partial z}=-\frac{\partial p}{\partial y}+\frac{1}{\mathrm{Re}}\left[\frac{\partial^2 v}{\partial x^2}+\frac{\partial^2 v}{\partial y^2}+\frac{\partial^2 v}{\partial z^2}\right] \tag{3.5}$$

$$\frac{\partial w}{\partial t}+\frac{\partial (uw)}{\partial x}+\frac{\partial (vw)}{\partial y}+\frac{\partial (w^2)}{\partial z}=-\frac{\partial p}{\partial z}+\frac{1}{\mathrm{Re}}\left[\frac{\partial^2 w}{\partial x^2}+\frac{\partial^2 w}{\partial y^2}+\frac{\partial^2 w}{\partial z^2}\right] \tag{3.6}$$

3. 3 Staggered grid

The major difficult encountered during solution of incompressible flow is the non-availability of any obvious equation for pressure. This difficulty can be resolved in the stream function–vorticity approach. But this approach loses its advantages when 3-D flow is computed because of the fact that a single scalar stream function does not exist in 3-D space. A 3-D problem demands a primitive variable approach. As a remedy it has been suggested to employ a different grid for each-dependent variables. Such a staggered grid for the dependent variables in a flow field was first used by Harlow and Welch (1965) [37] in their method MAC (Marker and Cell) method.

3.4 Solution of the Unsteady Navier-Stokes Equations

3.4.1 Introduction to the Marker and Cell (MAC) Method

This method necessarily deals with a poisons equation for the pressure and momentum equations for the computation of velocity. It was basically developed to solve problems with free surfaces, but can be applied to any compressible fluid flow problems. The method has been developed for use on a high speed electronic computer and would be impractical for hand solution purposes.

The solution technique makes use of finite difference approximations applied to the full Navier-Stokes equations. The primary dependent variables are the pressure and the two

components of velocity. Neither the vorticity nor the stream function enters explicitly into the analysis. The finite differences apply to both space and time variations. For the former the region is divided into numerous small rectangular zones or cells, and the field variables in each are characterized by single average values. For the time variations the changes are represented by a succession of field variable values separated by small increments of time. If both the finite space and time differences are small enough, the results will be sufficiently close to continuous, while large differences may destroy essential resolution.

For the case of free surface flows, it has been found in the marker and cell method that the primary physical variables, velocity and pressure, have several advantages over the stream function and vorticity. The free surface boundary condition of vanishing stress or of prescribed normal stress becomes more natural to apply.

3.4.2 Outline of Procedure:

The detailed derivation of the finite difference equations is based upon the following sequence of events by which the configuration is advanced from one time step to the next.

1. The complete field of velocities is known at the beginning of the cycle, either as a result of the previous cycle of calculation or from the prescribed initial conditions. It is assumed that this velocity field is conservative, i.e., that the finite difference analogy of velocity divergence vanishes everywhere. In addition, the coordinates of a set of marker particles are assumed to be known; these show which region is occupied by fluid and which is empty.

2. The corresponding field of pressures is calculated in such a way as to assure that the rate of change of velocity divergence also vanishes everywhere. This requires the solution of a Poisson's equation, which may be accomplished by a relaxation technique or any other suitable procedure.

3. The two components of acceleration are calculated; the products of these with the time increment per cycle then give the changes in velocity to be added to the old values.

4. The marker particles are moved according to the velocity components in their vicinities.

5. Adjustments are made for the passage of marker particles across cell boundaries. Whenever the result puts fluid into a previously empty cell or empties one which previously contained fluid, certain necessary velocity modifications are performed.

   This, then, completes the advancement of configuration to the end of the new cycle.

3.4.3 The algorithm of MAC method

The important ideas on which the MAC algorithm is based are

1. Unsteady Navier-Stokes equations for incompressible flow in weak conservative form and the Continuity equation are the governing equations.

2. Description of the problem is elliptic in space and parabolic in time. Solution will be marched in the time direction. At each time step, a converged solution in space domain is obtained but this converged solution at any time step may not be the solution of the physical problem.

3. If the problem is Steady, in its physical sense, then after a finite Number of steps in time direction, two consecutive time-steps will show identical solutions. However, in a machine-computation this is not possible. Hence a very small value, say 'STAT' is predefined. Typically STAT may be chosen between 10^{-3} and 10^{-5}.If the maximum discrepancy of any of the velocity components for two consecutive time steps at any location over the entire space does not exceed STAT then it can be said that the steady solution has been evolved.

4. If the physical problem is basically unsteady in nature, the aforesaid Maximum discrepancy of any dependent variable for two consecutive time steps will never be less than STAT. However for such a situation a velocity component can be stored over a long

duration of time and plot of the velocity component against time depicts the character of flow. Such a flow may be labeled as simply unsteady.

5. With the help of momentum equations, we compute explicitly a provisional value of the velocity components for the next time step.

6. Considering the weak conservative form of non-dimensional momentum equation in the X-direction:

$$\frac{\partial u}{\partial t}+\frac{\partial (u^2)}{\partial x}+\frac{\partial (uv)}{\partial y}+\frac{\partial (uw)}{\partial z}=-\frac{\partial p}{\partial x}+\frac{1}{\mathrm{Re}}\left[\nabla^2 u\right]$$

It is assumed that at t = nth level, we have a converged solution. Then for the next Time step.

$$\frac{\tilde{u}_{i,j,k}^{n+1}-u_{i,j,k}^{n}}{\Delta t}=\left[SDISCU\right]_{i,j,k}^{n}$$

Or

$$\tilde{u}_{i,j,k}^{n+1}=u_{i,j,k}^{n}+\Delta t\left[SDISCU\right]_{i,j,k}^{n} \qquad (3.7)$$

Where

SDISCU = Spatial discretization of the convective and diffusive terms of the x- Momentum equations and the pressure gradient.

Similarly, the provisional values for $\tilde{v}_{i,j,k}^{n+1}$ and $\tilde{w}_{i,j,k}^{n+1}$ can be explicitly computed.

These explicitly advanced velocity components may not constitute a realistic flow field. A divergence free velocity field has to exist in order to describe a plausible incompressible flow situation Now with these provisional $\tilde{u}_{i,j,k}^{n+1}$, $\tilde{v}_{i,j,k}^{n+1}$, $\tilde{w}_{i,j,k}^{n+1}$ values, the continuity equation is evaluated in each cell, If the calculation of $\nabla.u$ produces a non-zero value, there must be some amount of mass

accumulation or annihilation in each cell which is not physically possible, leading to an incorrect pressure field Therefore, pressure at any cell is directly linked with the value of $\nabla.u$ at that cell. Now on one hand the pressure has to be corrected with the help of non - zero divergence value and on the other hand, the velocity components have to be adjusted. The correction procedure continues through an iterative cycle till the divergence free velocity is ensured.

6. Boundary conditions are to be applied after each explicit evaluation for the time step is accomplished. Since the governing equations are elliptic in space, boundary Conditions on all confining surfaces are required. Moreover, the boundary Conditions are also to be applied after every pressure- velocity iteration.

The 5 principal kinds of boundary conditions to be considered are

- Rigid no slip walls,
- Free-slip walls,
- Inflow and outflow boundaries and
- Periodic (repeating) boundaries.

3.4.4 MAC – Formulation

1. The region in which computations are to be performed is divided into a set of small cells having edge lengths $\delta x, \delta y, \delta z$.

2. With respect to this set of computational cells, velocity components are located at the centre of the cell faces to which they are normal and pressure and temperature are defined at the centre of the cells.

3. Cells are labeled with an index (i, j, k) which denotes the cell number as counted from the origin in the x, y, and z directions. Also p_{ijk} is the pressure at the centre of the cell (i,j,k),

while u_{ijk} is the x-direction velocity at the centre of the face between cells (i,j,k) and (i+1,j,k) and so on.

4. Because of staggered grid arrangements, the velocities are not defined at the nodal points, but when ever required, they are to be found by interpolation.

   Ex:-

   With uniform grids, we can write

$$u_{i-\frac{1}{2},j,k} = \frac{1}{2}\left[u_{i-1,j,k} + u_{i,j,k}\right]$$

   Where a product or square of such quantity appears, it is to be averaged first and Then the product to be formed.

5. **Convective terms** are discritized using a weighted average of second upwind and space centered scheme.

6. **Diffusive terms** are discretized by a central difference scheme.

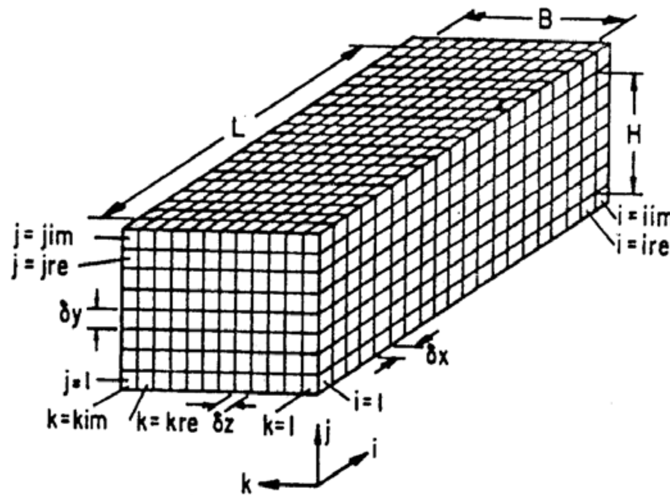

[Fig. 3.1] Discretization of a Three-Dimensional Domain

$$\frac{\partial(u^2)}{\partial x} = \frac{1}{4\delta x}[(u_{i,j,k} + u_{i+1,j,k})(u_{i,j,k} + u_{i+1,j,k}) + \alpha\left|(u_{i,j,k} + u_{i+1,j,k})\right|(u_{i,j,k} - u_{i+1,j,k})$$

$$-(u_{i-1,j,k}+u_{i,j,k})(u_{i-1,j,k}+u_{i,j,k})-\alpha\left|(u_{i-1,j,k}+u_{i,j,k})\right|(u_{i-1,j,k}-u_{i,j,k})]$$

$$=DUUDX$$

$$\frac{\partial(uv)}{\partial y}=\frac{1}{4\delta y}[(v_{i,j,k}+v_{i+1,j,k})(u_{i,j,k}+u_{i,j+1,k})+\alpha\left|(v_{i,j,k}+v_{i+1,j,k})\right|(u_{i,j,k}-u_{i,j+1,k})$$

$$-(v_{i,j-1,k}+v_{i+1,j,k})(u_{i,j-1,k}+u_{i,j,k})-\alpha\left|(v_{i,j-1,k}+v_{i+1,j-1,k})\right|(u_{i,j-1,k}-u_{i,j,k})]$$

$$=DUVDY$$

$$\frac{\partial(uw)}{\partial z}=\frac{1}{4\delta z}[(w_{i,j,k}+w_{i+1,j,k})(u_{i,j,k}+u_{i,j,k+1})+\alpha\left|(w_{i,j,k}+w_{i+1,j,k})\right|(u_{i,j,k}-u_{i,j,k+1})$$

$$-(w_{i,j,k-1}+w_{i+1,j,k})(u_{i,j,k-1}+u_{i,j,k})-\alpha\left|(w_{i,j,k-1}+v_{i+1,j,k-1})\right|(u_{i,j,k-1}-u_{i,j,k})]$$

$$=DUWDZ$$

$$\frac{\partial p}{\partial x}=\frac{p_{i+1,j,k}-p_{i,j,k}}{\delta x}=DPDX$$

$$\frac{\partial^2 u}{\partial x^2}=\frac{u_{i+1,j,k}-2u_{i,j,k}+u_{i-1,j,k}}{(\delta x)^2}=D2UDX2$$

$$\frac{\partial^2 u}{\partial y^2}=\frac{u_{i,j+1,k}-2u_{i,j,k}+u_{i,j-1,k}}{(\delta y)^2}=D2UDY2$$

$$\frac{\partial^2 u}{\partial z^2}=\frac{u_{i,j,k+1}-2u_{i,j,k}+u_{i,j,k-1}}{(\delta z)^2}=D2UDZ2$$

With $\alpha=1$, scheme is second upwind.

$\alpha=0$, Scheme is space centered

Factor α is chosen in such a way that the differencing scheme retains something of second order accuracy and the required unwinding is done for the sake of stability. A typical value of α is between 0.2 and 0.3. As mentioned earlier, the quantity $\tilde{u}^{n+1}_{i,j,k}$ is now evaluated explicitly from the discretized form of u-component equation as

$$\tilde{u}^{n+1}_{i,j,k} = u^{n}_{i,j,k} + \delta t\left[SDISCU\right]^{n}_{i,j,k}$$

Where

$$\left[SDISCU\right]^{n}_{i,j,k} = \begin{bmatrix} (-DUUDX - DUVDY - DUWDZ) - DPDX + \\ (1/\mathrm{Re})(D2UDX2 + D2UDY2 + D2UDY2 + D2UDZ2) \end{bmatrix}$$

Similarly

$$\tilde{v}^{n+1}_{i,j,k} = v^{n}_{i,j,k} + \delta t\left[SDISCV\right]^{n}_{i,j,k}, \qquad (3.8)$$

$$\tilde{w}^{n+1}_{i,j,k} = w^{n}_{i,j,k} + \delta t\left[SDISCW\right]^{n}_{i,j,k} \qquad (3.9)$$

As discussed earlier, the explicitly advanced tilde velocities may not necessarily lead to a flow field with zero mass divergence in each cell. At this stage the pressure distribution is not correct pressure in each cell will be corrected in such a way that there is no net mass flow in or out of the cell. In the original MAC [37] method the corrected pressures were obtained from the solution of a poisson equation for pressure. A related technique developed by chorine (1967) [38] involved a simultaneous iteration on pressures and velocity components. Viecelli (1971) [40] showed that the two methods as applied to MAC are equivalent. We shall make use of the iterative correction procedure of chorin (1967) [38] in order to obtain a divergence-free velocity field.

3.4.5 Pressure-Velocity Correction

3.4.5.1 The Philosophy of the Pressure correction method

The pressure correction technique is basically an iterative approach, where some innovative physical reasoning is used to construct the next iteration from the results of the previous iteration. The thought process is as follows:-

1. Start the iterative process by guessing the pressure field. Denote the guessed pressure by p^n.
2. Use the values of p^n to solve for *u, v,* and *w* from the momentum equations. Since these velocities are associated with the values of p^n, denote them by u^n, v^n, and w^n.

3. Since they were obtained from guessed values of p^n, the values u^n, v^n, and w^n, when substituted into the continuity equation, will not necessarily satisfy that equation. Hence, using the continuity equation, construct a pressure correction p', which when added to p^n will bring the velocity field more into agreement with the continuity equation. That is the corrected pressure p^{n+1} is

$$p^{n+1} = p^n + p' \tag{3.10}$$

4. corresponding velocity corrections u', v', w' can be obtained from P' such that

$$u^{n+1} = u^n + u'$$
$$v^{n+1} = v^n + v'$$
$$w^{n+1} = w^n + w'$$

5. In equation 3.10, designate the new value of *p* on the left hand side as the new value of p^n. Return to step-2 and repeat the process until a velocity field is found that does satisfy the continuity equation. When this is achieved, the correct flow field is at hand.

3.4.5.2 Pressure-Velocity Correction Procedure by MAC method

The relationship between the explicitly advanced velocity component and velocity at the previous time step may be written as

$$\tilde{u}^{n+1}_{i,j,k} = u^{n}_{i,j,k} + \delta t \frac{\left[p^{n}_{i,j,k} - p^{n}_{i+1,j,k}\right]}{\delta x} + \delta t \left[CONDIFU\right]^{n}_{i,j,k} \qquad (3.11)$$

Where

$$\left[CONDIFU\right]^{n}_{i,j,k} = \left[SDISCU\right]^{n}_{i,j,k} + \left[DPDX\right]^{n}_{i,j,k}$$

On the other hand, the corrected velocity-component (unknown) will be related to the correct pressure (also unknown) in following way..

$$u^{n+1}_{i,j,k} = u^{n}_{i,j,k} + \delta t \frac{\left[p^{n+1}_{i,j,k} - p^{n+1}_{i+1,j,k}\right]}{\delta x} + \delta t \left[CONDIFU\right]^{n}_{i,j,k} \qquad (3.12)$$

From Equations 3.11 and 3.12

$$u^{n+1}_{i,j,k} - \tilde{u}^{n+1}_{i,j,k} = \delta t \frac{\left[p'_{i,j,k} - p'_{i+1,j,k}\right]}{\delta x}$$

Where the pressure correction may be defined as

$$p'_{i,j,k} = p^{n+1}_{i,j,k} - p^{n}_{i,j,k}$$

Neither the pressure corrections nor $u^{n+1}_{i,j,k}$ are known explicitly at this Stage. Hence one cannot be calculated with the help of the other. Calculations are done in an iterative cycle and we write

$$u^{n+1}_{i,j,k} \rightarrow \tilde{u}^{n+1}_{i,j,k} + \delta t \frac{\left[p'_{i,j,k} - p'_{i+1,j,k}\right]}{\delta x}$$

In a similar way, we can formulate the following array:-

Corrected **Estimated** **Correction**

$$u^{n+1}_{i,j,k} \rightarrow \tilde{u}^{n+1}_{i,j,k} + \delta t \frac{\left[p'_{i,j,k} - p'_{i+1,j,k}\right]}{\delta x} \quad (3.13)$$

$$u^{n+1}_{i-1,j,k} \rightarrow \tilde{u}^{n+1}_{i-1,j,k} - \delta t \frac{\left[p'_{i,j,k} - p'_{i-1,j,k}\right]}{\delta x} \quad (3.14)$$

$$v^{n+1}_{i,j,k} \rightarrow \tilde{v}^{n+1}_{i,j,k} + \delta t \frac{\left[p'_{i,j,k} - p'_{i,j+1,k}\right]}{\delta y} \quad (3.15)$$

$$v^{n+1}_{i,j-1,k} \rightarrow \tilde{v}^{n+1}_{i,j-1,k} - \delta t \frac{\left[p'_{i,j,k} - p'_{i,j-1,k}\right]}{\delta y} \quad (3.16)$$

$$w^{n+1}_{i,j,k} \rightarrow \tilde{w}^{n+1}_{i,j,k} + \delta t \frac{\left[p'_{i,j,k} - p'_{i,j,k+1}\right]}{\delta z} \quad (3.17)$$

$$w^{n+1}_{i,j,k-1} \rightarrow \tilde{w}^{n+1}_{i,j,k-1} - \delta t \frac{\left[p'_{i,j,k} - p'_{i,j,k-1}\right]}{\delta z} \quad (3.20)$$

The correction is done through continuity equation. Plugging –in the above relationship into the continuity equation yields…

$$\left[\frac{u^{n+1}_{i,j,k} - u^{n+1}_{i-1,j,k}}{\delta x} + \frac{v^{n+1}_{i,j,k} - v^{n+1}_{i,j-1,k}}{\delta y} + \frac{w^{n+1}_{i,j,k} - w^{n+1}_{i,j,k-1}}{\delta z}\right]$$

$$= \left[\frac{\tilde{u}^{n+1}_{i,j,k} - \tilde{u}^{n+1}_{i-1,j,k}}{\delta x} + \frac{\tilde{v}^{n+1}_{i,j,k} - \tilde{v}^{n+1}_{i,j-1,k}}{\delta y} + \frac{w^{n+1}_{i,j,k} - w_{i,j,k-1}}{\delta z}\right]$$

$$-\delta t\left[\frac{p'_{i+1,j,k}-2p'_{i,j,k}+p'_{i-1,j,k}}{(\delta x)^2}+\frac{p'_{i,j+1,k}-2p'_{i,j,k}+p'_{i,j-1,k}}{(\delta y)^2}+\frac{p'_{i,j,k+1}-2p'_{i,j,k}+p'_{i,j,k-1}}{(\delta z)^2}\right]$$

$$=\left[\frac{\tilde{u}^{n+1}_{i,j,k}-\tilde{u}^{n+1}_{i-1,j,k}}{\partial x}+\frac{\tilde{v}^{n+1}_{i,j,k}-\tilde{v}^{n+1}_{i,j-1,k}}{\partial y}+\frac{w^{n+1}_{i,j,k}-w_{i,j,k-1}}{\partial z}\right]$$

$$+\frac{2\delta t(p'_{i,j,k})}{(\delta x)^2}+\frac{2\delta t(p'_{i,j,k})}{(\delta y)^2}+\frac{2\delta t(p'_{i,j,k})}{(\delta z)^2}$$

In deriving the above expression, it is assumed that the pressure corrections in the neighboring cells are zero. The first term between square brackets is the divergence of the velocity field in a finite difference form. Rewriting to the algebraic calculations.

$$0=(Div)_{i,j,k}+p'_{i,j,k}\left[2\delta t\left(\frac{1}{(\delta x)^2}+\frac{1}{(\delta y)^2}+\frac{1}{(\delta z)^2}\right)\right]$$

Or

$$p'_{i,j,k}=\frac{-(Div)_{i,j,k}}{\left[2\delta t\left(\frac{1}{(\delta x)^2}+\frac{1}{(\delta y)^2}+\frac{1}{(\delta z)^2}\right)\right]} \qquad (3.21)$$

In order to accelerate the calculations the pressure correction equation is modified as

$$p'_{i,j,k}=\frac{-\omega_0(Div)_{i,j,k}}{\left[2\delta t\left(\frac{1}{(\delta x)^2}+\frac{1}{(\delta y)^2}+\frac{1}{(\delta z)^2}\right)\right]} \qquad (3.22)$$

Where ω_0 is the over relaxation factor. The value of ω_0 that gives the most rapid convergence, should be determined by numerical experimentation.

After calculating $p^{'}_{i,j,k}$, the pressure in the cell (i, j, k) is adjusted as

$$p^{n+1}_{i,j,k} \rightarrow p^{n}_{i,j,k} + p^{'}_{i,j,k} \tag{3.23}$$

Now the pressure and velocity components for each cell are corrected through an iterative procedure in such a way that for the final pressure field, the velocity divergence in each cell vanishes. The process is continued till a divergence free velocity field is reached with a prescribed upper bound, have a value of 0.0001 is recommended.

3.4.6 Boundary Conditions

Different boundary conditions are shown in Fig. 3.2. Consider, for example, the bottom boundary of the computing (physical) Mesh. If this boundary is to be a rigid no slip wall, the normal velocity on the wall must be zero and the tangential velocity components should also be zero.

Here we consider a stationary wall,

$$v_{i,1,k} = 0$$
$$u_{i,1,k} = -u_{i,2,k} \qquad \text{For } i = 2 \text{ to } ire \text{ and } k = 2 \text{ to } kre.$$
$$w_{i,1,k} = -w_{i,2,k}$$

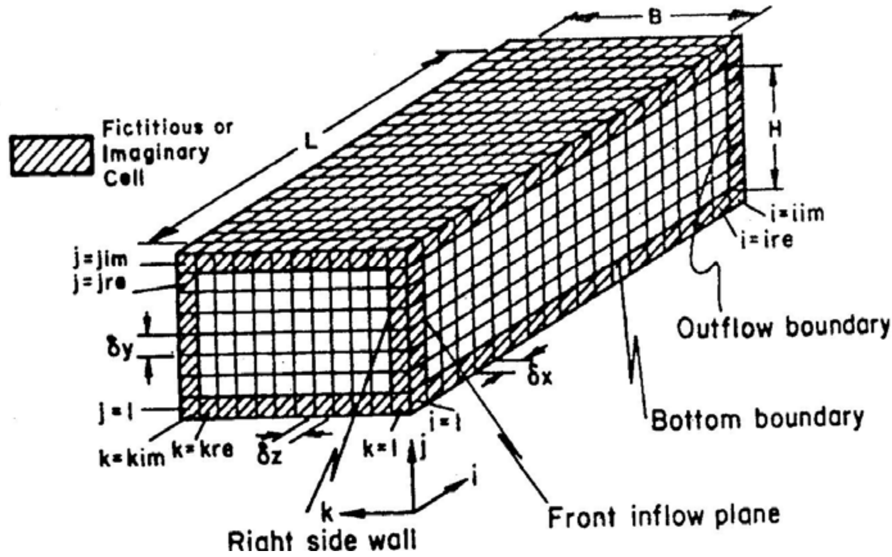

[Fig.3.2] Boundary Conditions and Imaginary Boundary Cells

For the right side wall, is a free-slip (vanishing shear) boundary, the normal velocity must be zero and the tangential velocities should have no normal gradient.

$$w_{i,j,1} = 0$$
$$u_{i,j,1} = u_{i,j,2}$$
$$v_{i,j,1} = v_{i,j,2}$$

For $i = 2$ to *ire* and $j = 2$ to *jre*

If the front plane is to be provided with inflow boundary condition, it should be specified properly. Any desired functional relationship may be recommended. Generally, normal velocity components are set to zero and a uniform or parabolic axial velocity may be deployed. Here we can write

$$v_{1,j,k} = v_{2,j,k}$$
$$w_{1,j,k} = -w_{2,j,k}$$
$$u_{1,j,k} = 1.0,, or$$
$$u_{1,j,k} = 1.5\left[1-((j_m - j)/\ j_m)^2\right]$$

For $j = 2$ to *jre* and $k = 2$ to *kre.*

Where

$J_{m,}$ is the horizontal midplane.

Continuative or outflow boundaries always pose a problem for low speed calculation, because what ever prescription is chosen it can affect the entire flow field upstream. What is needed is a prescription that permits fluid to flow out of the mesh with a minimum of upstream influence. Commonly used conditions for such a boundary is $\nabla u.n = 0,$ where n is the unit normal vector and u is the velocity vector.

In the MAC family of algorithms, the derivatives of the dependent variables in flow direction are set to zero in order to ensure smooth transition through the out flow boundary (Orlanski 1976)[39]

Symbolically

$$\frac{\partial \phi}{\partial t} + u_{av} \frac{\partial \phi}{\partial x} = 0$$

Here ϕ represents any of the velocity components (*u, v* or *w*) and u_{av} is the average stream wise velocity at the outflow section.

The outflow boundary condition is implemented as follows:-

For *i = ire, j = 2…..jre, k = 2….. kre.*

$$u_{i,j,k}^{n+1} = u_{i,j,k}^{n} - \frac{u_{av}\Delta t}{\Delta x}\left(u_{i,j,k}^{n} - u_{i-1,j,k}^{n}\right)$$

$$v_{i,j,k}^{n+1} = v_{i,j,k}^{n} - \frac{u_{av}\Delta t}{\Delta x}\left(v_{i,j,k}^{n} - v_{i-1,j,k}^{n}\right)$$

$$w_{i,j,k}^{n+1} = w_{i,j,k}^{n} - \frac{u_{av}\Delta t}{\Delta x}\left(w_{i,j,k}^{n} - w_{i-1,j,k}^{n}\right)$$

3.4.7 Numerical Stability Considerations

For accuracy, the mesh size must be chosen small enough to resolve the expected spatial variations in all dependent variables Once a mesh has been chosen, the choice of the time increment is governed by two restrictions, namely, the Courant-Friedrichs-Lewy (CFL) condition and the restriction on the basis of grid-Fourier numbers.

According to the CFL condition, material cannot move through more than one cell in one time step, because the difference equations assume fluxes only between the adjacent cells. Therefore the time increment must satisfy the inequality

$$\delta t < \min\left\{\frac{\delta x}{|u|},\frac{\delta y}{|v|},\frac{\delta z}{|w|}\right\} \tag{3.24}$$

Where the minimum is with respect to every cell in the mess. When the viscous diffusion terms are more important, the condition necessary to ensure stability is dictated by the restriction on the grid Fourier numbers, which results in

$$v\delta t < \frac{1}{2}\cdot\frac{\left(\delta x^2 \delta y^2 \delta z^2\right)}{\left(\delta x^2 + \delta y^2 + \delta z^2\right)} \tag{3.25}$$

In dimensional form. After nondimensionalization, this leads to

$$\delta t < \frac{1}{2}\cdot\frac{\left(\delta x^2 \delta y^2 \delta z^2\right)}{\left(\delta x^2 + \delta y^2 + \delta z^2\right)}\cdot \mathrm{Re} \tag{3.26}$$

The final δt for each time increment is the minimum of the values obtained from the above equations.

The last quantity needed to ensure numerical stability is the upwind parameter α . In general α should be slightly larger than the maximum value of

$$\text{Max} \left\{ \left| \frac{u\delta t}{\delta x} \right|, \left| \frac{v\delta t}{\delta y} \right|, \left| \frac{w\delta t}{\delta z} \right| \right\} \le \alpha < 1 \tag{3.27}$$

Normally, a value between 0.2 and 0.4 can be used for α . If it is too large, an unnecessary amount of numerical diffusion (artificial viscosity) may be introduced.

3.5 Solution of Energy Equation

The equation for incompressible flow, neglecting mechanical work and gas radiation, may be written as

$$\rho C_p \frac{DT}{Dt^*} = k\nabla^2 T + \mu\phi^* \tag{3.28}$$

Where, ϕ^* is the viscous dissipation given by

$$\phi^* = 2\left[\left(\frac{\partial u^*}{\partial x^*}\right)^2 + \left(\frac{\partial v^*}{\partial y^*}\right)^2 + \left(\frac{\partial w^*}{\partial z^*}\right)^2\right] + \left\{\frac{\partial u^*}{\partial x^*} + \frac{\partial u^*}{\partial y^*}\right\}^2 + \left\{\frac{\partial w^*}{\partial y^*} + \frac{\partial v^*}{\partial z^*}\right\}^2 + \left\{\frac{\partial w^*}{\partial x^*} + \frac{\partial u^*}{\partial z^*}\right\}^2$$

In the nondimensionalized manner, it is

$$u = \frac{u^*}{U_\infty}, v = \frac{v^*}{U_\infty}, w = \frac{w^*}{U_\infty}, \theta = \frac{T - T_\infty}{T_w - T_\infty},$$

$$x = \frac{x^*}{L}, y = \frac{y^*}{L}, z = \frac{z^*}{L} \text{ and } t = \frac{t^*}{L/U_\infty}$$

Substituting the above variables in eq. 3.28 We obtain

$$\frac{\rho C_p U_\infty (T_w - T_\infty)}{L}\left[\frac{\partial\theta}{\partial t} + u\frac{\partial\theta}{\partial x} + v\frac{\partial\theta}{\partial y} + w\frac{\partial\theta}{\partial z}\right] = \frac{(T_w - T_\infty)k}{L^2}\left[\frac{\partial^2\theta}{\partial x^2} + \frac{\partial^2\theta}{\partial y^2} + \frac{\partial^2\theta}{\partial z^2}\right] + \frac{\mu U_\infty^{\ 2}}{L^2}\phi$$

(3.29)

Where, ϕ is nondimensional form of ϕ^*. The normalized energy equation can be written as

$$\left[\frac{\partial \theta}{\partial t} + u\frac{\partial \theta}{\partial x} + v\frac{\partial \theta}{\partial y} + w\frac{\partial \theta}{\partial z}\right] = \frac{1}{Pe}\left[\frac{\partial^2 \theta}{\partial x^2} + \frac{\partial^2 \theta}{\partial y^2} + \frac{\partial^2 \theta}{\partial z^2}\right] + \frac{Ec}{\mathrm{Re}}\phi \tag{3.30}$$

Where Pe, the Peclet number is given as

$$\frac{1}{Pe} = \frac{k(T_w - T_\infty)}{L^2} \cdot \frac{L}{\rho C_p U_\infty (T_w - T_\infty)}$$

Or $$\frac{1}{Pe} = \frac{k}{L \cdot \rho \cdot C_p U_\infty} = \frac{k}{\mu C_p} \cdot \frac{\mu}{\rho L U_\infty} = \frac{1}{\mathrm{Pr}} \cdot \frac{1}{\mathrm{Re}}$$

and the Eckert number, Ec is given by

$$\frac{Ec}{\mathrm{Re}} = \frac{\mu U_\infty^{\ 2}}{L^2} \cdot \frac{L}{\rho C_p U_\infty (T_w - T_\infty)} = \frac{U_\infty^{\ 2}}{C_p (T_w - T_\infty)} \cdot \frac{1}{\rho U_\infty L/\mu}$$

3.5.1 Solution Procedure

The steady state energy equation, neglecting the dissipation term, may be written in the following conservative form as

$$\frac{\partial (u\theta)}{\partial x} + \frac{\partial (v\theta)}{\partial y} + \frac{\partial (w\theta)}{\partial z} = \frac{1}{Pe}\left[\frac{\partial^2 \theta}{\partial x^2} + \frac{\partial^2 \theta}{\partial y^2} + \frac{\partial^2 \theta}{\partial z^2}\right] \tag{3.31}$$

The above equation may be rewritten as

$$\nabla^2 \theta = Pe\ \left[CONVT\right]_{i,j,k}^{m} \tag{3.32}$$

Where, $[CONVT]_{i,j,k}$ is the discretized convective term on the left hand side of equation and *m* stands for iterative counter. To start with, we can assume any guess value of θ throughout the flow field. Since u, v, w are known from the solution of momentum equation, hence the above equation is now a linear equation. However, from the guess values of θ and known correct values of u, v, and w the left hand side of Eq. 3.30 is evaluated. A weighted average scheme or QUICK scheme may be adapted for discretization of the convective terms. After discretizing and evaluating R.H.S of Eq.3.31 we obtain a Poisson equation for temperature with a source term on the right hand side.

Now we will follow a SOR technique for solving Eq.3.29 considering a discretized equation as

$$\frac{\theta_{i+1,j,k} - 2\theta_{i,j,k} + \theta_{i-1,j,k}}{\delta x^2} + \frac{\theta_{i,j+1,k} - 2\theta_{i,j,k} + \theta_{i,j-1,k}}{\delta y^2} + \frac{\theta_{i,j,k+1} - 2\theta_{i,j,k} + \theta_{i,j,k-1}}{\delta z^2} = S^{*m}$$

Where

$$S^{*m} \equiv P_e [CONVT]^m_{i,j,k}$$

Or

$$A^{*m} - \theta_{i,j,k}\left[\frac{2}{(\delta x)^2} + \frac{2}{(\delta y)^2} + \frac{2}{(\delta z)^2}\right] = S^{*m}$$

Or
$$\theta_{i,j,k} = \frac{A^{*m} - S^{*m}}{\left[\frac{2}{(\delta x)^2} + \frac{2}{(\delta y)^2} + \frac{2}{(\delta z)^2}\right]} \qquad (3.33)$$

Where

$$A^{*m} = \frac{\theta^m_{i+1,j,k} + \theta^m_{i-1,j,k}}{(\delta x)^2} + \frac{\theta^m_{i,j+1,k} + \theta^m_{i,j-1,k}}{(\delta y)^2} + \frac{\theta^m_{i,j,k+1} + \theta^m_{i,j,k-1}}{(\delta z)^2}$$

$\theta_{i,j,k}$ In equation 3.32 may be assumed to be the most recent values and it may be written as $\theta^{m'}_{i,j,k}$. In order to accelerate the speed of computation we introduce an over relaxation factor ω. Thus

$$\theta^{m+1}_{i,j,k} = \theta^{m}_{i,j,k} + \omega\left[\theta^{m'}_{i,j,k} - \theta^{m}_{i,j,k}\right]$$

Where $\theta^{m}_{i,j,k}$ is the previous value, $\theta^{m'}_{i,j,k}$ the most recent value and $\theta^{m+1}_{i,j,k}$ the calculated better guess. The procedure will continue till the required convergence is achieved.

3.6 Computational Domain and Boundary Conditions

3.6.1 Computational Domain

In this computation we have considered total nodes along x-direction as 200 and along y-direction as 34. But the outer boundaries we have considered as imaginary boundaries, so there are total 199x33 nodes present in the domain. Hence the geometry becomes 197x31. Fig.3.3 shows the discretization of the computational domain.

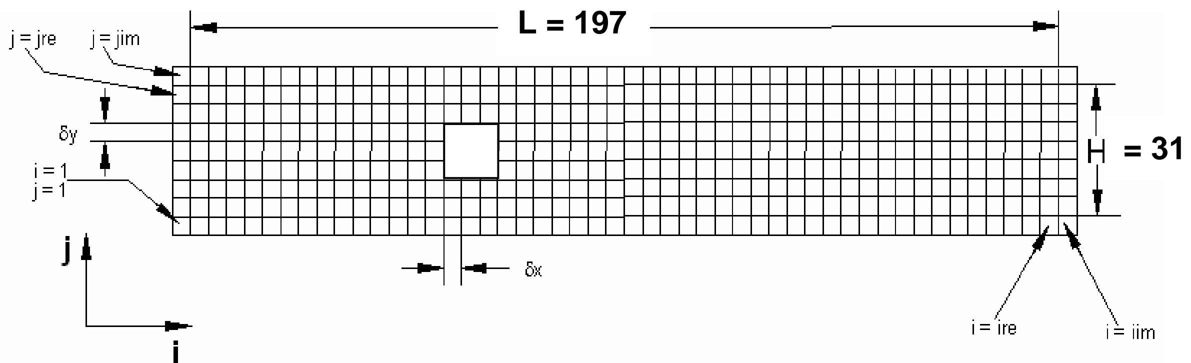

[Fig. 3.3] Discretization of the Domain

Now considering the boundary conditions of the problem. Bottom and Top boundaries are rigid, no slip walls, with a constant temperature of "1 (one)" (in non-dimensional form). Now for the Front plane here we have considered a uniform axial velocity, hence the normal velocity components are set to zero. The temperature of inlet air is considered to be '0' (zero). So that the temperature of the entire domain varies from zero to one. For outflow boundary the derivatives of *u, v,* and *w* are set to zero in order to ensure smooth transition through the outflow boundary. Finally the obstruction (chip) wall temperature was taken as 1 (one) in non-dimensional form. Fig. 3.4 shows the different boundary conditions with imaginary cells and obstruction (chip) of the computational domain.

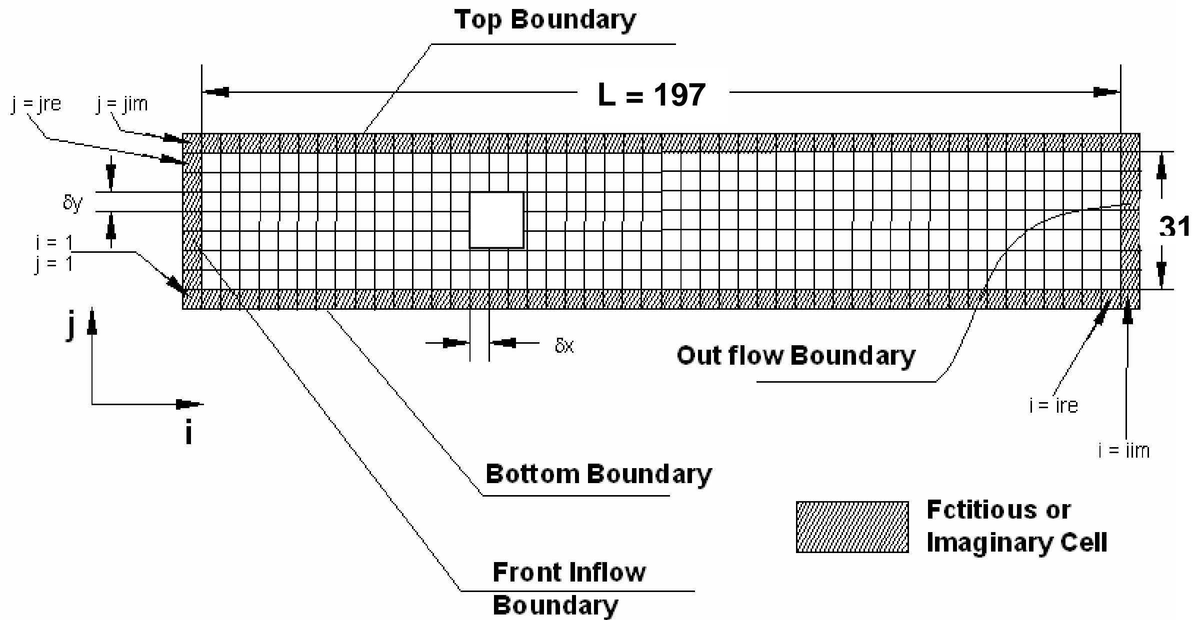

[Fig.3.4] Boundary Conditions and Fictitious Boundary Cells

When it comes to Computation, it was carried by taking different Reynolds numbers i.e. at Re = 300, Re = 600, Re = 900, and Re = 1200. Again the geometry of the obstruction also varied. Here throughout the computation square bodies of different sizes are considered i.e. the sizes are 3x3, 7x7, 11x11, and 15x15.

Let the height of the channel is H, and that of the chip (square) is B, then here the value of H is being fixed, i.e. H = 31, and that of B is varied. Hence the values of B/H in the calculation are as follows

$$\frac{B}{H} = \frac{3}{31}, \frac{7}{31}\frac{11}{31}, \frac{15}{31}.$$

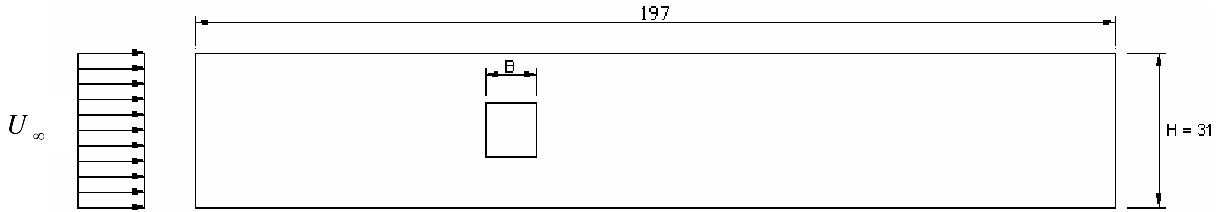

[Fig.3.5] Geometry of the Computational Domain Showing B, H

Hence different aspect ratios have been considered. Fig 3.5 shows the dimensions of B, H with the geometry configuration, and the inlet velocity profile being axially uniform velocity. The free stream velocity being U_∞ .

3.6.2 Boundary Conditions

Top and Bottom boundary

The computing (physical) mesh is rigid and no-slip wall

Hence

$$v_{i,1} = 0 \qquad u_{i,1} = -u_{i,2} \qquad \text{for } i = 2 \text{ to } 199$$

and

$$v_{i,34} = 0 \qquad u_{i,34} = -u_{i,33} \qquad \text{for } i = 2 \text{ to } 199$$

Front inflow boundary

It is provided with, normal velocity component are zero and an uniform axial velocity

$v_{1,j} = - v_{2,j}$

$u_{1,j} = 1.0$ for j = 2 to 33

Outflow Boundary

For i = 199, j = 2 to 33

$$u_{i,j}^{n+1} = u_{i,j}^{n} - \frac{u_{av}\Delta t}{\Delta x}\left(u_{i,j}^{n} - u_{i-1,j}^{n}\right)$$

$$v_{i,j}^{n+1} = v_{i,j}^{n} - \frac{u_{av}\Delta t}{\Delta x}\left(v_{i,j}^{n} - v_{i-1,j}^{n}\right)$$

Temperature boundary

$\theta = 1$ For j = 2 and 33

& i = 2 to 199

Again

$\theta = 1$ For i = ia to ib

& j = ja to jb

3.7 Closure

Different methods are available to solve the governing equations, mainly The Finite Difference Methods (FDM), Finite Element Methods (FEM) and Finite Volume Methods (FVM). Here we are using the Finite difference methods. Also in FDM different algorithms available and MAC is one of the most admired algorithm. In MAC either 2nd upwinding method or 3rd upwinding method can be used to discretize the convective term and we are using the 2nd upwinding method. In the next chapter we will discuss about the results obtained from this algorithm.

Chapter-4

Results and Discussions

- **Introduction**
- **Pressure Contours**
- **Temperature Contours**
- **Velocity Profile**
- **Nusselt Number**
- **Closure**

RESULTS AND DISCUSSIONS

4.1 Introduction

As explained earlier the Navier-Stokes equation and the Energy equation are solved using Marker and Cell method. The iterative method of solution is carried out in FORTRAN-90. In the analysis, the flow has been analyzed by varying the body dimension as 3x3, 7x7, 11x11, 15x15, and the Reynolds number as 300, 600, 900 and 1200. So the flow is in the range of laminar. In this chapter we will discuss the effects of these, on various parameters like pressure, temperature, velocity, and Nusselt number. The variations in these parameters are discussed in the subsequent part of this chapter.

4.2 Pressure Contours

Fig.4.1, 4.2, 4.3 and 4.4 represents the contours of pressure in the computational domain for different obstruction size. The obstruction is placed symmetrically placed along ordinate and the centre of the obstruction is 67.5 distance away from the front boundary. In the plot the maximum pressure is represented by red color and minimum is represented by green color. As the color changes from red to green the pressure decreases accordingly. Constant pressure lines (isobaric lines) with labels are also shown in the figure.

Now considering Fig.4.1, it is clear that the isobaric lines are vertical upto the distance of nearly 60 from the front boundary and from the distance of 80 onwards. These vertical lines show that the pressure variation along the y-direction is nil or all the points have same pressures. But between 60 to 80 the pressure variation or the isobaric lines are dense, specially near the obstruction. Near the obstruction the isobaric lines are dense and very close to the body. The nature of the isobaric lines near the obstruction is circular

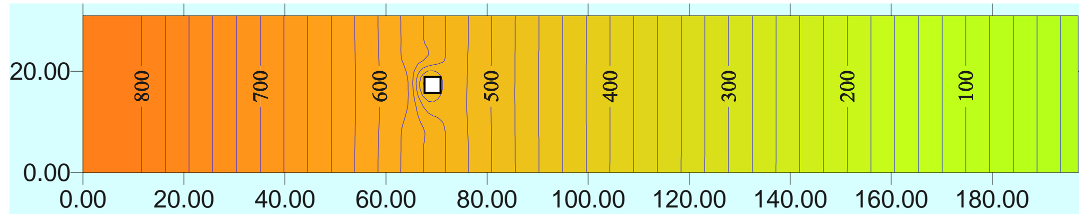

(a)

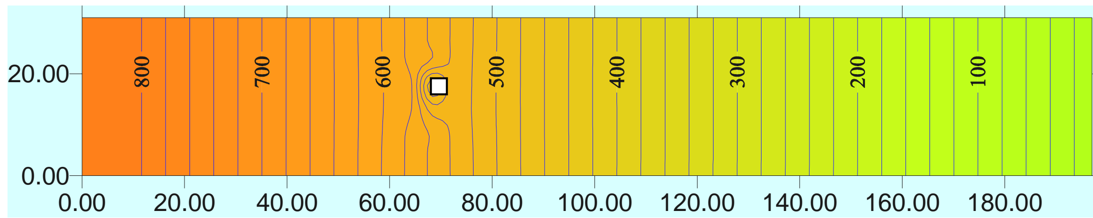

(b)

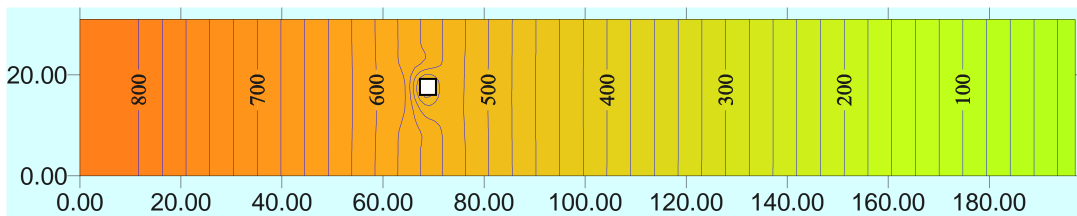

(c)

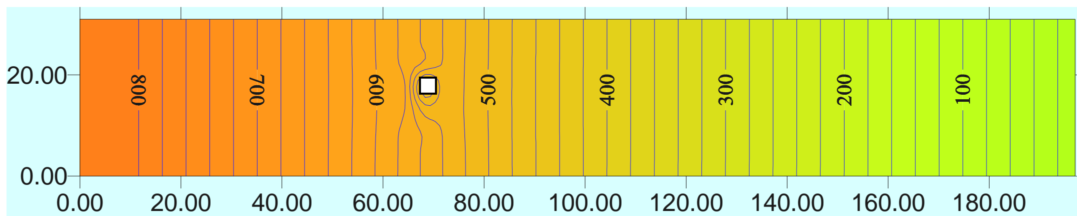

(d)

[Fig. 4.1] Pressure Contours for an obstruction size of 3x3 for various Reynolds Numbers, (a) Re = 300 (b) Re = 600 (c) Re = 900 (d) Re = 1200.

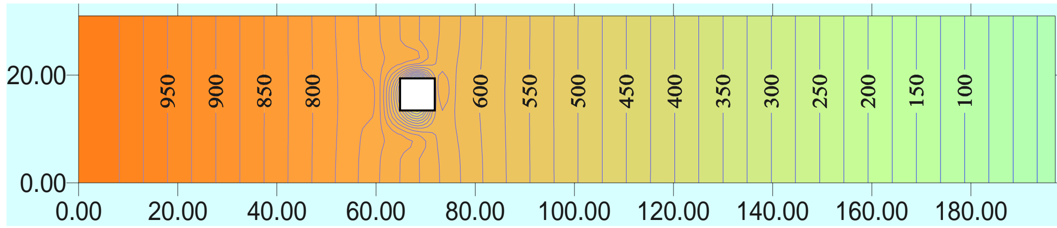

(a)

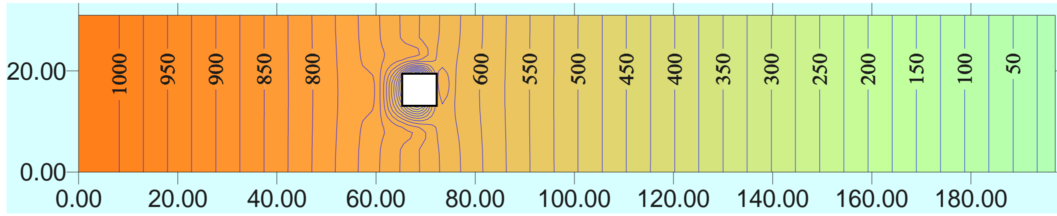

(b)

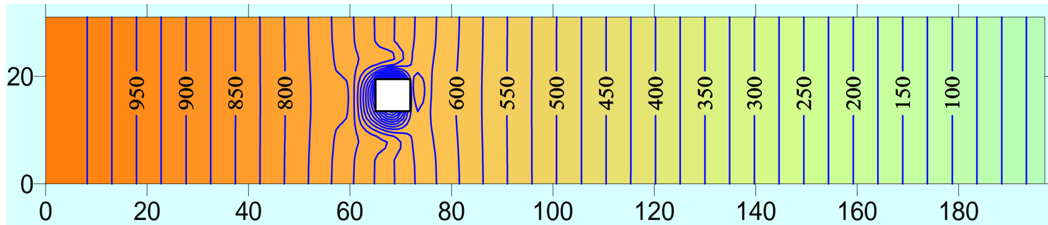

(c)

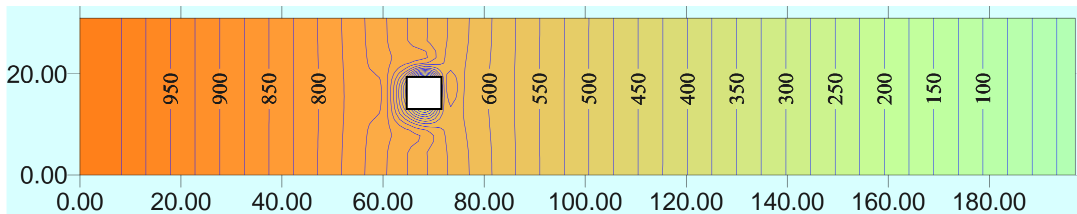

(d)

[Fig. 4.2] Pressure Contours for an obstruction size of 7x7 for various Reynolds Numbers, (a) Re = 300 (b) Re = 600 (c) Re = 900 (d) Re = 1200.

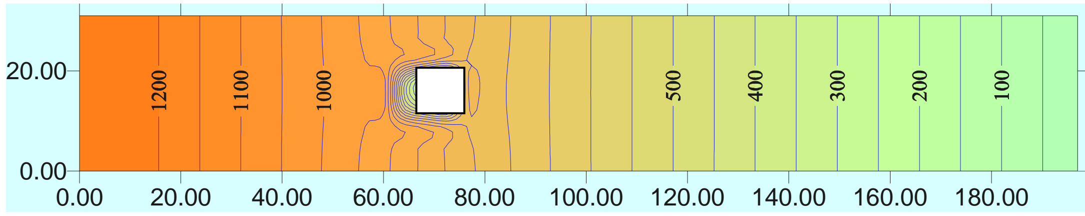

(a)

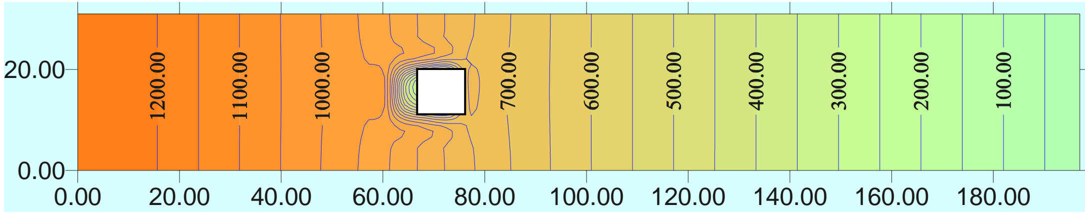

(b)

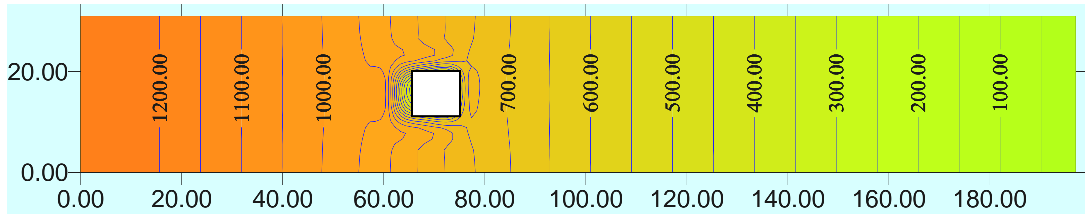

(c)

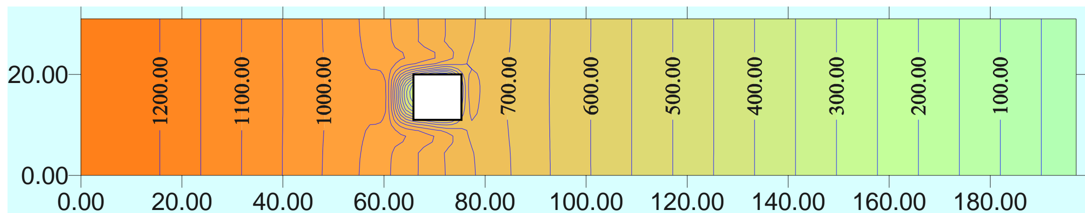

(d)

[Fig. 4.3] Pressure Contours for an obstruction size of 11x 11 for various Reynolds Numbers, (a) Re = 300 (b) Re = 600 (c) Re = 900 (d) Re = 1200.

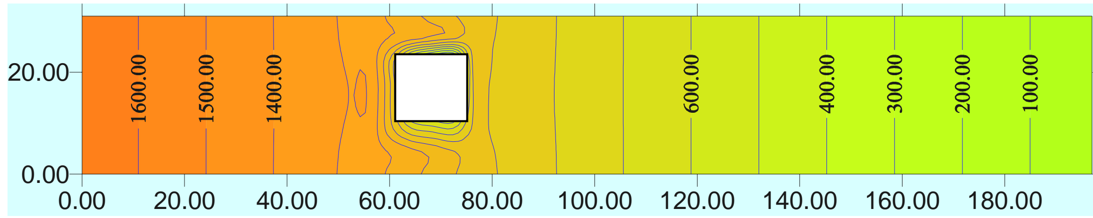

(a)

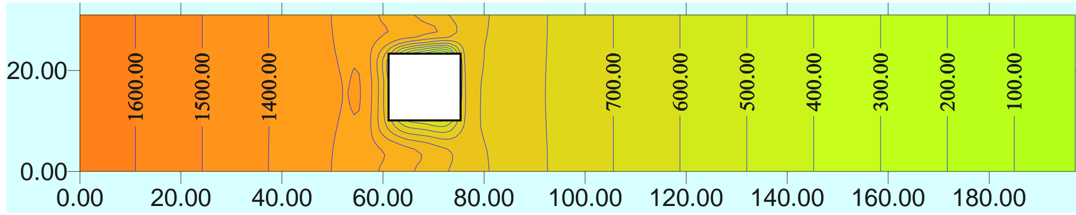

(b)

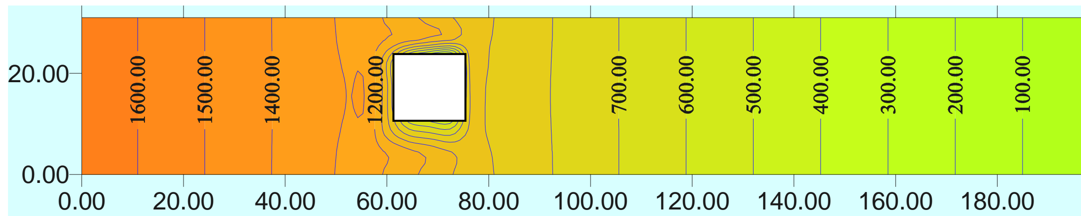

(c)

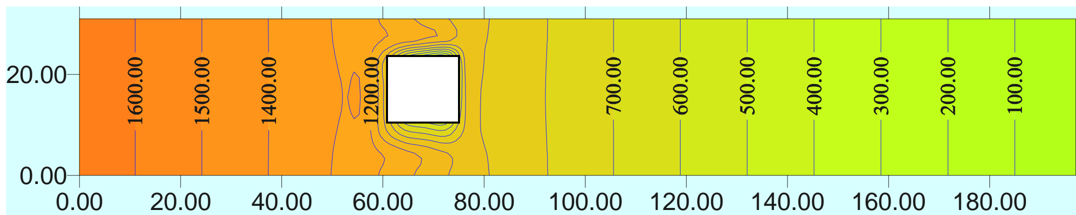

(d)

[Fig. 4.4] Pressure Contours for an obstruction size of 15x15 for various Reynolds Numbers, (a) Re = 300 (b) Re = 600 (c) Re = 900 (d) Re = 1200.

Fig.4.1 (a), (b), (c), (d), are four sets of contours showing the contours of pressure at Reynolds numbers of 300, 600, 900, and 1200 respectively. From the figure it is clear that the pressure at the inlet is around 850 and it decreases gradually along the axial direction finally reaching a value of nearly 5. It is clear from the graph that the Reynolds number has little impact on the pressure. As we know from theoretical point of view at the obstruction the velocity of the fluid suddenly decreases thus by increasing the pressure, known as stagnation pressure, which is clearly visible in the plot.

Now coming to Fig.4.2, here the obstruction size is 7x7, the front edge of the obstruction being at a distance of 64 from the front boundary and centrally placed in the y-direction. Here the maximum pressure is in the range of 1040 at the entry, and a minimum of 6 at the outlet. Near the obstruction high dense pressure lines are present.

Fig.4.3 represents pressure contours for an obstruction of 11x11. The front edge of the object is placed 62 unit distance from the inlet boundary. In this case the maximum pressure obtained at the entry is 1296, and the minimum pressure is 7.4, occurs at the outlet boundary.

And finally Fig.4.4 shows the pressure contours for an obstruction size of 15x15. Here the maximum pressure recorded is 1683, and minimum is 8.9. This is the largest obstruction size that has been considered in this calculation.

4.3 Temperature Contours

Fig 4.5 to 4.8 represents the contours of temperature for various body sizes and for various Reynolds numbers. Fig. 4.5 shows the temperature contour for an obstruction of 3x3. The isothermal lines are clearly visible in the figure. Now analyzing the figure it is clear that in each figure a contour of 0.08 isothermal line has been shown. When the Reynolds number is high i.e., 1200 means inlet velocity is high, this region is small. Because of high velocity most of the heat is carried by the air stream very rapidly, hence there is little time available to spread this region. Now as we decrease the Reynolds number, which means we will decrease the inlet velocity this region grows steadily. In the figure maximum temperatures are shown by red colors and minimum is shown by yellow colors. So near the chip and near the wall of the passage which are the maximum temperature of 1 (one) are red and the colors represent the temperature range. Various contour ranges would have been shown in the figure but in order to analyze the output only 0.8 temperature ranges has been prominently shown.

Similarly in Fig 4.6 the temperature ranges for a heated obstruction size of 7x7 are shown. Here a particular temperature range of 0.05 in all the contours bas been shown. Here also we are getting the same results as the velocity increases the temperature range of a particular range decreases. So as the velocity increases the heat removal rate also increases.

Now considering Fig. 4.7, here a temperature contour range of 0.1 is clearly shown in each figure for a chip size of 11x11. Here also we are getting the same results as before. As the body size gradually increases the temperatures are varying much more as the heat generating surface increases and an obstruction also increases so the flow field gets disturbed more.

In final temperature contour a body size of 15 x 15 bas been considered. In the high velocity case i.e., when Re = 1200, there is no range of 0.1, that’s why we have presented here a range of 0.09, which is very small. But in other cases a temperature range of 0.1 has been shown. Here the least count of the values shown are 0.1 and the colors represents accordingly from high (red) to low (yellow).

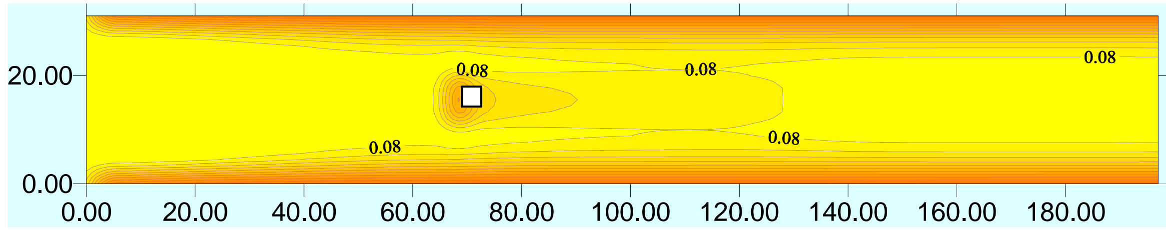

(a)

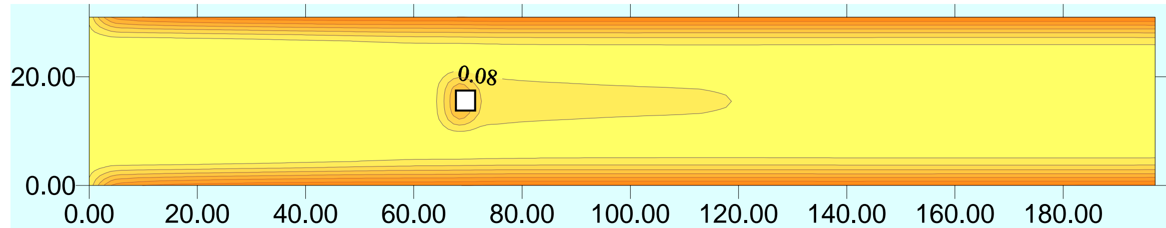

(b)

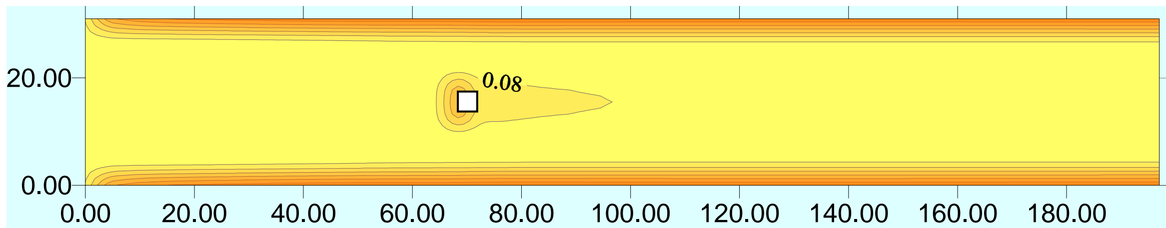

(c)

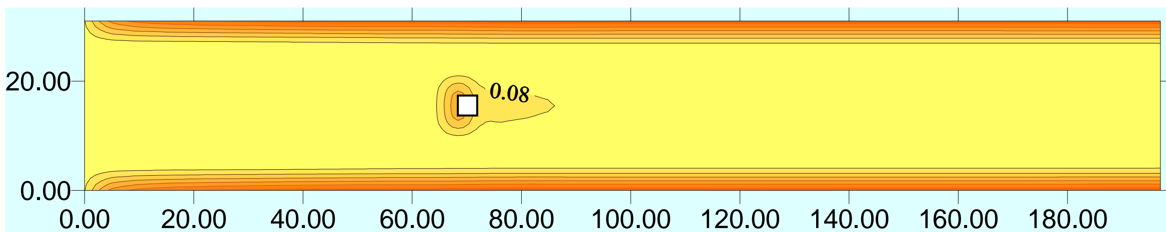

(d)

[Fig. 4.5] Temperature Contours for an obstruction size of 3x3 for various Reynolds no.s, (a) Re = 300 (b) Re = 600 (c) Re = 900 (d) Re = 1200.

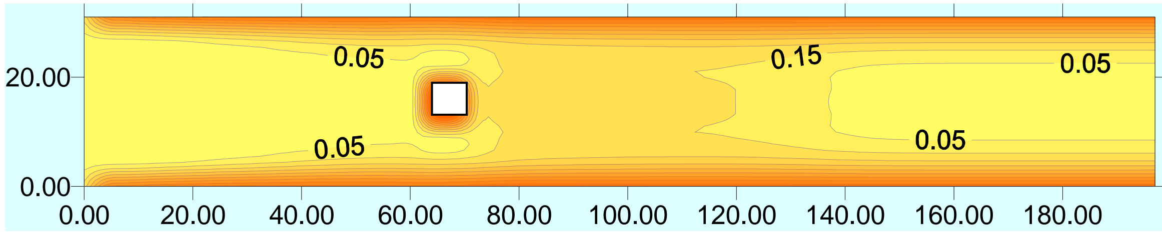

(a)

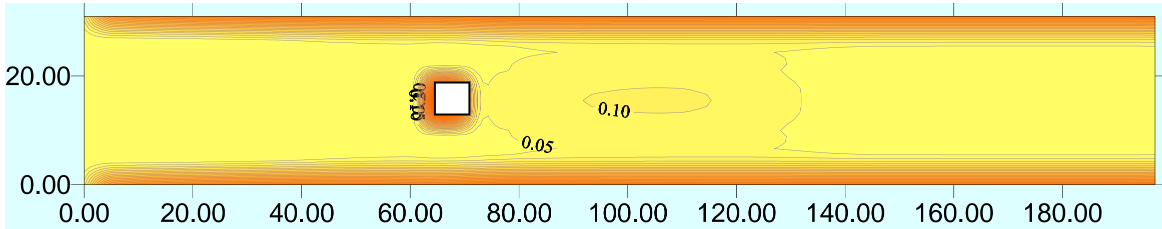

(b)

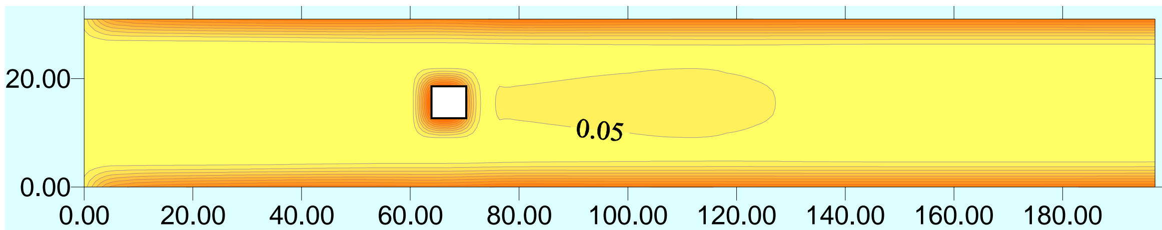

(c)

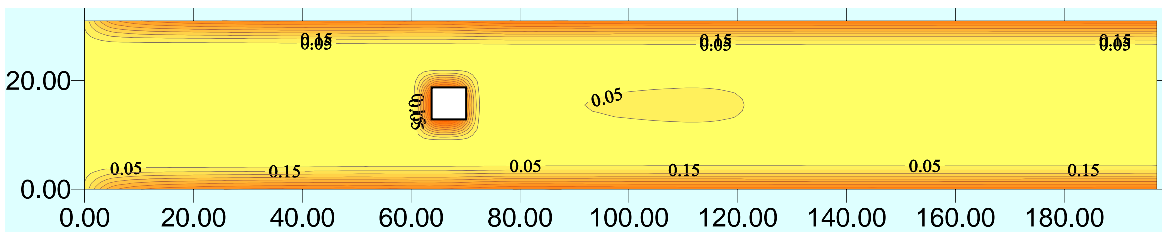

(d)

[Fig. 4.6] Temperature Contours for an obstruction size of 7x7 for various Reynolds no.s, (a) Re = 300 (b) Re = 600 (c) Re = 900 (d) Re = 1200.

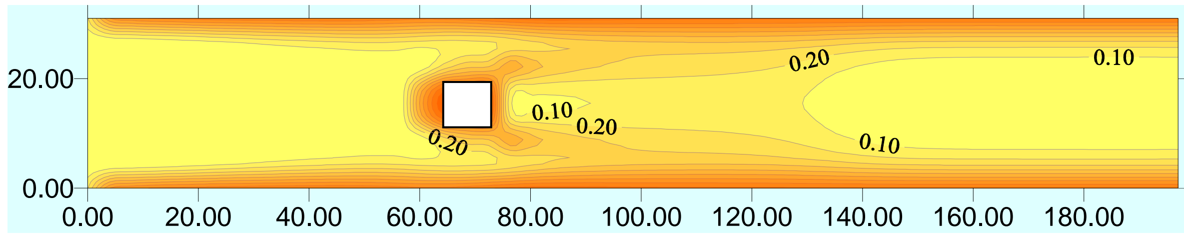

(a)

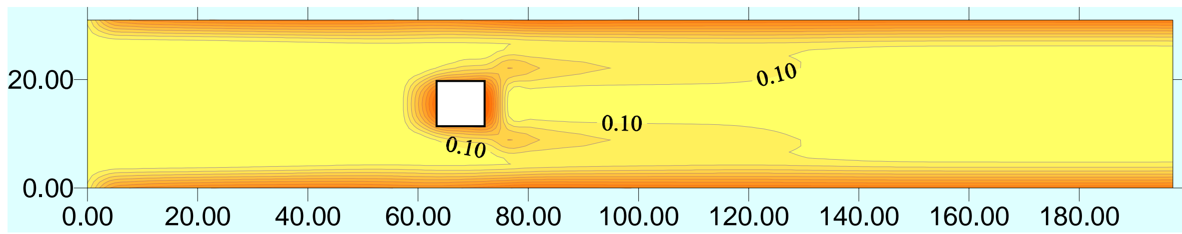

(b)

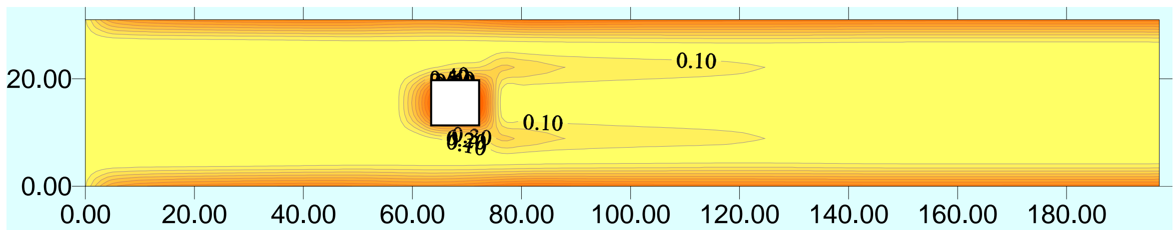

(c)

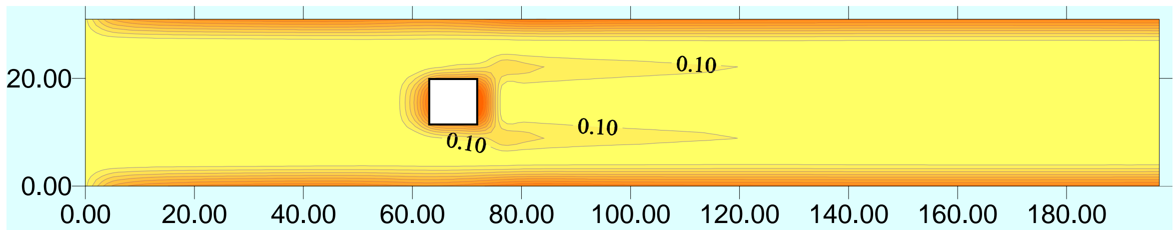

(d)

[Fig. 4.7] Temperature Contours for an obstruction size of 11x11 for various Reynolds no.s, (a) Re = 300 (b) Re = 600 (c) Re = 900 (d) Re = 1200

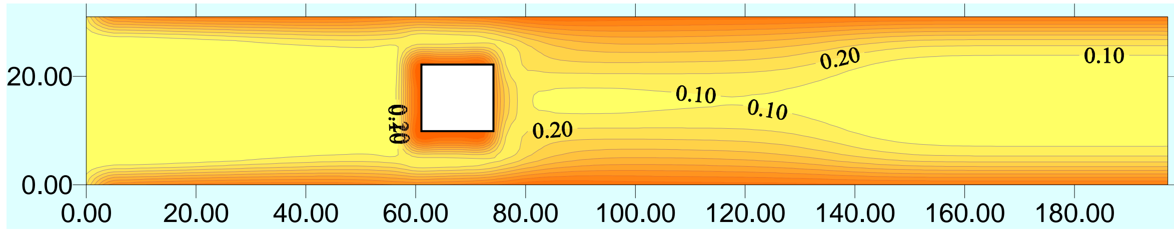

(a)

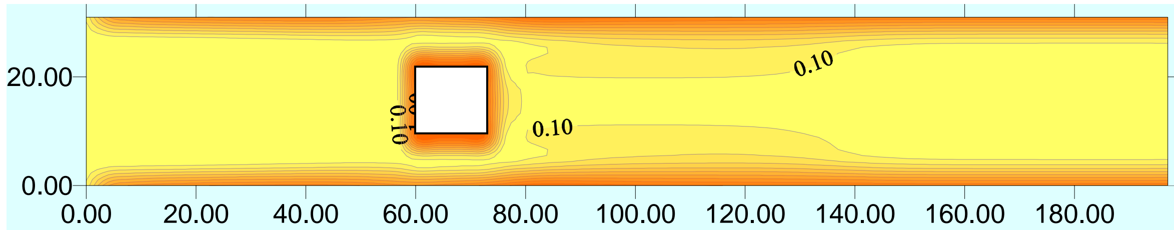

(b)

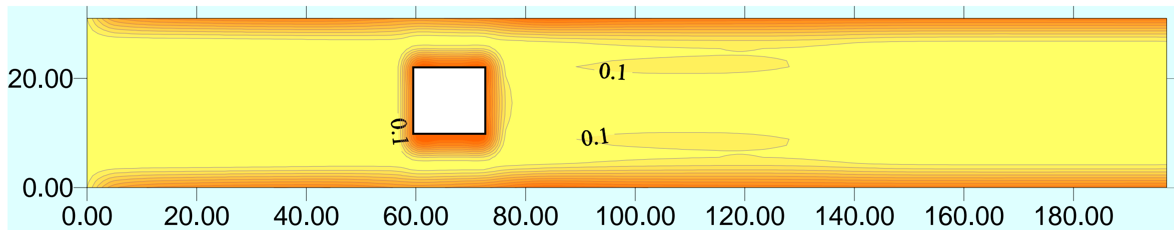

(c)

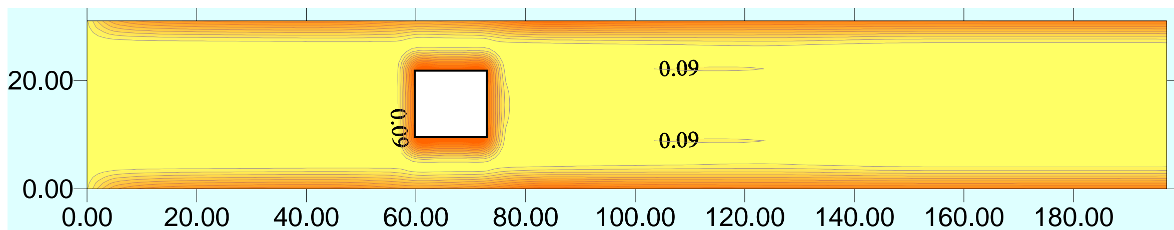

(d)

[Fig. 4.8] Temperature Contours for an obstruction size of 15x15 for various Reynolds no.s, (a) Re = 300 (b) Re = 600 (c) Re = 900 (d) Re = 1200.

4.4 Velocity Profile

Fig. 4.9 to Fig. 4.12 represents the velocity vector plots of different geometries and at different Reynolds numbers. From the plot it is clearly understood that the velocity vector directions changes as the fluid particles approach to the body and moves over the body. After crossing the body within few distance the velocity vectors again come back to their original directions showing that the flow is laminar. The change in direction of the velocity vectors increases as the body size increases.

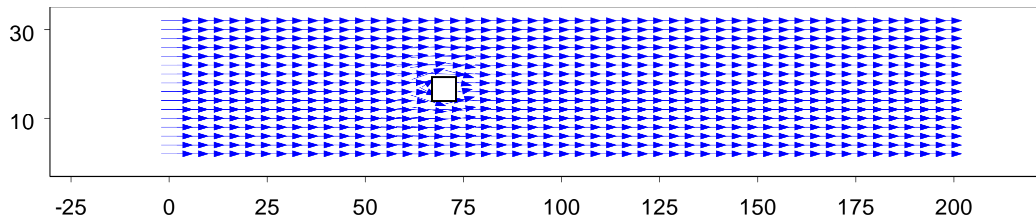

(a)

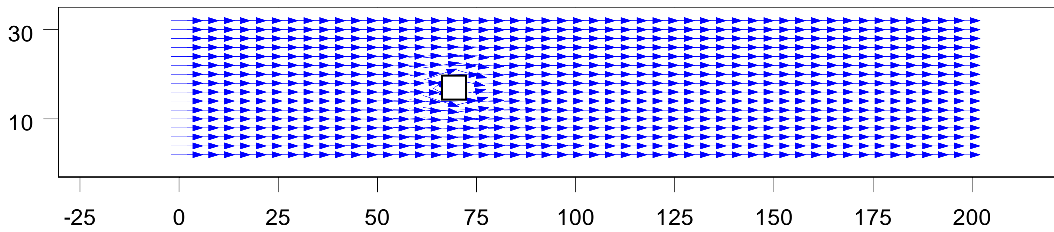

(b)

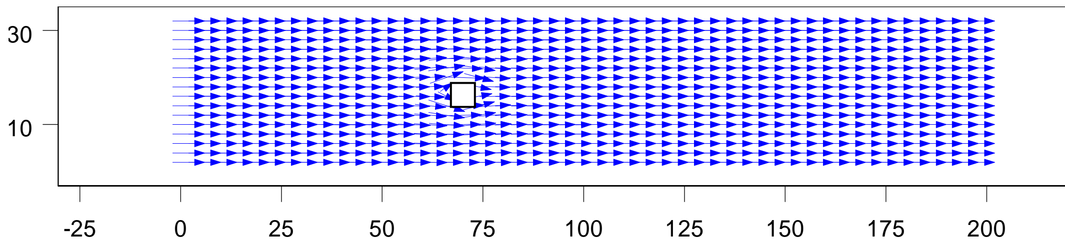

(c)

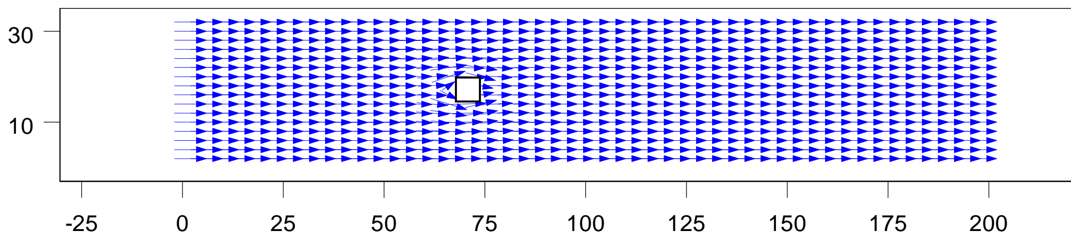

(d)

[Fig. 4.9] Velocity Profile for an obstruction size of 3x3 for various Reynolds Numbers (a) Re = 300 (b) Re = 600 (c) Re = 900 (d) Re = 1200.

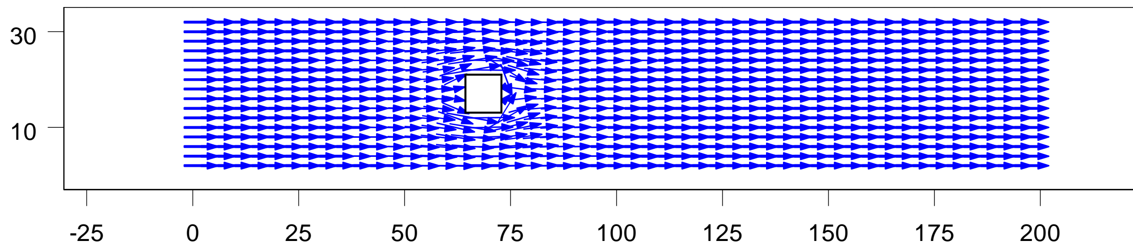

(a)

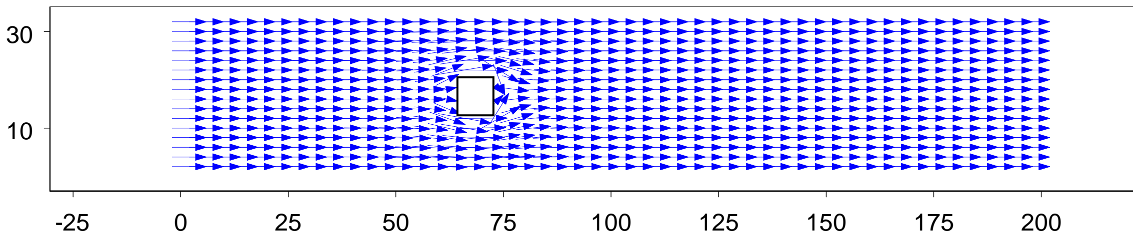

(b)

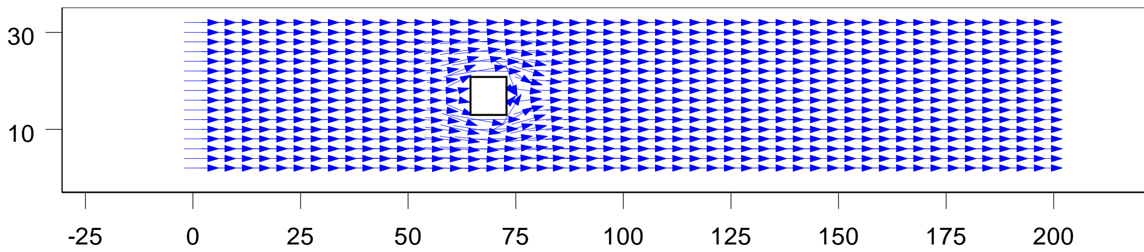

(c)

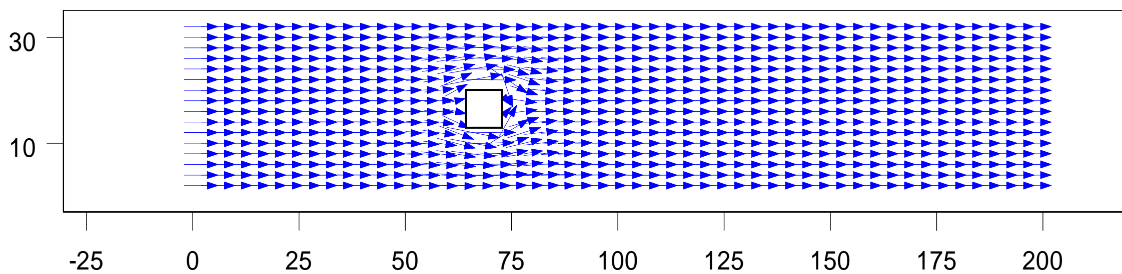

(d)

[Fig. 4.10] Velocity Profile for an obstruction size of 7x7 for various Reynolds Numbers (a) Re = 300 (b) Re = 600 (c) Re = 900 (d) Re = 1200.

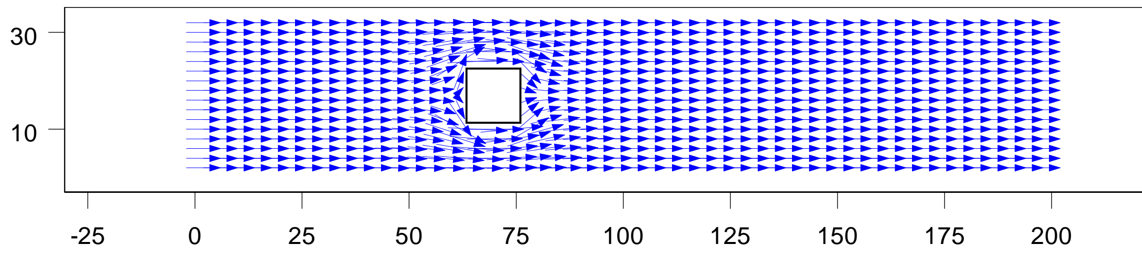

(a)

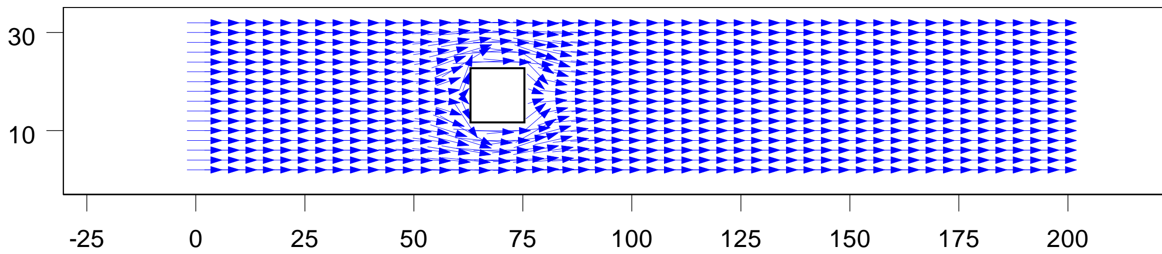

(b)

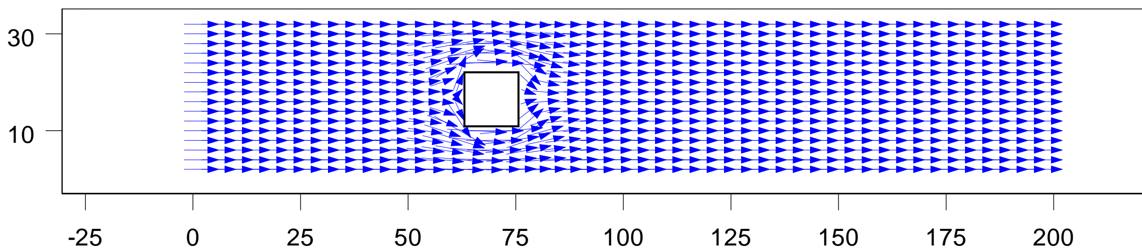

(c)

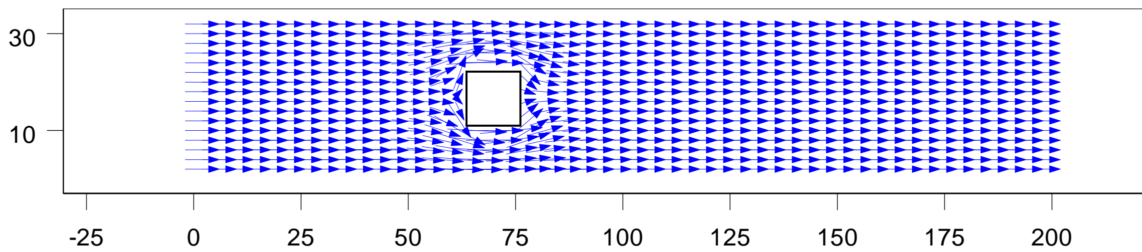

(d)

[Fig. 4.11] Velocity Profile for an obstruction size of 11x11 for various Reynolds Numbers (a) Re = 300 (b) Re = 600 (c) Re = 900 (d) Re = 1200.

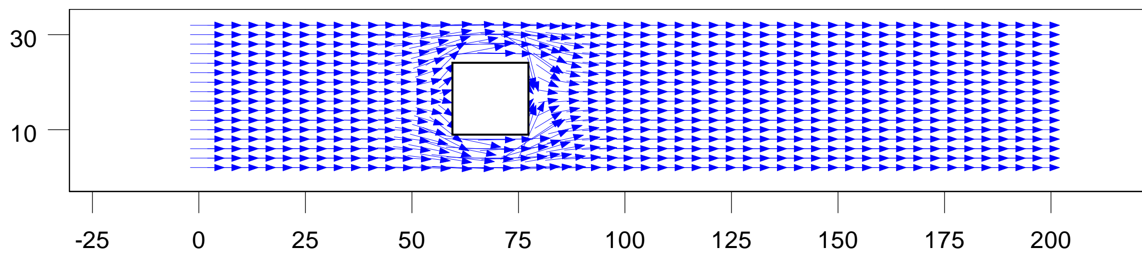

(a)

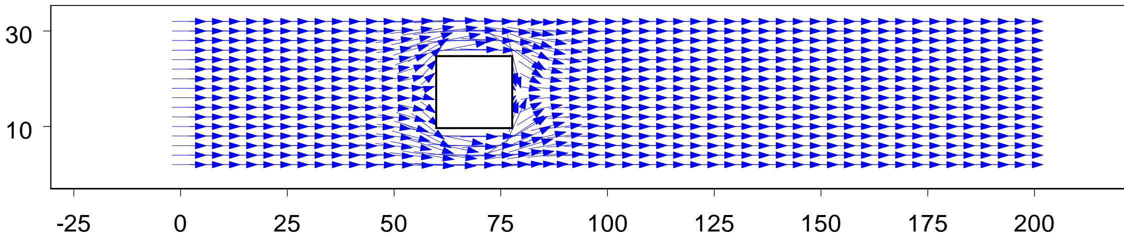

(b)

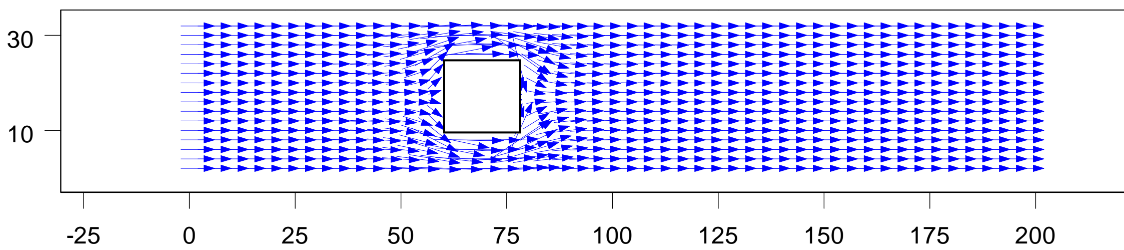

(c)

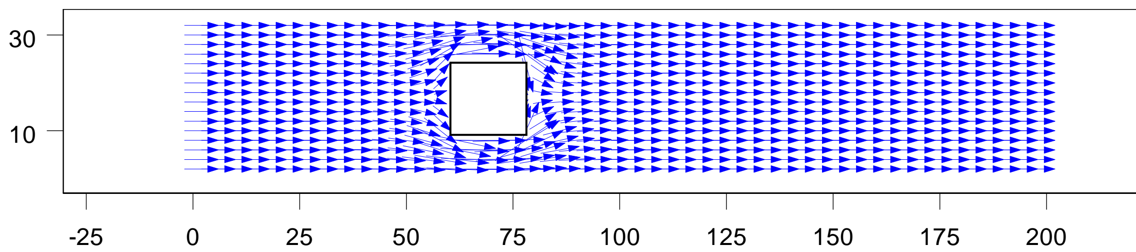

(d)

[Fig. 4.12] Velocity Profile for an obstruction size of 15x15 for various Reynolds Numbers (a) Re = 300 (b) Re = 600 (c) Re = 900 (d) Re = 1200.

4.5 Nusselt Number

Fig. 4.13 to fig.4.16 represents the variation of Nusselt number along axial direction for different B/H ratio. In the plot the blue lines represent the value of Nusselt number for Reynolds number 300, pink lines represent Re value of 600, green lines represent Re value of 900 and red lines represent Re value of 1200.

From the plot it is clear that as fresh air enters the channel the Nusselt number increases and it reaches a peak after that peak point the heat caring capacity of air decreases. But when the air passes through the chip the Nusselt number again increases. After passing the chip again the value of Nusselt number decreases due to wake formation behind the obstruction. Consequently the value of Nusselt number increases and it comes to a constant value. It can also be concluded from the plot that if the Reynolds number is small the initial heat caring capacity is low but it gradually increases towards the last section of the channel. On the other hand if the Reynolds number is high the initial value of Nusselt number is very high but after that it increases somewhat less in comparison to low Reynolds number. If we will observe for a particular Reynolds number, with increase in the obstruction size the saturation value of Nusselt number value comes early.

.

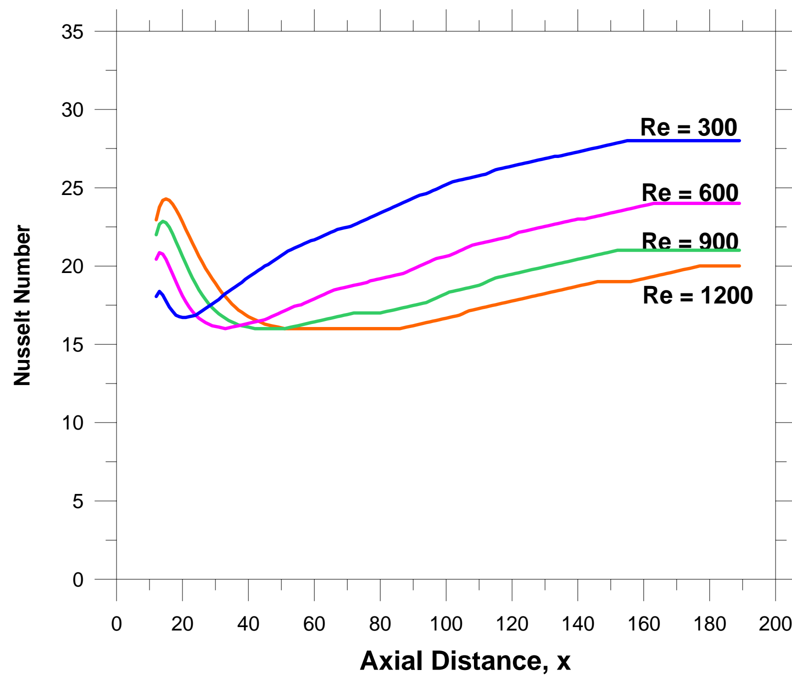

[Fig. 4.13] Variation of Nusselt Number along the Axial Direction for an Obstruction Size of 3x3, at Different Reynolds Number

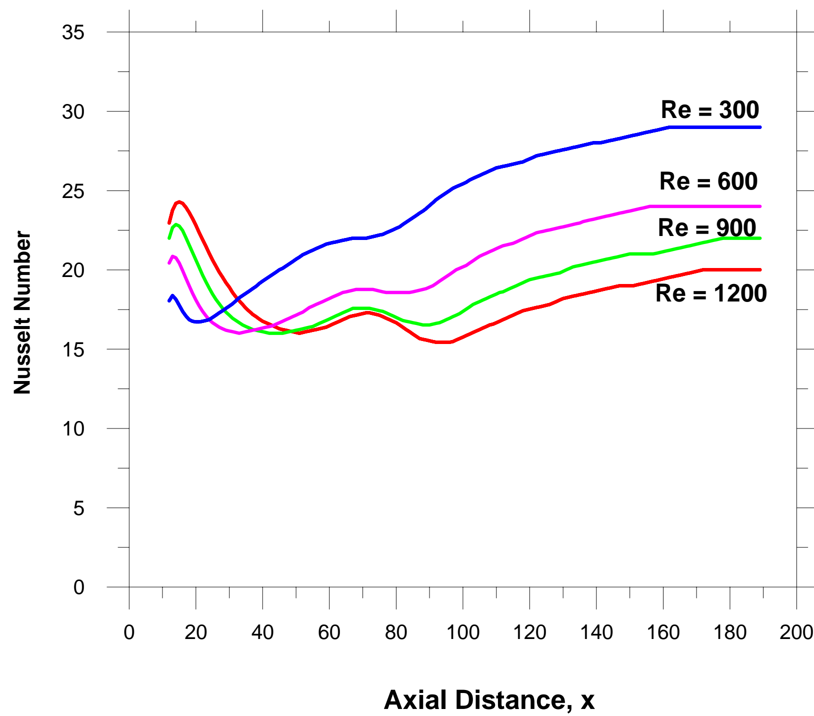

[Fig. 4.14] Variation of Nusselt Number along the Axial Direction for an Obstruction Size of 7x7, at Different Reynolds Number

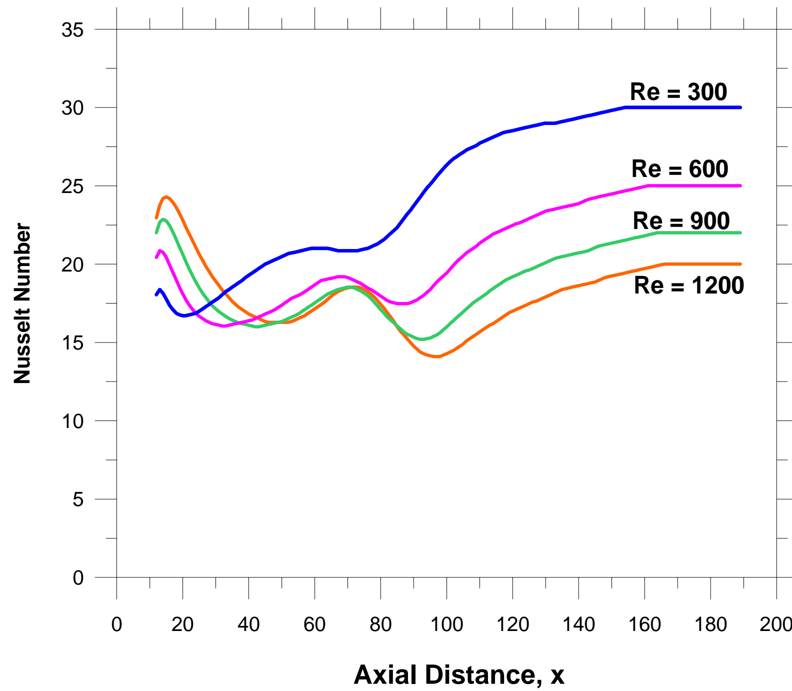

[Fig. 4.15] Variation of Nusselt Number along the Axial Direction for an Obstruction Size of 11x11, at Different Reynolds Number

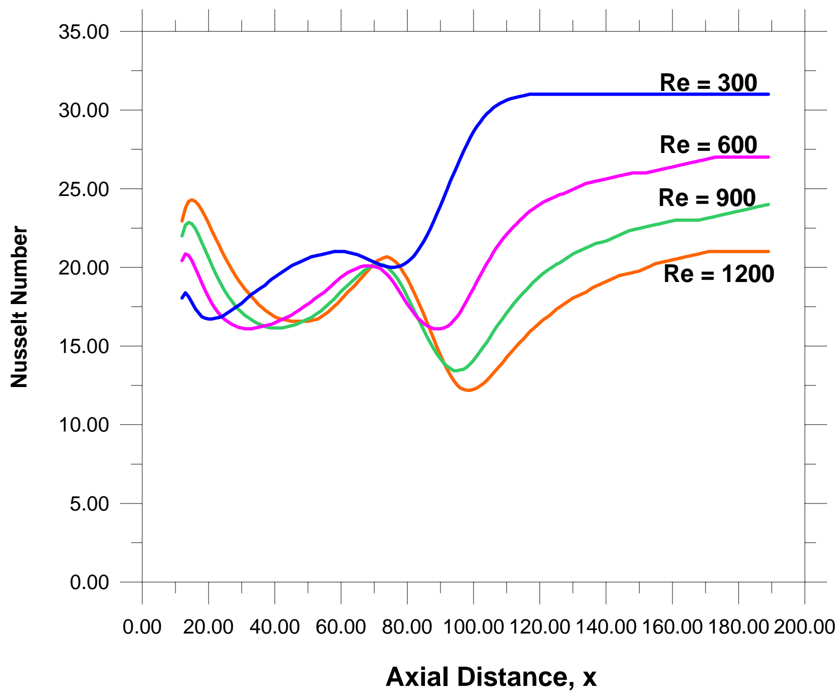

[Fig. 4.16] Variation of Nusselt Number along the Axial Direction for an Obstruction Size of 15x15, at Different Reynolds Number

4.6 Closure

Different contours of temperature, pressure, velocity profile and Nusselt number are plotted from the data output of the programme. We have analyzed the effects of various parameters like the inlet velocity, body geometry etc. One can understand the areas which can be given more attention to keep the temperature of the chip. The results of the analysis were presented as a summary in chapter-5 and suggestions for further work are given.

Chapter-5

Conclusions

And

Suggestions for Further Work

CONCLUSIONS AND SUGGESTIONS FOR FURTHER WORK

A numerical investigation on flow past a heated obstruction (chip cooling) has been successfully carried out to analyze the complex heat transfer phenomena involved in the process. General conclusions that stemmed from this analysis are presented here, together with a brief recapitulation of some of the important remarks made earlier.

5.1 Conclusion

A numerical code has been developed to solve the continuity equation, momentum equation and energy equation with certain boundary conditions, for flow through a channel via an obstruction for laminar, transient flow. Different contours of pressure, temperature, velocity profiles along with the variation of Nusselt number are plotted. Few of the conclusions are presented here

- The pressure is more concentrated near the obstruction and in other places its constant along the transverse direction. The pressure is more at the entry and gradually decreases along the axial direction, x, being the minimum value at the exit. The isobaric lines are more close to each other near the obstruction.
- From the temperature contour it can be concluded that more the Reynolds number, more the heat removal rate. In each figure a particular contour (isothermal line) has been shown to compare the effects of velocity on the cooling process.
- From the velocity profile it concludes that the velocity vectors are deviating or changing the direction near the obstruction presenting the real case of fluid flow.
- Finally from the Nusselt number graph it concludes that more the Reynolds number more is the value of Nusselt number showing that more heat transfer rate. The value of Nusselt number initially increases as the fresh air enters and after that it decreases but when the obstruction comes the value of Nusselt number again increases showing more heat transfer rate. After the obstruction again it decreases due to wake formation, but finally it increases and comes to a steady state.

With this analysis we can able to predict the zone where more temperatures are produced accordingly care can be taken. So we can predict the thermal behavior of the system. Any type of geometry can be formed and we can analyze the effect of temperature. But in the results some deficiency is that, presently there is no wake formation behind the obstruction and also the variation of pressure along the y- direction is also very little. Also the impact of inlet velocity on pressure distribution is felt less. Due to shortage of time these problems were not solved in the present investigation but can be sort-out and can even be better analyzed in the future work. Also this problem can be extended to multi chip problems and three dimensional problems. Also all these can be used to validate the capabilities of the commercially available CFD packages in the market.

5.2 Suggestions for further work

In this analysis we have considered a two dimensional case with a single obstruction in transient case. There exists much more scope to extend this work. For example, the analysis can be carried out with multi chip or multi-obstruction problem with or without heated wall. Further the same problem can be carried out in three dimensional domain, which can be validated with same boundary conditions by any of the commercially available CFD packages in the market. The case of laminar case may be extended to Turbulent case in each of the case i.e., two dimensional single chip/multi chip and three dimensional single chip/multi chip

Appendix-A: RESULTS BY "FLUENT"

The results of the code can be compared with the results of the CFD package "FLUENT", which is presented here. FLUENT is a commercially available CFD package, which solves the problems by Finite Volume Method. The problem is simulated in FLUENT by considering the same geometry and same boundary conditions, except that here the things are not nondimensionalized. The following geometry and boundary conditions are considered while the problem is simulated in FLUENT.

Geometry

Computational domain is 0.197 m x 0.031 m

Obstruction sizes are 3x3, 7x7, 11x11, 15x15, and individually each are considered

Boundary Conditions

Inlet velocity = 0.02224469 m/s ($\equiv$ Re is 300)

= 0.04448938 m/s ($\equiv$ Re is 600)

= 0.066734 m/s ($\equiv$ Re is 900)

= 0.08897 m/s ($\equiv$ Re is 1200)

Pressure outlet = Atmospheric pressure.

Inlet temperature of air = 300 K

Chip wall Temperature = 400 K

Wall temperature of the passage = 400 K

Fluid considered is air and rest all values are default values.

While calculating the corresponding velocity from the Reynolds number, the Characteristic length considered was the axial distance i.e., 0.197 m.

The results are almost same as that of we got from the code, but for the case of pressure contours and velocity profiles the results deviate somewhat more.

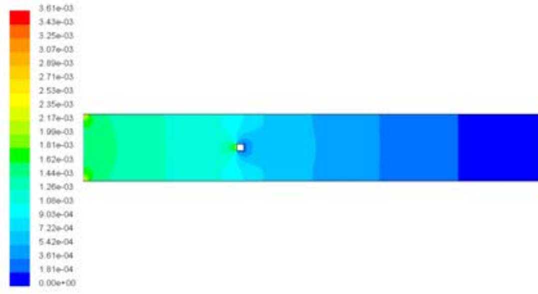

(a)

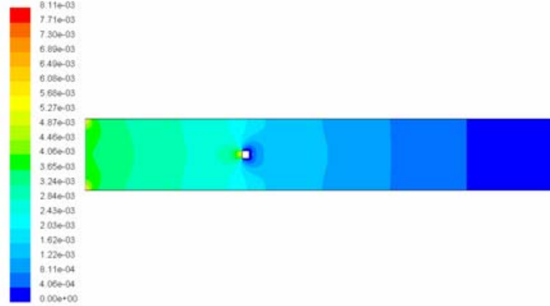

(b)

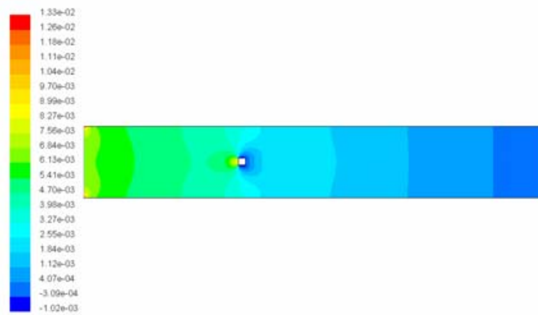

(c)

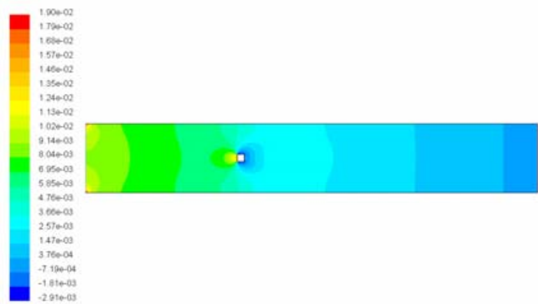

(d)

[Fig.A.1] Pressure (Static) Contours for an Obstruction Size of 3x3 at Various Reynolds No. (a) 300, (b) 600, (c) 900, (d) 1200

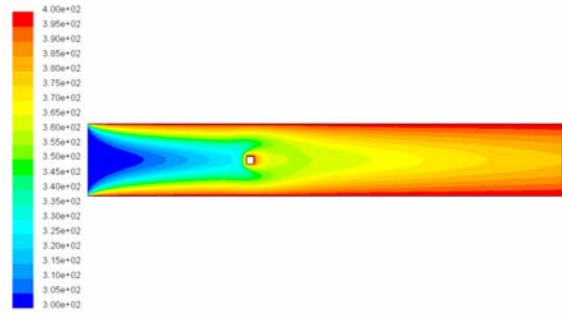

(a)

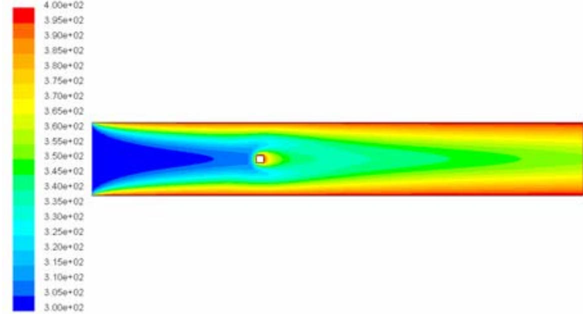

(b)

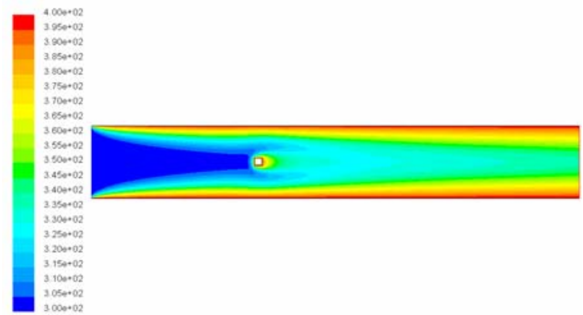

(c)

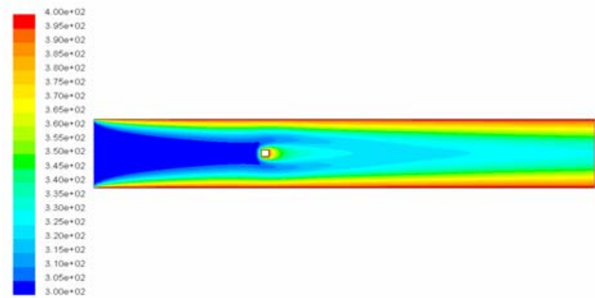

(d)

[Fig.A.2] Temperature (Static) Contours for an Obstruction Size of 3x3 at Various Reynolds No. (a) 300, (b) 600, (c) 900, (d) 1200

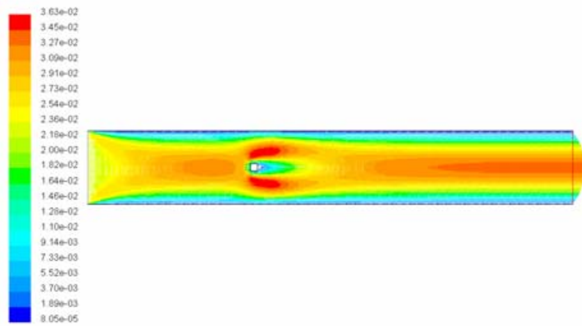

(a)

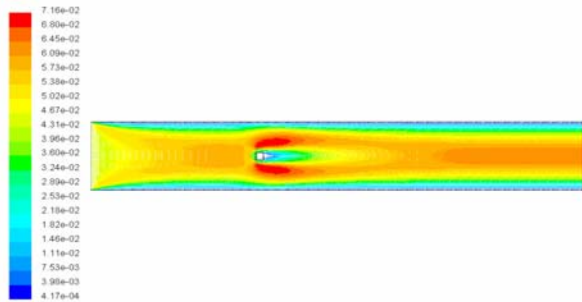

(b)

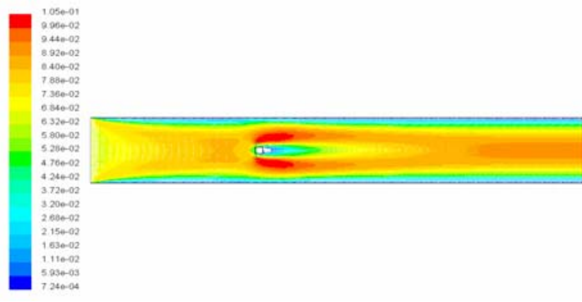

(c)

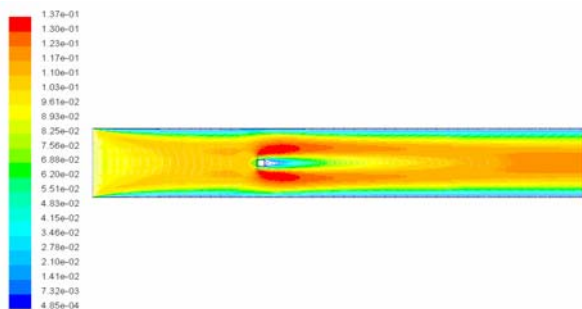

(d)

[Fig.A.3] Velocity Profile for an Obstruction Size of 3x3 at Various Reynolds Number (a) 300, (b) 600, (c) 900, (d) 1200

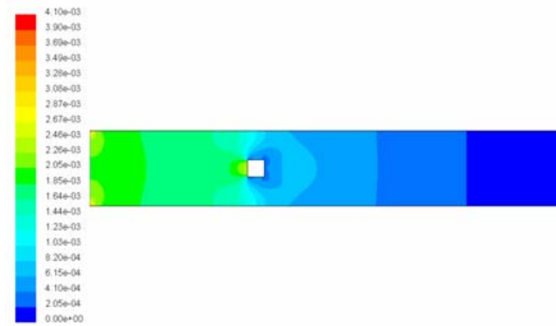

(a)

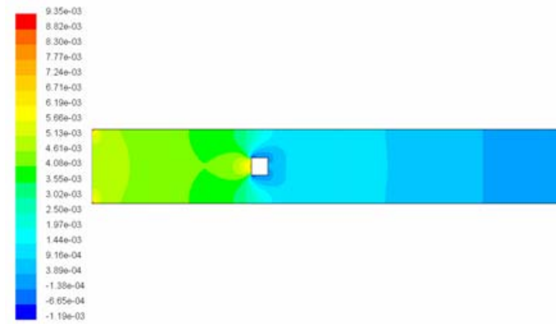

(b)

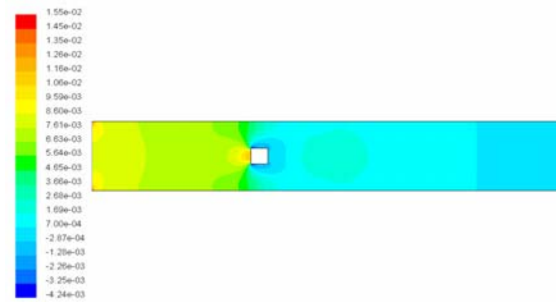

(c)

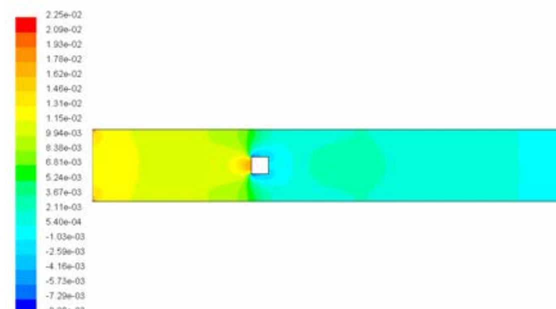

(d)

[Fig.A.4] Pressure (Static) Contours for an Obstruction Size of 7x7 at Various Reynolds No. (a) 300, (b) 600, (c) 900, (d) 1200

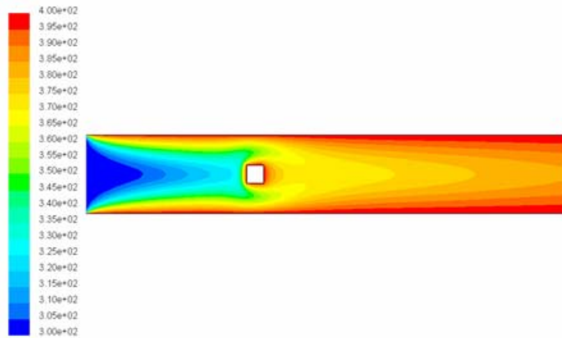

(a)

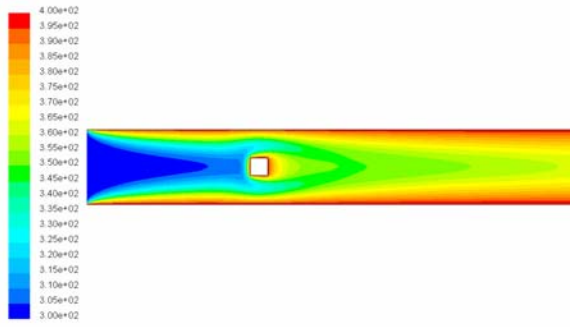

(b)

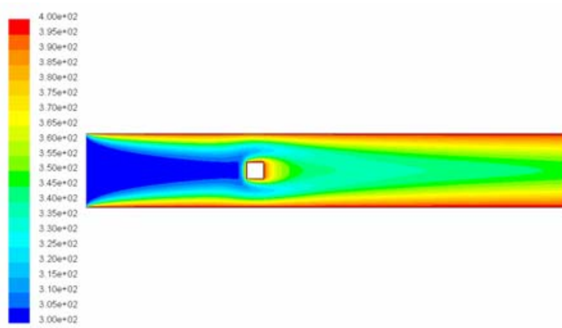

(c)

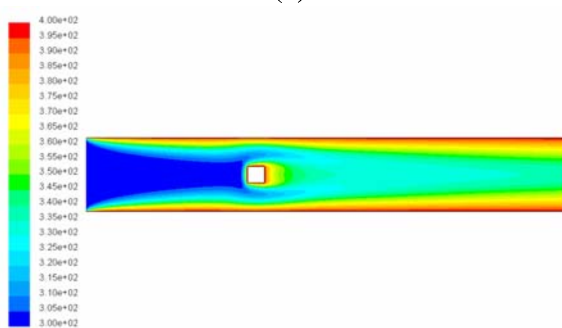

(d)

[Fig.A.5] Temperature (Static) Contours for an Obstruction Size of 7x7 at Various Reynolds No. (a) 300, (b) 600, (c) 900, (d) 1200

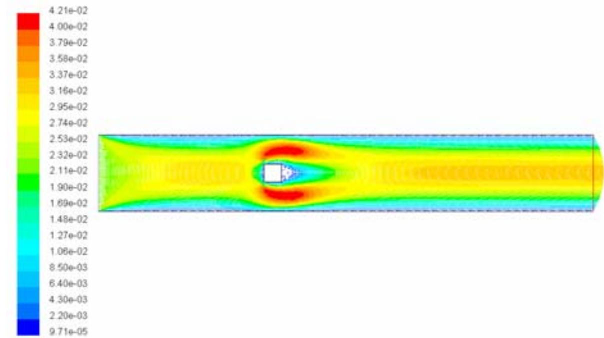

(a)

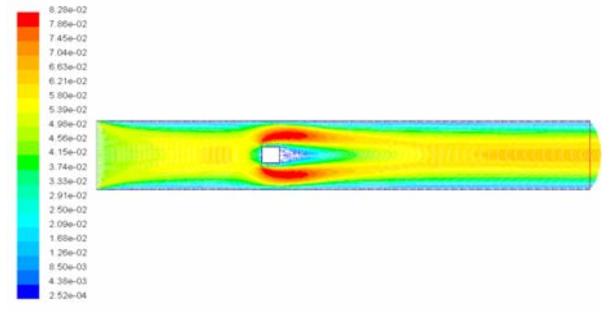

(b)

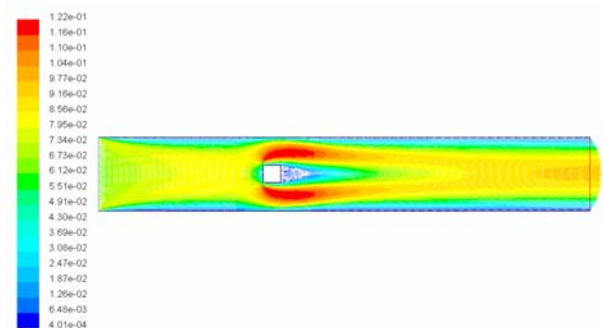

(c)

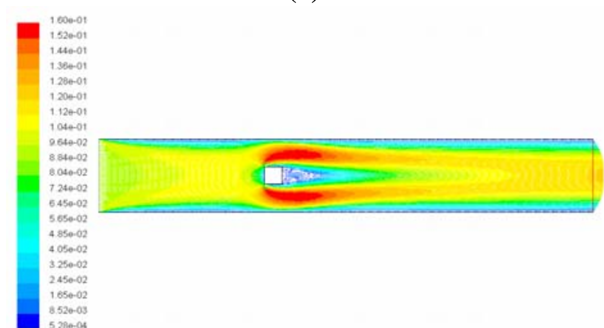

(d)

[Fig.A.6] Velocity Profiles for an Obstruction Size of 7x7 at Various Reynolds No. (a) 300, (b) 600, (c) 900, (d) 1200

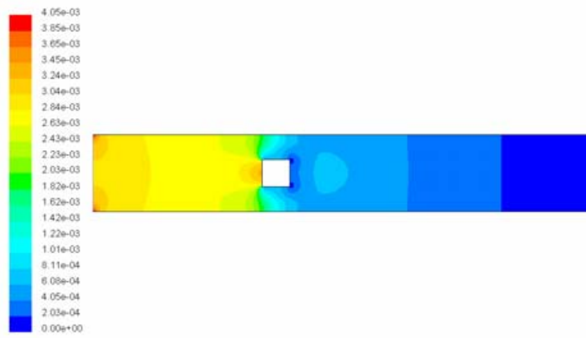

(a)

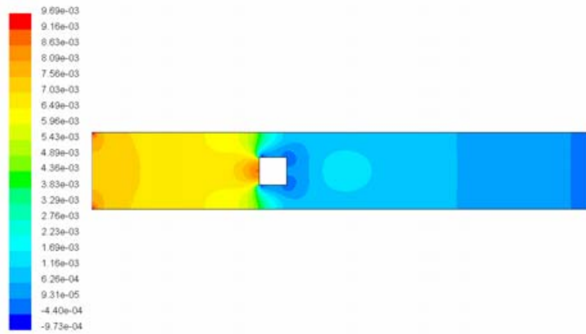

(b)

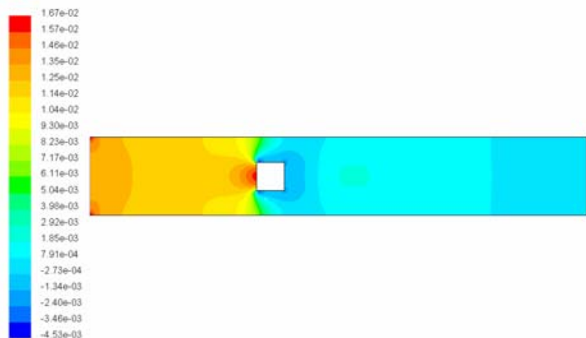

(c)

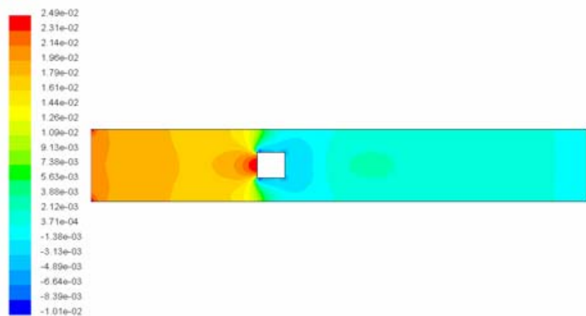

(d)

[Fig.A.7] Pressure (Static) Contours for an Obstruction size of 11x11 at Various Reynolds Number (a) 300, (b) 600, (c) 900, (d) 1200

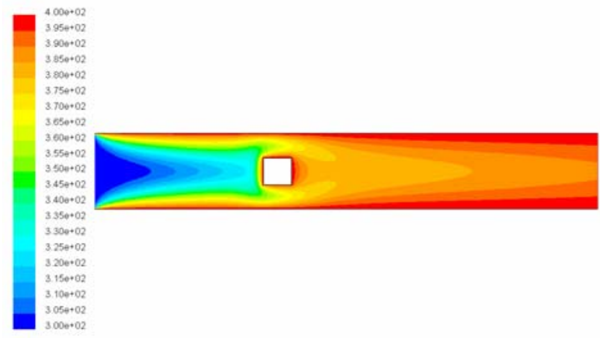

(a)

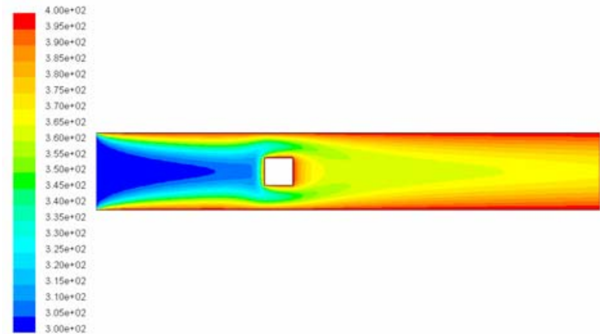

(b)

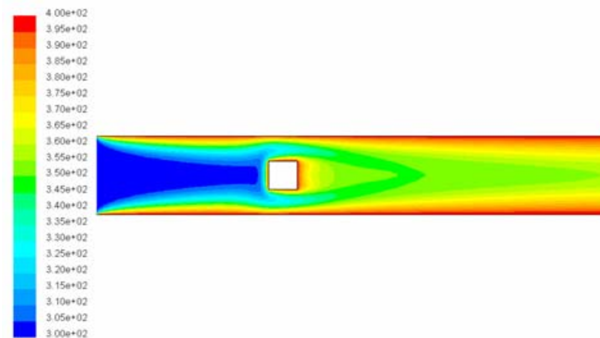

(c)

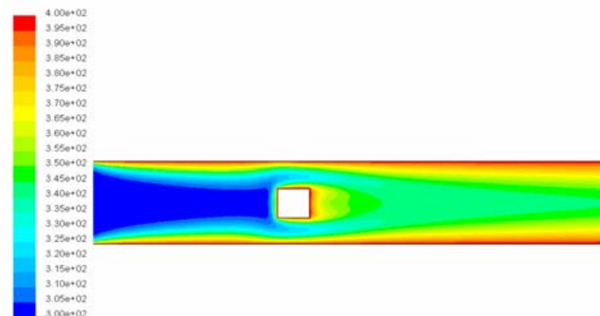

(d)

[Fig.A.8] Temperature (Static) Contours for an Obstruction Size of 11x11 at various Reynolds Number (a) 300, (b) 600, (c) 900, (d) 1200

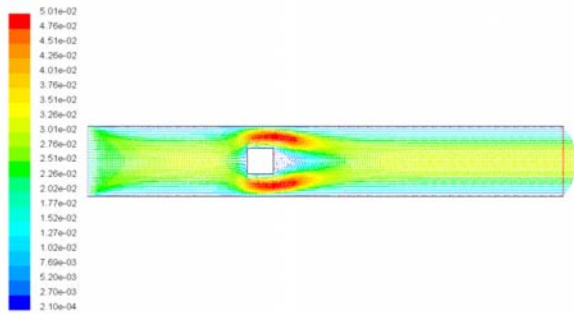

(a)

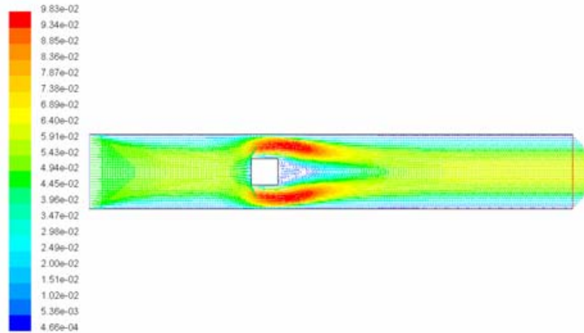

(b)

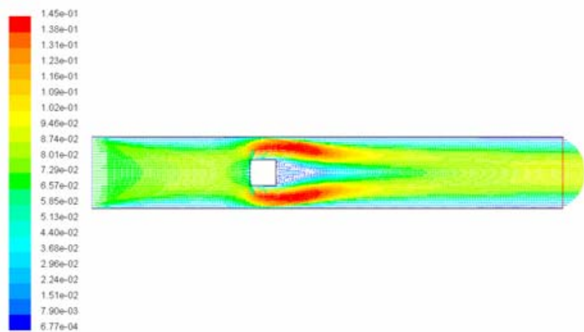

(c)

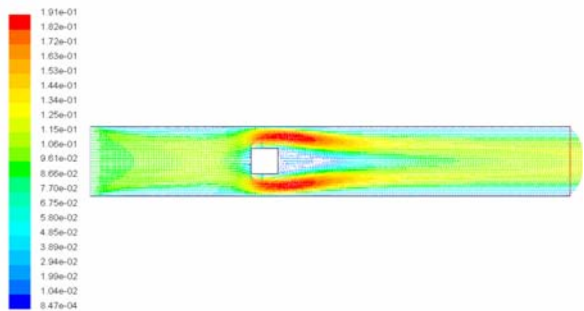

(d)

[Fig.A.9] Velocity Profiles for an Obstruction Size of 11x11, for Various Reynolds No. (a) 300, (b) 600, (c) 900, (d) 1200

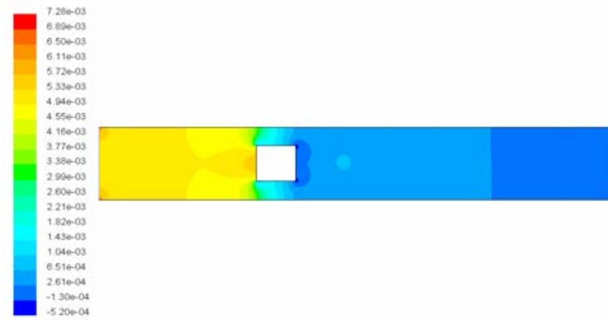

(a)

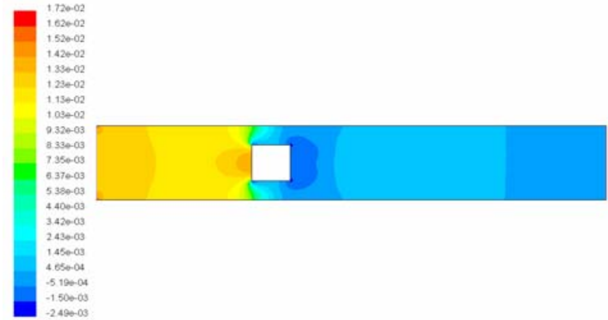

(b)

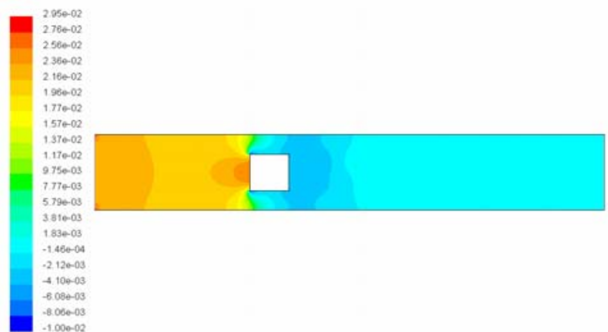

(c)

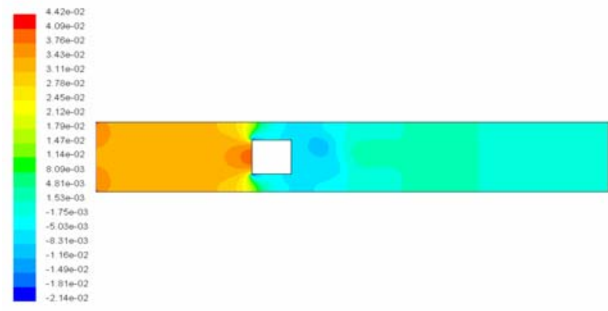

(d)

[Fig.A.10] Pressure (Static) Contours for an Obstruction of 15x15, for Various Reynolds Number (a) 300, (b) 600, (c) 900, (d) 1200

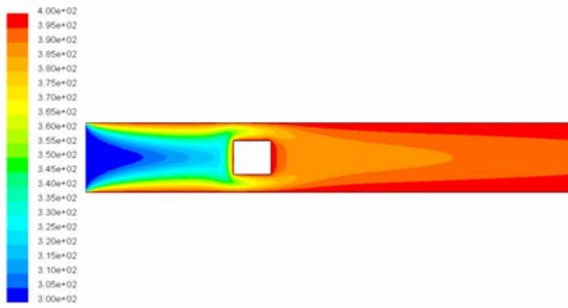

(a)

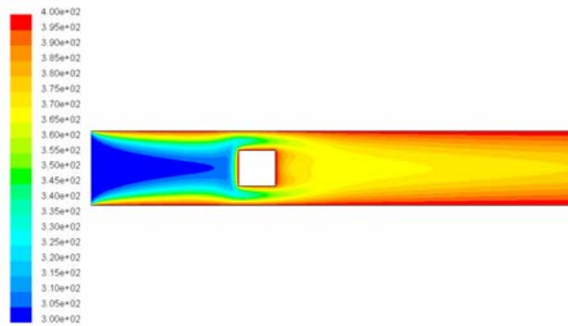

(b)

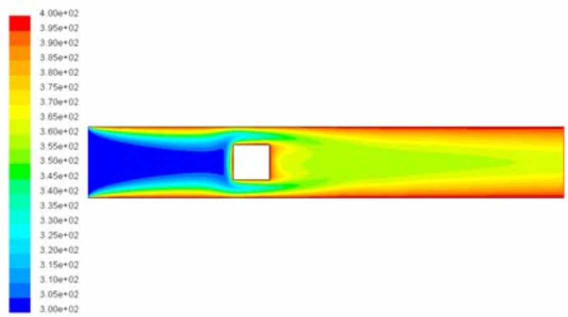

(c)

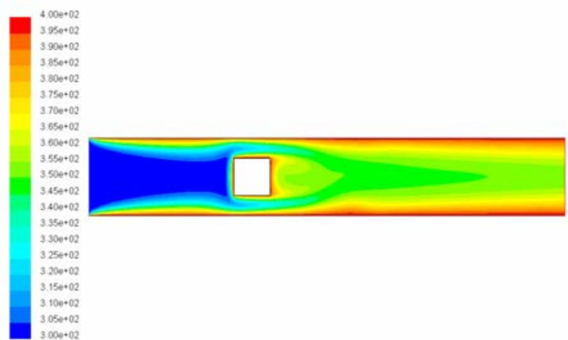

(d)

[Fig.A.11] Temperature (Static) Contours for an Obstruction Size of 15x15 at various Reynolds Number (a) 300, (b) 600, (c) 900, (d) 1200

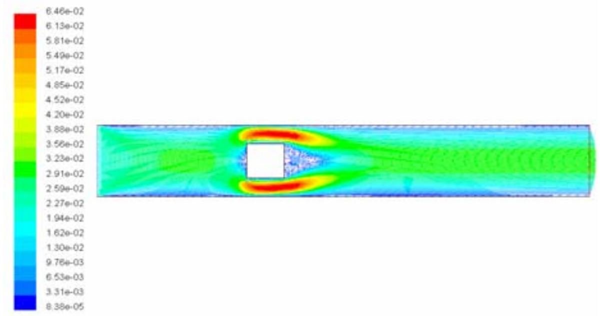

(a)

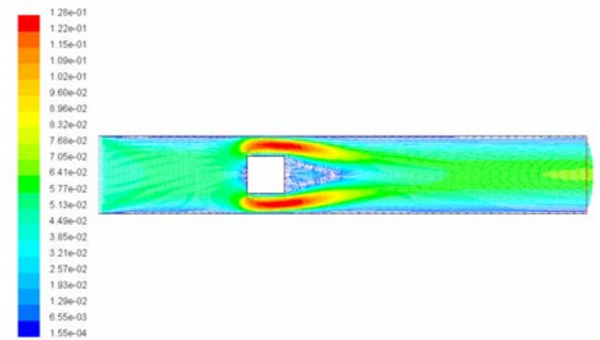

(b)

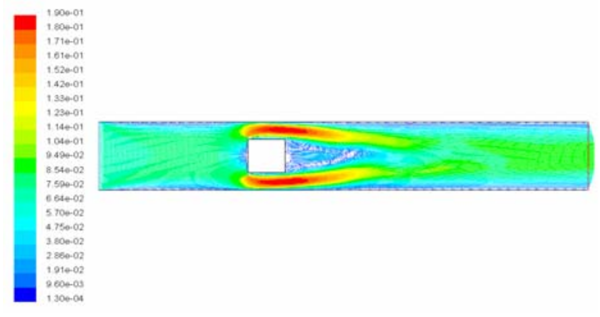

(c)

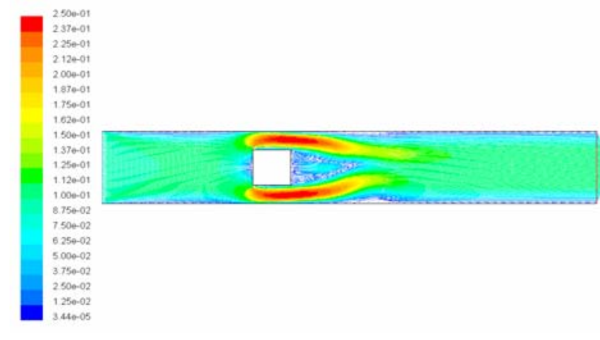

(d)

[Fig.A.12] Velocity Profiles for an Obstruction Size of 15x15, for Various Reynolds Number (a) 300, (b) 600, (c) 900, (d) 1200

Appendix-B: PROGRAMME FOR CHIP COOLING

```
cmmmmmmmmmmmmmmmmmmmmmmmmmmmmmmmmmmmmmmmmmmmmmmmmmmmmmmmmmmm
c       program willi
c*****************************************************************
c*      program  willi for computing flow field in a channel
c*      with built in square cylinder
c* tape1 = restart field
c* tape2 = symmetry and frequency
c* tape3 = output for restart
c* tape8 = input data
c*****************************************************************
            include  'header.h'
c           ianf=mclock()
            write(*,23)
 23         format('has entered willi')
            call init
            if ( irest.eq.0) call start
            if ( irest.eq.1) call restar
 10        call conti
c
            open (3,file='iwrite',form='formatted')
            read (3,*)iwrite
            close(3)
c
c           if(iwrite.eq.1) then
c           call otre
c           end if
            call bcns
            call ticorr
            call otpt
            call energy
            call nseqcp
            call bcns
            call tigrad
c
c     **************************************
            if(ita.gt.400) epsi=0.005
            if(ita.lt.400.and.ita.gt.300)epsi=0.01
            if(ita.lt.300.and.ita.gt.200)epsi=0.05
            if(ita.lt.200.and.ita.gt.100)epsi=0.1
            if(ita.lt.100)epsi=0.5
            write(*,123) epsi
```

```
 123      format(  'epsi  = ',e10.4,$)
          goto 10
          end
c
mmmmmmmmmmmmmmmmmmmmmmmmmmmmmmmmmmmmmmmmmmmmmmmmmmmmmmmmmmmm
          subroutine init
c       initiation of computing data
cccccccccccccccccccccccccccccccccccccccccccccccccccccccccccccccccccccccc
c
          include 'header.h'
c
          write(6,*)'has entered init'
          open(8,file='daten')
          read(8,*)irest,iuprof,iexit,stab,updef,iim,jim,jn1,
     &            jnim,ia,ib,ja,jb,itamax,fx,fy,epsi,stat,
     &            tstat,beta0,alphat,re,pr,twall,
     &            tobs,tentry,grf,ifcp
         write(*,*)' irest =',irest,' iuprof =',iuprof,'iexit =',
     &    iexit,'stab =',stab,'updef =',updef,'iim =',iim,' jim =',
     &    jim,'jn1 =',jn1
          write(*,*)' jnim=',jnim,' ia =',ia,' ib =',ib,' ja =',ja,
     &    ' jb =',jb,'itamax =',itamax,'fx =',fx,'fy =',fy,'epsi=',
     &    epsi,' stat =',stat
          write(*,*)' tstat =',tstat,' beta0=',beta0,' alphat =',alphat,
     &   ' re =',re,' pr =',pr,'twall =',twall,' tobs =',tobs,
     &   ' tentry =',tentry,'grf =',grf,'ifcp =',ifcp

c                   initialize vectors
                    do 120 i=1,mf
             do 120 j=1,nf
                    u2(mf,nf)=0.0
                    v2(mf,nf)=0.0
                    u1(mf,nf)=0.0
                    v1(mf,nf)=0.0
           t1(mf,nf)=0.0
                    t2(mf,nf)=0.0
         p(mf,nf)=0.0
             psi(mf,nf)=0.0
                    udym(mf,nf)=0.0
                    vdxm(mf,nf)=0.0
 120                continue
             do 140 i=1,mf
                    x(mf)=0.0
             nux(mf)=0.0
 140                continue
                    do 160 j=1,nf
                    qinlet(nf)=0.0
                    y(nf)=0.0
```

```
        tinlet(nf)=0.0
 160             continue
c
          ire=iim-1
          jre=jim-1
          ita=0
          isum=0
c
          deltay=fy/(jre-1)
          deltax=fx*deltay
          dtmax=1.0
c
          rdx=1.0/deltax
          rdy=1.0/deltay
c
          do 10 i=1,ire
          x(i)=real(i-1)*deltax
c         write(*,*)i,x(i)
 10      continue
c
         do 20 j=1,jre
         y(j)=real(j-1)*deltay
c        write(*,*)j,y(j)
 20      continue

c         pause
          deltx2=deltax**2
          delty2=deltay**2
c
c  *********  constant properties   ************
c
          deltat=stab*deltay
          rev=1.0/re
          pev=1.0/(re*pr)
          idt=iim-2
          jdt=jim-2
c
          return
          end

ccccccccccccccccccccccccccccccccccccccccccccccccccccccccccccccccccccccccccccccccc
          subroutine start
c         start conditions
cccccccccccccccccccccccccccccccccccccccccccccccccccccccccccccccccccccccccccccccccccc
c
          include 'header.h'
c
          zeit=0.0
```

```
c
c  ******  start of a parabolic calculation  ******
c
          write(6,*)'has entered start'
c
          jpr=jim-1
          jp1=2
          rpmj=(jpr+jp1)*0.5
          rj=real(jpr)+0.5-rpmj
c
          if((dabs(fy-1.0)).le.0.001) then
          do 30 j=1,jim
c
c  ****** parabolic velocity profile  ******
c
          if(iuprof.eq.2) then
          qinlet(j)=1.5*(1.-(((rpmj-real(j))**2)/(rj**2)))
          else
          qinlet(j)=1.0
          endif
c
c  ****** constant temperature profile ******
c
          tinlet(j)=tentry
 30       continue
          endif
c  ****** defining the inlet profile  ********
c
          do 31 i=1,iim
          do 31 j=1,jim
          u2(i,j)=qinlet(j)
          v2(i,j)=0.0
          p(i,j)=1.0
          t1(i,j)=tentry
 31       continue
c
          return
          end
cccccccccccccccccccccccccccccccccccccccccccccccccccccccccccccccccccccccccccccccc
          subroutine restar
ccccccccccccccccccccccccccccccccccccccccccccccccccccccccccccccccccccccccccccccccc
          include 'header.h'
c
          write(6,*) 'has entered restar'
          open (1,file='result1',form='formatted')
          read(1,*)ita,zeit,deltat
          do 200 i=1,iim
          do 200 j=1,jim
```

```
      read(1,*)l,m,u2(i,j),v2(i,j),p(i,j),t1(i,j)
 200  continue
      close (1)
      i=1
      do 202 j=1,jim
      qinlet(j)=u2(i,j)
 202  continue
c
      return
      end
cccccccccccccccccccccccccccccccccccccccccccccccccccccccccccccc
      subroutine conti
c     pressure iteration
cccccccccccccccccccccccccccccccccccccccccccccccccccccccccccccc
c
      include 'header.h'
      write (6,*)'has entered conti'
      iti=0
      ita=ita+1
      beta=beta0/(2.0*deltat*(1.0/deltx2+1.0/delty2))
 40   call bcc
      call ceqcp
c     ende=second()
c     if((ende-anf).ge.550. .and. (ende-anf).1e.560.)call otre
c
      if(divmax.ge.epsi) goto 40
c
      write(6,41)ita,iti,isum,divmax,imax,jmax
 41   format(2x,3i7,4x,e15.8,2i5,1x,'from ceqcp')
c
      return
      end

cccccccccccccccccccccccccccccccccccccccccccccccccccccccccccccc
      subroutine bcc
c     boundary conditions for the mass continuity equation
c     conditions for the confining surfaces
cccccccccccccccccccccccccccccccccccccccccccccccccccccccccccccc
c
      include 'header.h'
c
      i=1
      do 50 j=1,jim
      u2(i,j)=qinlet(j)
 50   continue
c
      j=1
      do 51 i=1,iim
```

```
          v2(i,j)=0.
 51       continue
c
          j=jim
          do 52 i=1,iim
          v2(i,j-1)=0.0
 52       continue
c
c  ******  obstacle boundary conditions  ********
          call bcobw
c ************************************************
c
          if(iti.ge.1) goto 55
c
          if (iexit.eq.1) then
          i=iim-2
          do 53 j=1,jim
          u2(i+1,j)=u2(i,j)
          v2(i+1,j)=v2(i,j)
 53       continue
          end if
          if (iexit.eq.2) then
          i=iim-2
          do 54 j=1,jim
          u2(i+1,j)=2.*u2(i,j)-u2(i-1,j)
          v2(i+1,j)=2.*v2(i,j)-v2(i-1,j)
 54       continue
          end if
 55       return
          end

ccccccccccccccccccccccccccccccccccccccccccccccccccccccccccccc
          subroutine bcobw
c      bstacle-boundary-conditions for bcc,bcns
cccccccccccccccccccccccccccccccccccccccccccccccccccccccccccccc
c
c  ****** boundary conditions for the obstacle *********
c
          include 'header.h'
          do 60 i=(ia-1),ib
          do 60 j=ja,jb
          u1(i,j)=0.0
          u2(i,j)=0.0
 60       continue
c
          do 61 i=ia,ib
          do 61 j=(ja-1),jb
          v1(i,j)=0.
```

```
      v2(i,j)=0.
 61   continue
      return
      end
ccccccccccccccccccccccccccccccccccccccccccccccccccccccccccc
      subroutine ceqcp
c     mass continuity equation for constant properties
ccccccccccccccccccccccccccccccccccccccccccccccccccccccccccc
c
      include 'header.h'
      divmax=0.
      dalt=0.
      imax=0
      jmax=0
c
      do 70 i=2,ire
      do 70 j=2,jre
c
      div=(u2(i,j)-u2(i-1,j))/deltax
      $   +(v2(i,j)-v2(i,j-1))/deltay
      deltap=-beta*div
      a=deltat*deltap
      ax=a/deltax
      ay=a/deltay
c
      p(i,j)=p(i,j)+deltap
      u2(i,j)=u2(i,j)+ax
      u2(i-1,j)=u2(i-1,j)-ax
      v2(i,j)=v2(i,j)+ay
      v2(i,j-1)=v2(i,j-1)-ay
c
      dab=dabs(div)
      if(dab.gt.dalt) then
      divmax=dab
      imax=i
      jmax=j
      end if
      dalt=divmax
c
 70   continue
c
      iti=iti+1
      isum=isum+1
c
      if(iti.eq.1 .or.iti.eq.(iti/50*50)) then
      write(6,71)ita,iti,isum,divmax,imax,jmax
 71   FORMAT(2x,3i7,4x,e15.8,2i5,1x,'from ceqcp')
      end if
```

```
c           write (6,*)'leaving ceqcp'
            return
            end
ccccccccccccccccccccccccccccccccccccccccccccccccccccccccccccccc
            subroutine otre
ccccccccccccccccccccccccccccccccccccccccccccccccccccccccccccccc
c
            include 'header.h'
c
            write(6,*)'has entered otre'
            open(1,file='result1',form='formatted')
            write(1,*) ita,zeit,deltat
            do 190 i=1,iim
            do 190 j=1,jim
            write(1,*) i,j,u2(i,j),v2(i,j),p(i,j),t2(i,j)
 190        continue
            close(1)
            stop
            end
ccccccccccccccccccccccccccccccccccccccccccccccccccccccccccccccc
            subroutine bcns
c       boundary conditions for the       navier stokes equations
c       conditions for the confining surfaces
ccccccccccccccccccccccccccccccccccccccccccccccccccccccccccccccc
            include 'header.h'
c
            j=2
            do 170 i=1,iim
            u2(i,j-1)=jn1*u2(i,j)
            v2(i,j-1)=0.0
 170        continue
c
            j=jim
            do 171 i=1,iim
            u2(i,j)=jnim*u2(i,j-1)
            v2(i,j-1)=0.0
 171        continue
c
            i=1
            do 172 j=1,jim
            u2(i,j)=qinlet(j)
            v2(i,j)=-v2(i+1,j)
 172        continue
c
c   ********  obstacle boundary conditions  ***********
            call bcobw
            return
            end
```

```
cccccccccccccccccccccccccccccccccccccccccccccccccccccccccccccccc
      subroutine velalt
c     alternation of the velocity arrays
cccccccccccccccccccccccccccccccccccccccccccccccccccccccccccccccc
      include 'header.h'
c
      do 80 i=1,iim
      do 80 j=1,jim
      u1(i,j)=u2(i,j)
      v1(i,j)=v2(i,j)
 80   continue
      return
      end

cccccccccccccccccccccccccccccccccccccccccccccccccccccccccccccccc
    subroutine ticorr
c     calculation of time time-increment
cccccccccccccccccccccccccccccccccccccccccccccccccccccccccccccccc
c
      include 'header.h'
c
      utop=0.0
       vtop=0.0
c
      do 90 i=2,ire
      do 90 j=2,jre
      uchek=0.5*(u2(i,j)+u2(i-1,j))
      vchek=0.5*(v2(i,j)+v2(i,j-1))
      utop=dmax1(utop,abs(uchek))
      vtop=dmax1(vtop,abs(vchek))
 90   continue
c
      if(vtop.le.0.0) goto 91
c
      umax=deltax/utop
      vmax=deltay/vtop
c
      deltat=dmin1(umax,vmax)
      goto 92
 91   continue
c
      deltat=deltax/utop
c
 92   continue
c
      deltat=stab*deltat
      deltch=0.5*(deltx2*delty2/(deltx2+delty2))*re
c
```

```
      write(*,93)deltat
      write(*,94)deltch
c
 94   format(3x,'deltch  ',e13.5)
 93   format(3x,'deltat  ',e13.5)
      deltat=dmin1(deltat,deltch)
      write(*,*)'deltamin=  ',deltat
c
c  **** alpha factor  *******
c
      udel=deltat/umax
      vdel=deltat/vmax
c
      alpha=updef*dmax1(udel,vdel)
c
      write(*,95)alpha
 95   format(3x,' alpha = ',e13.5)
c
      return
      end
cccccccccccccccccccccccccccccccccccccccccccccccccccccccccccccccc
      subroutine otpt
cccccccccccccccccccccccccccccccccccccccccccccccccccccccccccccccc
c
      include 'header.h'
c
      write(6,*) 'has entered otpt'
      open (2, file='fre1000', form='formatted')
      t0=ita*deltat
      write(2,*)t0,v2(100,17)
      open (12, file='cl1000', form='formatted')
c
c ****   calculation of cl ******
c
      cpsum=0.0
      do 192 i=ia,ib
      q1=8.*re*deltay
      q2=3.*(v2(i,ja-2)-2.*v2(i,ja-1))
      q3=9.*p(i,ja-1)/8.
      q4=p(i,ja-2)/8.
      ppb=q3-q4+(q2/q1)
      q5=3.*(v2(i,jb+2)-2.*v2(i,jb+1))
      q6=9.*p(i,jb+1)/8.
      q7=p(i,jb+2)/8.
      ppt=q6-q7-(q5/q1)
      cpsum=cpsum+2.*(ppb-ppt)
 192  continue
      cp1=cpsum/(ib-ia)
```

```
      sl=0.
      sr=0.
      s1=2./re
      cfsum=0.
      do 193 j=ja,jb
      y1=3.*deltax
      y2=9.*v2(ia-1,j)-v2(ia-2,j)
      sl=sl+(y2/y1)
      y3=9.0*v2(ib+1,j)-v2(ib+2,j)
      sr=sr+(y3/y1)
      cfsum=cfsum+s1*(sl+sr)
 193  continue
      cf1=cfsum/(jb-ja)
      cl=cp1+cf1
c
c ***** writing cl into file cl *******
      write(12,*)t0,cl
c
      if(dtmax.le.stat.or.ita.ge.itamax) then
     open (1, file='uv800',form='formatted')
      open (2, file='pt800',form='formatted')
      open (11, file='nux800',form='formatted')
      write(1,*)ita,zeit,deltat
      write(2,*)ita,zeit,deltat
      do 197 i=1,iim
      do 197 j=1,jim
      write(1,*)i,j,u2(i,j),v2(i,j)
      write(2,*)i,j,p(i,j),t2(i,j)
 197  continue
      close(1)
      close(2)
      call psifunc
c     calculate the nusselt number
      j=2
      do 120 i=2,ire
      nux(i)=-(-25.0*t2(i,j)+48.0*t2(i,j+1)-36.0*t2(i,j+2)
     1  +t2(i,j+3)-3.0*t2(i,j+4))/(12.0*deltay)
      write(11,*)i,nux(i)
 120 continue
     close(11)
      stop
      endif
      return
      end

cccccccccccccccccccccccccccccccccccccccccccccccccccccccccccccc
      subroutine nseqcp
c   navier stokes equations for constant properties
```

```
cccccccccccccccccccccccccccccccccccccccccccccccccccccccccccccccc
c
      include 'header.h'
      write(6,*)'has entered nseqcp'
c
      zeit=zeit+deltat
      do 150 i=2,(ire-1)
     do 150 j=2,jre
c
c ************ obstacle boundary conditions  *****************
      if (i.ge.(ia-1).and.i.le.ib) then
      if (j.eq.ja) then
      u1(i,j)=-u1(i,j-1)
      endif
      if(j.eq.jb) then
      u1(i,j)=-u1(i,j+1)
      endif
      endif
c
      if(i.eq.(ia-1)) then
      if(j.ge.(ja-1).and.j.le.jb) then
      v1(i+1,j)=-v1(i,j)
      endif
      endif
c
      if(i.eq.(ib+1)) then
      if(j.ge.(ja-1).and.j.le.jb) then
      v1(i-1,j)=-v1(i,j)
      endif
      endif
c
ccccccccccccccccccc  d i f f - u  cccccccccccccccccccccccccccccccc
c     duudx
      u1a=u1(i-1,j)+u1(i,j)
      u22=u1(i-1,j)-u1(i,j)
      u3=u1(i,j)+u1(i+1,j)
      u4=u1(i,j)-u1(i+1,j)
c
c     duv /dy
      u5 =u1(i,j-1)+ u1(i,j)
      u6 =u1(i,j-1)-u1(i,j)
      u7 =u1(i,j)+u1(i,j+1)
      u8 =u1(i,j)-u1(i,j+1)
c
c     duv /dx
      u13=u1(i-1,j)+u1(i-1,j+1)
      u14=u7
c
```

```
cccccccccccccccccccccccc  d i f f - v ccccccccccccccccccccccccccccc
c
c          dvu /dx
           v1a=v1(i,j-1) + v1(i+1,j-1)
           v22=v1(i,j)   + v1(i+1,j)
c
c          duv /dx
           v3 =v1(i-1,j) + v1(i,j)
           v4 =v1(i-1,j) -          v1(i,j)
           v5 =v1(i,j)   + v1(i+1,j)
           v6 =v1(i,j)   - v1(i+1,j)
c
c          dvv /dy
           v7 =v1(i,j-1) + v1(i,j)
           v8 =v1(i,j-1) - v1(i,j)
           v9 =v1(i,j)   + v1(i,j+1)
           v10=v1(i,j)   - v1(i,j+1)
c
ccccccccccccccccccccccccccc u - deq    ccccccccccccccccccccccccccccc
c
           d2udx2=(u22 - u4)/deltx2
           d2udy2=(u6 - u8)/delty2
            dpdx=(p(i,j)-p(i+1,j))/deltax
c
            duudx=0.25*(u1a*u1a + alpha*dabs(u1a)*u22 -
    $        u3*u3 - alpha*dabs(u3)*u4)/deltax
            dvudy=0.25*( v1a*u5 + alpha *dabs(v1a)*u6 -
    $           v22*u7 - alpha*dabs(v22)*u8)/deltay
c
            u2(i,j)=deltat*(duudx+dvudy+dpdx+rev*(d2udx2+d2udy2))+u1(i,j)
c
cccccccccccccccccccccccc   v  - deq   cccccccccccccccccccccccccccc
c
            d2vdx2=(v4 - v6)/deltx2
            d2vdy2=(v8 - v10)/delty2
c
            dpdy = (p(i,j) - p(i,j+1))/deltay
c
            duvdx = 0.25*(u13*v3 +alpha*dabs(u13)*v4-
    $         u14*v5 - alpha*dabs(u14)*v6)/deltax
c
            dvvdy = 0.25*(v7*v7 +alpha*dabs(v7)*v8 -
    $           v9*v9 - alpha*dabs(v9)*v10)/deltay
c
c           body force due to buoyancy
            thf= t1(i,j) +t1(i,j+1)
            gy = 0.5*grf*rev*thf*rev*ifcp
c
```

```
          v2(i,j) = deltat*(duvdx +dvvdy +dpdy +rev*(d2vdx2 +d2vdy2)
     $   +gy)+v1(i,j)
c
 150      continue
c
          return
          end

ccccccccccccccccccccccccccccccccccccccccccccccccccccccccccccccc
          subroutine tigrad
c         maximum of the velocity alternation during a zeit increment
ccccccccccccccccccccccccccccccccccccccccccccccccccccccccccccccc
          include 'header.h'
c
          dtmax=0.
          dumax=0.
          dvmax=0.
c
          do 180 i=2,(ire -1)
          do 180 j=2,jre
c
          dudt=dabs(u1(i,j)-u2(i,j))/deltat
          dvdt=dabs(v1(i,j)-v2(i,j))/deltat
c
          dact=dtmax
          dtmax=dmax1(dtmax,dudt,dvdt)
          if(dtmax.le.dact) goto 180
          idtm=i
          jdtm=j
 180      continue
c
c  ********  constant properties   **********
c
          write(6,182) idtm,jdtm,dtmax
 182      format(2x,'maximum change in velocity ',2x,2i5,e13.5)
          if (dtmax*.1 .le. epsi) epsi = dtmax*.1
          return
          end
ccccccccccccccccccccccccccccccccccccccccccccccccccccccccccccccc
          subroutine energy
c         solution of the energy equation
ccccccccccccccccccccccccccccccccccccccccccccccccccccccccccccccc
          include 'header.h'
c
          write(6,*) 'has entered energy'
c
c  ******* plate fin with stamping  ********
          itt=0
```

```
 100      call bctc
c  *****  constant properties   ********
c
          call teqcp
c
          call temalt
c
          if(dt.ge.tstat) goto 100
c
          call bctc
c
          write(6,102) itt,dt,itmax,jtmax
 102      format(2x,'temp.iter.= ',i5,2x,'delta.temp.= ',e18.10,1x,2i4)
c
          return
          end
cccccccccccccccccccccccccccccccccccccccccccccccccccccccccccccccc
          subroutine bctc
          temperature - boundary - conditions for the confining surfaces
cccccccccccccccccccccccccccccccccccccccccccccccccccccccccccccccc
c
          include 'header.h'
c
          write (6,*) 'has entered bctc'
          s1=(1-jn1)*0.5
          s2=(1+jn1)*0.5
          s3=(1-jnim)*0.5
          s4=(1+jnim)*0.5
c
          tw5=5.*twall
          te4=4.*tentry
          f112=11./2.
          f32=3./2.
c
          i=1
          do 110 j=1,jim
          t1(i,j)=te4-4.*t1(i+1,j)+t1(i+2,j)
 110     continue
c
          j=1
          do 111 i=1,iim
          t1(i,j)=s1*(tw5-f112*t1(i,j+1)+f32*t1(i,j+2))
          &    +s2*t1(i,j+1)
 111      continue
c
          j=jim
          do 112 i=1, iim
          t1(i,j)=s3*(tw5-f112*t1(i,j-1)+f32*t1(i,j-2))
```

```
     $    +s4*t1(i,j-1)
 112      continue
c
          i=iim
          do 113 j=1,jim
          t1(i,j)=2.*t1(i-1,j)-t1(i-2,j)
 113      continue
          write (6,*)'leaving bctc'
          return
          end

ccccccccccccccccccccccccccccccccccccccccccccccccccccccccccccccc
          subroutine teqcp
c         energy equation for constant properties
ccccccccccccccccccccccccccccccccccccccccccccccccccccccccccccccc
c
          include 'header.h'
c
          write(6,*) 'has entered teqcp'
          al=alphat
          dt=0.
          dalt=0.
          deltt=0.0010
          itt=itt+1
c
c
          do 120 i=2,ire
          do 120 j=2,jre
c
c  *******   temperature obstacle boundary conditions  **********
c
          if(i.ge.ia.and.i.le.ib) then
          if(j.eq.ja) then
          t1(i,j)=2.*tobs-t1(i,j-1)
          end if
          if(j.eq.jb) then
          t1(i,j)=2.*tobs-t1(i,j+1)
          end if
          end if
c
          if(i.eq.ia) then
          if(j.ge.ja.and.j.le.jb) then
          t1(i,j)=2.*tobs-t1(i-1,j)
          end if
          end if
c
          if(i.eq.ib) then
          if(j.ge.ja.and.j.le.jb) then
```

```
      t1(i,j)=2.*tobs-t1(i+1,j)
      end if
      end if
c
      t1a=t1(i,j)+t1(i+1,j)
      t2a=t1(i,j)-t1(i+1,j)
      t3=t1(i-1,j)+t1(i,j)
      t4=t1(i-1,j)-t1(i,j)
      t5=t1(i,j)+t1(i,j+1)
      t6=t1(i,j)-t1(i,j+1)
      t7=t1(i,j-1)+t1(i,j)
      t8=t1(i,j-1)-t1(i,j)
c
      dtudx=(u2(i,j)*t1a+al*dabs(u2(i,j))*t2a
     &   -u2(i-1,j)*t3-al*dabs(u2(i-1,j))*t4)*0.5/deltay
      dtvdy=0.0
c
      d2tdx2=(t4-t2a)/deltx2
      d2tdy2=(t8-t6)/delty2
c
      residt=deltt*(-dtudx-dtvdy+pev*(d2tdx2+d2tdy2))
c
      t2(i,j)=t1(i,j)+residt
c
      if(i.ge.ia .and. i.le.ib) then
      if(j.ge.ja .and. j.le.jb) then
      t1(i,j)=tobs
      t2(i,j)=tobs
      end if
      end if
c
      dab=dabs(t2(i,j)-t1(i,j))
      if(dab.gt.dalt) then
      dt=dab
      itmax=i
      jtmax=j
      end if
      dalt=dt
c
 120  continue
c
      if(itt.eq.1 .or. itt.eq.(itt/25*25)) then
      write(*,121) itt,dt,itmax,jtmax
 121  format(2x,'temp.iter.=',i5,2x,'delta.temp.=',e18.10,1x,2i4)
      end if
c
      return
      end
```

```
cccccccccccccccccccccccccccccccccccccccccccccccccccccccccccccccc
      subroutine temalt
c      alternation of the temperature arrays
cccccccccccccccccccccccccccccccccccccccccccccccccccccccccccccccc
c
      include 'header.h'
      do 140 i=1,iim
      do 140 j=1,jim
      t1(i,j)=t2(i,j)
 140  continue
      return
      end

cccccccccccccccccccccccccccccccccccccccccccccccccccccccccccccccc
      subroutine psifunc
c     calculation of psi
cccccccccccccccccccccccccccccccccccccccccccccccccccccccccccccccc
c
      include 'header.h'
c
c
       do 10 i=3,ire-1
       do 10 j=3,jre-1
       udy1=0.5*(u2(i,j)+u2(i,j+1))*deltay
       udy2=0.5*(u2(i,j)+u2(i,j-1))*deltay
       udym(i,j)=0.5*(udy1+udy2)
 10    continue

       do 30 j=3,jre-1
       do 30 i=3,ire-1
       vdx1=0.5*(v2(i,j)+v2(i+1,j))*deltax
       vdx2=0.5*(v2(i,j)+v2(i-1,j))*deltax
       vdxm(i,j)=0.5*(vdx1+vdx2)
 30    continue

       do 40 i=2,ire
       do 40 j=2,jre
 40    psi(i,j)=udym(i,j)-vdxm(i,j)
       do 60 i=ia-1,ib+1
       do 60 j=ja-1,jb+1
       psi(i,j)=0.0
 60    continue
c
       open (3, file='psi800',form='formatted')
       do 20 i=1,iim
       do 20 j=1,jim
 20    write(3,*)i,j,psi(i,j)
```

```
          close(3)
          open (12, file='vector800',form='formatted')
          do 100 i=2,ire
          do 100 j=2,jre
          vmagnitude(i,j)=dsqrt(u2(i,j)*u2(i,j)+v2(i,j)*v2(i,j))
          if(dabs(u2(i,j)).le.0.0d00)then
          vangle(i,j)=0.5*3.14159265
          else
          vangle(i,j)=datan(v2(i,j)/u2(i,j))
          endif
 100      continue
c
          do 120 i=ia,ib
          do 120 j=ja,jb
          vmagnitude(i,j)=0.0
          vangle(i,j)=0.0
 120      continue
          do 140 i=2,ire,4
          do 140 j=2,jre,2
          if((i.ge.ia.and.i.le.ib).and.(j.ge.ja.and.j.le.jb))goto 140
          write(12,*)i,j,vangle(i,j),vmagnitude(i,j)
 140      continue
          close(12)
          return
          end
cccccccccccccccccccccccccccccccccccccccccccccccccccccccccccccccc
          header.h
cccccccccccccccccccccccccccccccccccccccccccccccccccccccccccccccc
          implicit real*8(a-h,o-z)
          parameter (mf=210,nf=40)
          common /fix/stab,updef
          common /vari1/ iim,jim,ire,jre,idt,jdt,icn,itmax,jtmax,imax,jmax
          common /vari2/ deltax,deltay,deltx2,delty2,epsi,dtmax,stat
          common /vari3/ itamax,divmax,dt,re,rev,pr,pev
          common /vari4/ tentry,twall,alphat,grf,tobs,zeit,anf,ende
          common /vari5/ beta0,tstat,deltat,utop,ita,iti,isum,beta
          common /vari6/ itt,ia,ib,ja,jb,rdx,rdy,fx,fy,iwrite
          common /vari7/ jn1,jnim,alpha,iuprof,iexit,ifcp,irest
          common /vector/ u2(mf,nf),v2(mf,nf),u1(mf,nf),v1(mf,nf),
          common /vector/ t1(mf,nf),t2(mf,nf),p(mf,nf),qinlet(nf),x(mf)
          common /vector/ y(nf),nux(mf),tinlet(nf),psi(mf,nf),
          common /vector/ udym(mf,nf),vdxm(mf,nf),uinlet(nf),vinlet(nf)
          common /vector/ vangle(mf,nf),vmagnitude(mf,nf)

              common /corbx/ u1a,u22,u3,u4,u5,u6,u7,u8,u13,u14,
   &           v1a,v22,v3,v4,v5,v6,v7,v8,v9,v10
              common /corbxt/t1a,t2a,t3,t4,t5,t6,t7,t8
cccccccccccccccccccccccccccccccccccccccccccccccccccccccccccccccc
```

daten file

```
cccccccccccccccccccccccccccccccccccccccccccccccccccccccccccccccc
0,1,2,0.35,1.35,200,34,-1,-1,68,72,16,19,2000,1.0,1.0,0.5,0.001,
0.01,1.8,1.0,1200,0.7,1.0,
1.0,0.0,0.0,0
cccccccccccccccccccccccccccccccccccccccccccccccccccccccccccccccc
read(8,*)irest,iuprof,iexit,stab,updef,iim,jim,jn1,
     &          jnim,ia,ib,ja,jb,itamax,fx,fy,epsi,stat,
     &          tstat,beta0,alphat,re,pr,twall,
     &          tobs,tentry,grf,ifcp
cccccccccccccccccccccccccccccccccccccccccccccccccccccccccccccccc
```

BIBLIOGRAPHY

1. Culham, J. R. , Yovanovich, M. M., Lemczyk T. F., "Thermal Characterization of Electronic Packages Using a Three-Dimensional Fourier Series Solution", Journal of Electronic Packaging" ASME, September 2000, Vol. 122 , Page 233 -239.
2. Davies, Mark R. D., Cole, Reena., Lohan, John., "Factors Affecting the Operational Thermal Resistance of Electronic Components", Journal of Electronic Packaging, ASME, September 2000, Vol. 122, Page 185-191.
3. Chen, Han-Ting., Horng, Jenn-Tsong., Chen, Po-Li., Hung, Ying-Huei., " Optimal Design for PPF Heat Sinks in Electronics Cooling Applications", Journal of Electronic Packaging, ASME, December 2004, Vol. 126, Page 410-422.
4. Pucha, Raghuram V., Tunga,James, Krishna., "Accelerated Thermal Guidelines for Electronic Packages in Military Avionics Thermal Environment", Journal of Electronic Packaging, ASME, June 2004, Vol. 126, Page 256-264.
5. Zhao, C.Y. , Lu, T.J., "Analysis of Micro Channel Heat Sinks For Electronics Cooling", International Journal of Heat and Mass Transfer, 2002, Vol.45, Page 4857-4869
6. Mukhopadhyay, A., Biswas, G., Sundararajan, T., "Numerical investigation of confined wakes behind a square cylinder in a channel", Int. J. Numerical Methods in Fluids, Vol. 14, pp 1473-1484, 1992.
7. Lee, Tien-Yu Tom., Chambers, Ben., "Application of CFD Technology to Electronic Thermal Management", IEEE Transactions on Components, Packaging, and Manufacturing Technology-Part-B, Vol.18, No.3, August 1995.
8. Hung, T. C., Wangi S. K., & Peter F., "Simulation of Passively Enhanced Conjugate Heat Transfer Across an Array of Volumetric Heat Sources" Communications in Numerical Methods in Engineering, John Wiley & Sons, Ltd. Vol.13, 1997,Page 855-866
9. Bebnia, Masud., Nakayama, Wataru., and Wan, Jeffrey., "CFD Simulations of Heat Transfer from a Heated Module in an Air Stream: Comparison with

Experiments and a Parametric Study" IEEE 1998, Inter Society Conference on Thermal Phenomena

10. Egan, Eric., Amon Cristina H., "Thermal Management Strategies fir Embedded Electronic Components of Wearable Computers", Journal of Electronic Packaging, June 2000, Vol.122, Page 98-106.
11. Gauch, Paul., and Xu, Weiran., "Modelling Phase Change Material in Electronics Using CFD- A Case Study", International Conference on High Density Inter-Connect and Systems Packaging, 2000.
12. Chang, J. Y. , Yu, C. W., Webb, R. L., " Identification of Minimum Air Flow Design for a Desktop Computer using CFD Modelling" Journal of Electronic Packaging, ASME, September 2001, Vol. 123, Page 225-231.
13. Rodgers, Peter J., Eveloy, Valerie C., Davies, Mark R. D., " An Experimental Assessment of Numerical Predictive Accuracy for Electronic Component Heat Transfer in Forced Convection-Part 2, Results and Discussions", Journal of Electronic Packaging, ASME, March 2003, Vol-125, Page 76-83.
14. Leon1, Octavio., Mey, Gilbert De., Jan Vierendeels, Erik Dick., " Comparison Between The Standard and Staggered Layout for Cooling Fins in Forced Convection Cooling", Journal of Electronic Packaging, ASME, September 2003, Vol-125, Page 442-446.
15. Kitamura, Yoji., Ishizuka, Masaru., "Chimney Effect on Natural Cooling of Electronic Equipment Under Inclination.", Journal of Electronic Packaging, December 2004, Vol.126., Page 423-429.
16. Nakayama, W., Matsoukis, R., Hacho, Y., Yakima. "A new role of CFD Simulation in Thermal design of compact electronic equipment: Application of the Build-up approach to thermal analysis of a benchmark model". Journal of electronic packaging, ASME, vol.126, December 2004, Page-440-448.
17. Bhopte, Siddharth.,. Alshuqairi, Musa S., Agonafer, Dereje., Ahmed, Gamal Refai., "Mixed Convection of Impinging Air Cooling Over Heat Sink in Telecom System Application", Journal of Electronic Packaging, ASME, December 2004, Vol. 126, Page 519-523..

18. Jin, L.F., Tou., K.W., Tso., C.P., "Effects of Rotation on Natural Convection Cooling From Three Rows of Heat Sources in a Rectangular Cavity", International Journal of Heat and Mass Transfer, 2004, Vol.48, Page 3982-3994.
19. Roy, A., Bandyopadhyay, G., "Numerical Investigation of Confined Flow past a Square Cylinder Placed in a Channel." IE (I), Vol 85, November 2004.
20. Srikanth, J., and.Tulapurkara, E.G., Biswas. G., "Large Eddy Simulation of Flow Past Built-in-Winglet-Pair in a Rectangular Channel", American Institute of Aeronautics and Astronautics, June 2005.
21. Dhiman, A.K., "Chhabra, R.P., Eswaran, V., "Flow and Heat Transfer Across a Confined Square Cylinder in the Steady Flow Regime: Effect of Pectet Number", International Journal of Heat and Mass Transfer, 48 (2005), Page 4598-4614.
22. Kumara, K. S., "Tulapurkaraa, E.G., Biswasb, G., Gowdac, B.H.L., "Reverse Flow in Channel with Obstruction at Entry", Fluid Dynamic Research, (37) 2005 Page 387-398.
23. Cheng.Y.P , Lee.T.S & Low.H.T, "Numerical Analysis of Mixed Convection in Three Dimensional Rectangular Channel with Flush Mounted Heat Sources Based on Field Synergy Principle", International Journal for numerical methods in fluids(in press)(2006) John Wiley & Sons Ltd,
24. Carlson, D. M., Sullivan, D. C., Bach, R. E, and Resnick, D. R., "The ETA-10 liquid-nitrogen-cooled supercomputer system," IEEE Trans. Electron. *Devices*, vol. 36, no. 8, pp. 1404–1413, Aug. 1989.
25. Schwall, R. E., and Harris, W. S., "Packaging and cooling of low temperature electronics," in Advances in Cryogenic Engineering. New York: Plenum Press, 1991, pp. 587–596.
26. Fujisaki, A., Suzuki, M., and Yamamoto, H., "Packaging technology for high performance CMOS server fujitsu GS8900," IEEE Trans. Adv. Package., vol. 24, pp. 464–469, Nov. 2001.
27. Devoe, Jason., Ortega, Alfonso., "An Investigation of Board Level Effects on Compact Thermal Models of Electronics Chip Packages", IEEE 2000, 18th IEEE SEMI-THERM Symposium

28. Wong, Henry., Peck, Robert E., “Experimental Evaluation of Air-Cooling Electronics at High Altitudes”, Journal of Electronic Packaging” ASME, December 2001, Vol. 123, Page 356-365.
29. Haider, S. I.,. Joshi, Yogendra, K., Nakayama, Wataru., “A Natural Circulation Model of the Closed Loop Two Phase Thermo Syphon for Electronics Cooling” Journal of Heat Transfer, ASME, October 2002, Vol. 124, Page 881-890.
30. Lorenzini, Giulio., Biserni, Cesare., “A Vepotron Effect Application for Electronic Equipment Cooling”, Journal of Electronic Packaging, ASME, December 2003, Vol. 125, Page 475-479.
31. Yoo, Seong-Yeon., Park, Jong-Hark., Chung, Min-Ho., “Local Heat Transfer Character in Simulated Electronic Modules”, Journal of Electronic Packaging, ASME, September 2003, Vol. 125, Page 362-368.
32. Grimes, Ronan., Davies, Mark., “Air Flow and Heat Transfer in Fan Cooled Electronic Systems”, Journal of Electronic Packaging, ASME, Vol.126, March 2004, Page 124-134.
33. Gima, Satoru., Nagata, Takashi., Zhang, Xing., and Fujii, Motoo., “ Experimental Study on CPU Cooling System of Closed Loop Two Phase Thermosyphon”, Heat Transfer- Asian Research 34(3) -2005 Wiley Periodicals.
34. Simionescu, F., Meir, A. J., and Harris, D. K., “Approximation of an optimal convective heat transfer coefficient”, Optim. Control Appl. Meth. (In press), John Wiley & Sons, Ltd. 2006.
35. Rhee, Jinny., Moffat, Robert J., “Experimental Estimate of the Continuous One-Dimensional Kernel Function in a Rectangular Duct with Forced Convection”, Journal of Heat Transfer, ASME, August 2006, Vol-128, Page 811-818.
36. Tae Ho Ji a, Seo Young Kim b, and Jae Min Hyuna, “Heat Dissipation from a Heated Square Cylinder in Osvillating Channel Flow”, IEEE 2006.
37. Harlow, F.H and Welch, J.E., “Numerical Calculation of Time dependent Viscous incompressible flow of Fluid with free surfaces”, The Phys of Fluid, Vol.8, pp2182 2188, 1965
38. Chorin, A.J., “A Numerical Method for Solving Incompressible Viscous Flow Problems”, Journal of Computational Physics, Vol.2, Page 12-26, 1967.

39. Orlanski, I., “A Simple Boundary Condition for Unbounded Flows”, Journal of Computational Physics, Vol. 21, Page 251-269, 1976.

40. Viecelli, J. A., “A Computing Method for Incompressible Flows Bounded by Moving Walls”, Journal of Comput. Phys., Vol8, pp 119-143, 1971.

41. Bergles, A. E. “The evolution of cooling technology for electrical, electronic, and microelectronic equipment,” *ASME HTD*, vol. 57, pp. 1–9, 1986.